Università degli Studi di Padova

Head Office: Università degli Studi di Padova

Department of Biology
Ph.D. COURSE IN BIOMEDICAL SCIENCE
CURRICULUM: Cell Biology and Physiology
SERIES: 36° cycle

OPA1-DRIVEN CRISTAE REMODELING PROMOTES PANCREATIC CANCER PROGRESSION

Thesis written with the financial contribution of AIRC

Coordinator: Prof. Chiara Romualdi
Supervisor: Prof. Luca Scorrano
Co-Supervisor: Prof. Alessandro Carrer

Ph.D. student : Carlotta Paoli

Abstract

Mitochondria are dynamic organelles that participate in various cellular processes such as bioenergetic homeostasis, signaling cascades and redox state control, ultimately influencing cell fate decisions. The diversity of mitochondrial functions resonates in the dynamic nature of their morphology. Indeed, both mitochondrial ultrastructure and network organization influence mitochondrial function and are both highly dynamic to respond to cellular demands quickly. As signaling organelles, mitochondria communicate with other cellular compartments through several mechanisms, including the release of metabolites, ROS production, and changes in their localization and shape. These alterations occur in response to environmental cues making mitochondria essential cellular stress sensors. In cancer, where low nutrient and oxygen levels often characterize local microenvironments, mitochondria play a central role in adaptation to stress, facilitating cancer cell proliferation in harsh conditions. This is well exemplified in pancreatic ductal adenocarcinoma (PDAC), which is one of the deadliest cancers worldwide and is characterized by a prominent desmoplastic reaction and a near avascular microenvironment that hampers nutrient/oxygen supply. Notably, over the last years, a compelling body of work has shown that metabolism is profoundly altered in PDAC.

My thesis aims to dissect the significance of the rewiring of mitochondrial function and morphology during PDAC progression to identify potential targetable mechanisms driving tumor aggressiveness. Quantitative analysis of the mitochondrial proteome in cellular models of stepwise pancreatic carcinogenesis revealed increased levels of proteins involved in metabolic pathways, protein import, and mitochondrial translation. These alterations included unexpected upregulation of components of the oxidative phosphorylation pathway, validated by the increase in mitochondrial respiration in late-stage PDAC cells. Changes in mitochondrial respiration correlated with modifications in mitochondrial ultrastructure both in vitro and in vivo. Further investigation identified members of the NDPK family, including NME4, as drivers of these changes in mitochondrial ultrastructure. Indeed, NME4 has been associated with the regulation of the GTPase activity of OPA1, the master regulator of cristae stability. NME4, in a complex with OPA1, has a crucial role in the regulation of mitochondrial ultrastructure, as its silencing in HeLa cells disrupts mitochondrial cristae. Accordingly, NME4 loss reshapes mitochondrial ultrastructure and impairs mitochondrial respiration in pancreatic cancer cells.

High protein levels of either NME4 or OPA1 are associated with poorer survival outcomes, highlighting their clinical relevance. These data highlight the crucial role of mitochondrial ultrastructure in promoting pancreatic carcinogenesis, but mechanisms remained elusive.

We leveraged both functional genomics to manipulate Opa1 expression and autochthonous mouse models of pancreatic carcinogenesis. Our results demonstrated that OPA1 elevation promotes active DNA duplication, histone hyper-acetylation, and cellular proliferation both in vitro and in vivo. These phenotypes have all been linked to PDAC development. Accordingly, OPA1 overexpression accelerates PDAC progression in vivo, while targeting OPA1 hinders pancreatic cancer cell growth, without affecting non-transformed pancreatic ductal cells.

In summary, this research significantly advances our understanding of mitochondrial reshaping during pancreatic carcinogenesis, revealing the intricate interplay between mitochondrial dynamics, cell cycle regulation, and tumor progression. Key players like NME4 and OPA1 can be envisaged as exciting therapeutic targets. Nonetheless, future research could delve deeper into the molecular intricacies of NME4 and OPA1 function and explore in more detail the molecular mechanisms beyond their role in pancreatic tumorigenesis.

INDEX

List of Abbreviations

5-hmC – 5-hydroxylmethylcytosine

α-KG – α-ketoglutarate

α-SMA – α-smooth muscle actin

ACCS2 – acyl-CoA synthetase short chain family member

ACLY – ATP-citrate lyase

ADM – acinar to ductal metaplasia

ADP – adenosine diphosphate

AIFM1 – apoptosis inducing factor mitochondria associated 1

AML – acute myeloid leukemia

AMPK – AMP-activated protein kinase

ARMC1 – armadillo repeat containing 1

ASXL1 – additional sex combs like 1

ATP – adenosine triphosphate

BAK – BCL2 antagonist/killer

BAX – BCL2 associated X

BCA – bicinchoninic acid assay

BCL – B-cell CLL/lymphoma

BET – bromodomain and extra-terminal motif

BH3 – BCL2 homology 3

BMI – body mass index

BPE – bovine pituitary extract

BSA – bovine serum albumin

CAF – cancer associated fibroblast

CCCP – carbonyl cyanide m-chlorophenyl hydrazone

CCD – coiled-coil domain

CCK – cholecystokinin

CCL5 – chemokine C-C motif ligand 5

CDKN2A – cyclin-dependent kinase inhibitor 2A

cGAS – cyclic GMP-AMP synthase

CHCHD – coiled-coil-helix-coiled-coil-helix domain

CI-IV – complex I-IV

CJ – cristae junction

CPA1 – carboxypeptidase A1

CPT1α – carnitine acetyl-transferase 1α

CS – calf serum

DAMP – damage-associated molecular pattern

DISC1 – disrupted in schizophrenia 1

DMEM – Dulbecco's modified Eagle medium

DNA – deoxyribonucleic acid

DNAJC11 – DnaJ heat shock protein family member C11

DHODH – dihydroorotate dehydrogenase

DRP1 – dynamin-related protein 1

ECAR – extracellular acidification rate

ECM – extracellular matrix

EDTA – ethylenediaminetetraacetic acid

EGF – epidermal growth factor

EM – electron microscopy

EMT – epithelial-mesenchymal transition

ER – endoplasmic reticulum

ERK – extracellular signal-regulated kinases

ETC – electron transport chain

Et-OH – ethanol

$FAD^+/FADH_2$ – flavin adenine dinucleotide (oxidized/reduced form)

FAO – fatty acid oxidation

FBS – fetal bovine serum

FCCP – carbonyl cyanide-4-(trifluoromethoxy) phenylhydrazone

FSC-A – forward scatter

GED – GTPase effector domain

GEF – guanidine exchanging factor

GI – gastrointestinal

GLS – glutaminase

GLUD – glutamate dehydrogenase

GMP – guanosine monophosphate

GOT – glutamic-oxaloacetic transaminase

GTP – guanosine triphosphate

HBSS – Hanks’ balanced salt solution

HBP – hexosamine biosynthesis pathway

Hh – hedgehog

HK2 – hexokinase 2

IBM – inner boundary membrane

IGF1 – insulin-like growth factor

IMM – inner mitochondrial membrane

IMMT – inner membrane mitochondrial protein

IPO – Importin

IMS – intermembrane space

KO – knock-out

KPBS – potassium phosphate buffered saline

KRAS – kirsten rat sarcoma viral oncogene homolog

KRT19 – keratin 19

LDLR – low-density lipoprotein receptor

LKB1 – liver kinase B1

MAP – mitogen-activated Protein

MCT – monocarboxylate transporters

MDH1 – malate dehydrogenase

MDM2 – mouse double minute 2 homologue

ME1 – malic enzyme 1

MEF – mouse embryonic fibroblast

MEK – mitogen-enhanced kinase

MFF – mitochondrial fission factor

MFN – mitofusin

MICOS – mitochondrial contact site and cristae organizing system

Mid49 – mitochondrial dynamics protein of 49 kDa

Mid51 – mitochondrial dynamics protein of 51 kDa

Miro – mitochondrial rho

MIST1 – muscle, intestine and stomach expression 1

MiT-TFE – microphthalmia-transcription factor E

MOMP – mitochondria outer membrane permeabilization

MPP – mitochondrial protein peptidase

mt – mitochondrial

mTORC – mechanistic target of rapamycin complex

MTS – mitochondrial targeting sequence

MUC1 – mucin 1

MYC – myelocytomatosis viral oncogene homolog

NAD^+/NADH – nicotinamide adenine dinucleotide (oxidized/reduced form)

$NADP^+$/NADPH – nicotinamide adenine dinucleotide phosphate (oxidized/reduced form)

NDP – nucleoside diphosphate

NDPK – nucleotide diphosphate kinase

NME4/6 – non-metastatic cells 4/6

NP-40 – nonyl phenoxypolyethoxylethanol-40

NRF2 – nuclear factor erythroid 2-related factor 2

NTP – nucleoside triphosphate

OCR – oxygen consumption rate

OMA1 – overlapping with the M-AAA protease 1 homolog

OMM – outer mitochondrial membrane

OPA1 – optic atrophy protein 1

OXPHOS – oxidative phosphorylation

PanIN – pancreatic intraepithelial neoplasia

PCR – polymerase chain reaction

PDAC – pancreatic ductal adenocarcinoma

PDX1 – pancreatic and duodenal homeobox 1

PINK1 – PTEN induced kinase 1

PKA – protein kinase A

PPP – pentose phosphate pathway

PSC – pancreatic stellate cells

PTF1 – pancreatic transcription factor 1

PUFA – polyunsaturated fatty acid

RCC1L – regulator of chromosome condensation 1 like

ROS – reactive oxygen species

rRNA – ribosomal ribonucleic acid

SAM – S-adenosylmethionine

SC – supercomplex

SLC – solute carrier family

SSC-A – side scatter-A

STING – stimulator of interferon response CGAMP interactor 1

SWI/SNF – switch/sucrose non-fermentable

TAM – tumor associated macrophage

t-Bid – truncated-BH3 interacting domain death agonist

TCEP – tris (2-carboxyethyl)phosphine

TCGA – the cancer genome atlas

TET – ten-eleven translocase

TF – transcription factor

TFAM – transcription factor A mitochondrial

TGFβ – transforming growth factor beta

TIMM – translocase of inner mitochondrial membrane

TM – transmembrane

TMA – tissue microarray

TME – tumor microenvironment

TNBC – triple negative breast cancer

TNF – tumor necrosis factor

TOMM20 – translocase of outer mitochondrial membrane

tRNA – transfer ribonucleic acid

TCA – tricarboxylic acid

UPR – unfolded protein response

UDP-GlcNAc – uridine diphosphate N-acetylglucosamine

US – United States

VDAC – voltage dependent anion channel

WAT – white adipose tissue

Wnt – Wingless-related integration site

INTRODUCTION

The first evidence of the impact of metabolism on neoplastic transformation stems from a seminal work by Otto Warburg in 1927, which described how cancer cells rely preferentially on glycolysis rather than OXPHOS to sustain their proliferation [1]. However, in the century spanning from this discovery and the present days, numerous studies have portrayed an extremely intricate scenario; indeed, the metabolic reprogramming observed in cancer cells is not limited to an altered balance between glycolytic and oxidative pathways, but involves a general alteration of the cellular metabolic state, with effects on both catabolic and anabolic processes [2,3]. Moreover, it has been proven that tumors are metabolically heterogeneous, with consistent rewiring during cancer development and variations dependent on the tumor type and stage. Furthermore, increasing evidence underlines that an additional level of metabolic modifications may be provided by intratumoral heterogeneity, with different cellular subpopulations relying on diverse metabolic pathways for their survival [4].

Given its extensive and multi-layered complexity, published studies have only begun to characterize the full extent of the metabolic rewiring occurring in cancer cells, and just in the recent years these processes have started to be investigated as a putative vulnerability exploitable for new therapeutic approaches [5]. Nevertheless, these alterations might display enormous potential in the treatment of undruggable malignancies, and therefore deserve further attention.

A prime example of such context is represented by pancreatic ductal adenocarcinoma (PDAC), which is one of the deadliest cancers worldwide and is characterized by a dismal 5-year survival rate of less than 10%. The extremely high mortality of PDAC is mainly due to the long latency of its symptoms, often leading to a late diagnosis, and to the consequent lack of effective therapeutic approaches [6]. Notably, over the last years, a compelling body of work has shown that metabolism is profoundly altered in PDAC [7]. In particular, most PDAC patients harbor an activating mutation in the KRAS gene, which has been associated with the reprogramming of several metabolic pathways, including glutaminolysis and the pentose phosphate pathway [8]. Strikingly, a central spot during pancreatic cancer metabolic reprogramming is represented by mitochondria, key organelles able to not only regulate the bioenergetic homeostasis of the cell but also able to play crucial signaling roles both in physiological and pathological contexts [7,9].

MITOCHONDRIA: BEYOND BIOENERGETICS

From their discovery, our understanding of mitochondria changed profoundly. Primarily known as the powerhouse of the cell for their ability to generate large amounts of ATP, this analogy no longer describes the full extent of the functions of these dynamic organelles. In fact, mitochondrial activity extends well beyond bioenergetic homeostasis, as it partakes in signaling cascades, redox state control, epigenetic organization, and cellular quality control [10]. The spectrum of mitochondrial functions is as wide as dynamic is their morphology. Indeed, both mitochondrial ultrastructure and the organization of mitochondrial network heavily impact mitochondrial function [11].

Moreover, these organelles have evolved several mechanisms to communicate with the rest of the cell, through direct contact sites and indirect signal mediators. Hence, mitochondria must be considered as signaling organelles, employing a wide range of functions that can affect cellular homeostasis in physiologic and pathologic contexts, altogether contributing to the determination of cell identity and to regulate cell functioning [9].

Mitochondrial morphology and dynamics

Mitochondrial morphology is extremely dynamic, and it is intrinsically linked to the regulation of the organelle function. Two main layers of complexity can be identified to describe the structural features of mitochondria: at the single mitochondrion level, the conformation of its membranes constitutes the mitochondrial ultrastructure, while the spatial organization of multiple mitochondria in the cells is referred to as mitochondrial network dynamics.

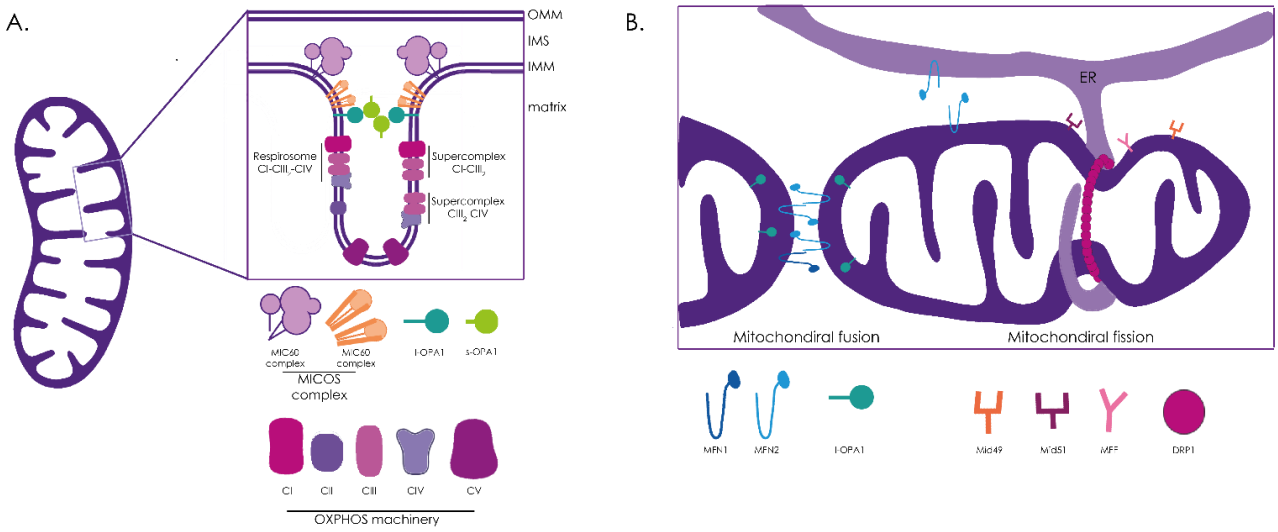

Fig. 1 A. **Schematic representation of regulators of mitochondrial cristae morphology and mitochondrial network dynamics.** The MICOS complex and OPA1 cooperate in the regulation of CJs and cristae biogenesis and stability. At cristae rims, F_1F_0-ATPsynthase dimers increases cristae stability. Mitochondrial cristae harbor the components of the ETC organized in supercomplexes with different stoichiometry. B. Mitochondrial fusion is mediated by MFN1 and MFN2 in the OMM and OPA1 in the IMM. Mitochondrial fission is dependent on DRP1 oligomerization at ER-mitochondria contact sites. Additionally, DRP1 has different adaptors on the OMM, including Mid49, Mid51 and MFF.

Mitochondrial ultrastructure

Mitochondria are bounded by two distinct membranes, which define different functional regions of the organelle. In contact with the cytosol, the outer mitochondrial membrane (OMM) is a semipermeable membrane which prevents small-molecule diffusion while allowing the exchange of metabolites and cations between the cytosol and the intermembrane space (IMS). Instead, the inner mitochondrial membrane (IMM) is completely impermeable and it divides the IMS from the mitochondrial matrix. Furthermore, this internal membrane can be subdivided into different functional compartments: the inner boundary membrane (IBM), the cristae and the cristae junctions (CJs) [11].

The IBM is the portion of the IMM that runs parallel to the OMM and it is characterized by contact sites among the two lipid bilayers, participating in processes like protein import and apoptosis [12]. The cristae are deep invaginations of the IMM protruding into the mitochondrial matrix; these dynamic structures are enriched in cardiolipin and in proteins involved in iron-sulfur biogenesis, protein

translocation and synthesis, and mtDNA maintenance [13]. Mitochondrial cristae are especially relevant for the organellar function; in particular, their structural features are pivotal in the compartmentalization of soluble molecules, which is mechanistically allowed by the third functional compartment of the IMM, the cristae junctions. Indeed, the IMM is constricted at the cristae base into CJs, narrow openings of approximately 20-50 nm diameter that limit the diffusion of solutes between the IMS and the cristae lumen [13].

Interestingly, mitochondrial cristae are not static structures, but undergo continuous cycles of biogenesis and disruption to meet the specific spatiotemporal needs of the cell. The mechanism through which cristae are formed is completely unknown, but all the proposed models concur that it must depend on the coordinated action of proteins and lipids to allow the formation of positive and negative curvatures in the IMM [14]. In particular, membrane curvature is allowed by the presence in the IMM of cardiolipin, which is present only in the mitochondria and constitutes almost the 20% of all the organelle phospholipids. Structurally, cardiolipin is characterized by a conical shape, which is conferred by the combination of an anionic polar head group and four esterified fatty acyl chains and allows the stabilization of negatively curved membranes [15,16].

After their formation, cristae are stabilized by the dimerization of the F_1F_0-ATP synthase at the cristae rims (Fig. 1A) [17]. Notably, the downregulation of subunits *e* or *g* of the F_1F_0-ATPsynthase (responsible for the oligomerization of the protein complex) results in the formation of onion-shaped cristae in yeast [18]. On the other hand, CJs morphology and stability are principally regulated by the MICOS complex (Fig. 1A), which is overall highly conserved along evolution and, in mammals, is composed by MIC10, MIC12, MIC19, MIC25, MIC26, MIC27, and MIC60. The ablation of any of these subunits results into the destabilization of CJs and in the formation of onion-shaped cristae, emphasizing the centrality of this complex in the stabilization these structures [19–24]. The number of new interactors of the MICOS subunits is constantly increasing. The list includes CHCHD10, CHCHD2, DNAJC11, ARMC1, DISC1, VDAC, SLC25A46, OPA1, PINK1, Miro, TFAM and OMA1 [24].

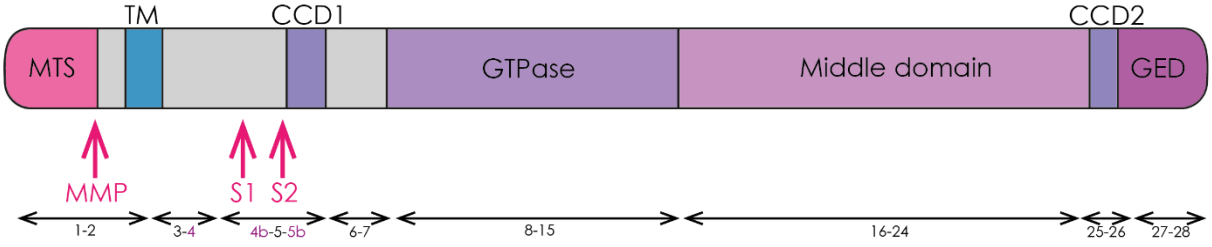

Fig. 2 Schematic representation of OPA1 structure. OPA1 shares several structural features with dynamins including the GTPase domain a middle domain and a GTPase effector domain (GED). Before the GTPase domain, Opa1 displays a mitochondrial targeting sequence (MTS) followed by a transmembrane domain (TM) and coiled-coil regions (CCD1). These domains are found in all OPA1 variants. OPA1 exons (numbers) are schematized by double arrow. Intra-mitochondrial proteolytic cleavage sites for mitochondrial processing peptidase (MPP), OMA1 (S1) and YME1L (S2) are indicated.

In particular, OPA1 is a crucial regulator of cristae biogenesis and morphology, as its acute ablation reshapes dramatically mitochondrial ultrastructure, resulting in cristae disruption [13,25].

Structurally, the N-terminus of OPA1 is characterized by a mitochondrial targeting sequence, a transmembrane domain that anchor the protein to the IMM, and a coil-coiled domain. The subsequent region of the protein includes a GTPase domain, a middle domain, a second coiled-coil domain, and a GTPase effector domain at the conserved C-terminus (Fig. 2). Precursors translated from the mRNA variants of OPA1 are targeted to mitochondria through their MTS, which is then cleaved by MPP after the import. This processing gives rise to the long isoforms of OPA1 (l-OPA1), that are anchored to the IMM and can be further processed at site 1 and 2 (S1 and S2) at the N-terminus (Fig.2) producing the short forms of OPA1 (s-OPA1), which are soluble into the IMS (Fig. 1A) [25–27]. The processing of l-OPA1 is mediated by two IMM peptidases: the zinc metalloprotease OMA1, that cleaves OPA1 at S1 in exon 5, and the ATP-dependent metalloprotease YME1L, that processes OPA1 at S2 in exon 5b. While YME1L is constitutively active, OMA1 can be activated by stress conditions and in response to mitochondrial dysfunction [26,28,29].

Both forms of OPA1 seem to be sufficient to maintain mitochondrial cristae structure [26,30,31]. Additionally, it has been proposed that s-OPA1 in the IMS serves as a bridge between l-OPA1 molecules regulating cristae width (Fig. 1A) [14,32–35]. Indeed, CJs are kept tight by oligomers containing a balanced proportion of both l-OPA1 and s-OPA1. The induction of cristae remodeling results in the unbalance of this proportion and the destabilization of the 720 kDa OPA1-containing complex, accompanied with the consequent widening of cristae [13,32,36,37]. Notably, OPA1 slight overexpression in mice decreases cristae width while its downregulation or ablation *in vitro* widens cristae and CJs, increasing cytochrome c release and inducing apoptosis [11,13,32,37].

In addition to its oligomerization, OPA1 activity depends also on the activation of its GTPase domain. In this context, the ablation of OPA1 interactors involved in GTP loading or in the regulation of GTP levels phenocopies OPA1 loss [38,39]. In this category, two proteins have been described to affect the GTPase activity of OPA1: NME4 and RCC1L.

NME4 is the only member that harbors an MTS among the NDPK family of proteins, which are involved in the reversible phosphorylation of NDPs into NTPs [40,41]. In particular, it has been shown that this protein is anchored to the IMM facing the IMS and that, in this location, it interacts with OPA1. Furthermore, the knockout of NME4 in HeLa cells induces the disruption of mitochondrial ultrastructure with cristae loss. Additionally, in presence of liposomes mimicking the IMM composition NME4 is able to increase the GTPase activity of OPA1, that further increases in the presence of native mitochondrial GTP concentration [38].

Conversely, RCC1L was initially described as necessary for mitochondrial respiration in a genome-wide screening [42]. Thereafter, this protein was shown to localize in the IMM facing the IMS where it acts as an OPA1-specific guanidine nucleotide exchanging factor. Indeed, RCC1L interacts with OPA1 and *in vitro* GEF assay shows that it can acts as a strong and rapid GEF for OPA1 in a concentration-dependent manner [39,43].

In conclusion, OPA1 is a crucial player in the regulation of mitochondrial ultrastructure and cristae formation and stability, which is a multifaceted and complex process that can regulate crucial mitochondrial pathways, including apoptosis and OXPHOS.

Mitochondrial network dynamics

In the cytosol, mitochondria are organized into a dynamic network, that constantly reshapes its morphology through fusion and fission events. Mitochondrial network is dynamically reshaped in response to several stimuli, including starvation and apoptosis, reinforcing the notion that mitochondrial morphology and function are tightly linked.

Mitochondrial fusion in mammals is a two-step process, that allows the exchange of mtDNA, lipids, and metabolites [11]. It is principally mediated by three large GTPases of the dynamin superfamily, namely MFN1/MFN2 and OPA1, which mediate respectively the fusion of the OMM and of the inner membranes [44–46]. The fusion process starts with the docking of two molecules of MFN1/MFN2 on the OMM of two mitochondria. The formation of these homo/hetero dimers induces conformational changes that drives GTP hydrolysis by MFNs, ultimately leading to the fusion of the two OMMs. In the second step of this process, OPA1 tethers the inner membranes of the two mitochondria allowing fusion, after an additional docking step [14]. Interestingly, cell fusion assays suggested that the presence of OPA1 and cardiolipin on either side of the membranes could represent the minimal IMM fusion machinery [47]. Notably, the mechanism by which OPA1 mediates the IMM fusion seems to be independent of its regulation of cristae morphology and reshaping [13,32,48].

On the other hand of the dynamic spectrum of mitochondrial network reshaping stand the fission machinery, whose main actor is DRP1, a protein recruited in a phosphorylation-dependent manner on the mitochondrial surface. In this specific location, several proteins function as adaptors for DRP1, including MFF, Mid49, and Mid51. Once recruited on the OMM surface, DRP1 oligomerizes around the mitochondrion and drives its division in a GTP-dependent manner. Although the role of DRP1 in initiating mitochondrial fission is clear, its capability to terminate this process has been subject of extensive debate. Indeed, cryo-EM imaging showed that the minimal diameter or the DRP1 *ring* upon GTP addition is 50-60 nm, suggesting the involvement of other unknown players in the fission process [14,49,50].

Summarizing, mitochondrial dynamics proteins act as receptors and transduce cytosolic and environmental stimuli into tightly regulated alterations in mitochondrial network shape, and consequently function, that are required for cellular adaptations. Blocking this axis by manipulating the ability of mitochondria to adapt and respond to certain stimuli compromises cellular physiology [11].

Mitochondrial function

Historically, mitochondrial function has mainly coincided with the generation of ATP by the TCA cycle through oxidative phosphorylation. This process mainly takes place into the mitochondrial matrix and it is constituted by a series of enzymatic steps able to release stored chemical energy through the oxidation of acetyl-CoA derived from fatty acids, amino acids, and pyruvate generated from glucose via glycolysis [51,52].

The TCA cycle is an amphibolic pathway, being involved both in anabolism, through the production of intermediates for the synthesis of macromolecules, and catabolism, generating reducing equivalents (such as NADH and $FADH_2$) to ultimately produce ATP through oxidative phosphorylation [53–55].

The TCA cycle is a crucial biosynthetic hub: in fact, oxalacetate can be converted into phosphoenolpyruvate (substrate of gluconeogenesis), α-ketoglutarate can be converted in glutamate and then to glutamine feeding purine synthesis, and lastly citrate can be exported into the cytosol where is converted into acetyl-CoA and oxalacetate. In the cytosol, oxalacetate can generate aspartate, while acetyl-CoA is a precursor for lipid synthesis and it is the unique acetyl donor for acetylation of histones and other proteins [54].

Importantly, when TCA cycle intermediates are employed for biosynthetic purposes, the cycle has to be replenished, and this happens through several entry points, in a process termed anaplerosis. The more relevant anaplerotic pathways are the conversion of pyruvate to mitochondrial oxalacetate by pyruvate carboxylase and the conversion of glutamine into glutamate and subsequently into α-ketoglutarate, in a pathway known as glutaminolysis. Additionally, it has to be taken into account that the TCA cycle is heavily dependent on substrate availability and is therefore controlled allosterically by many key intermediates, such as acetyl-CoA, succinyl-CoA, ATP, ADP and NADH. Exemplifying, when the cell has ATP and NADH in excess, the TCA cycle slows down. In contrast, high demand for ATP increases the ATP/ADP ratio resulting in a stimulation of the enzymes of the cycle [56].

Other than glycolysis, also fatty acids oxidation can feed the TCA cycle producing acetyl-CoA. FAO enzymes are mainly localized into the mitochondrial matrix and the oxidation of fatty acids is the main source of ATP when levels of glucose are low. The first mitochondrial step of FAO is the transport of fatty acyl-CoA into the mitochondrial matrix, a process mediated by the carnitine transport cycle. In this cycle, CPT1α in the OMM replaces the CoA moiety with a molecule of carnitine, forming fatty acyl-carnitine that is transported through the IMM by the carnitine-acylcarnitine translocase in exchange for a carnitine molecule. In the matrix, the fatty acyl-carnitine is converted firstly in fatty acyl-CoA and then into acetyl-CoA, with the generation of NADH and $FADH_2$. The limiting step of FAO is the one catalyzed by CPT1α, which is allosterically inhibited by

malonyl-CoA, one of the intermediates of fatty acids synthesis in the cytosol, to prevent simultaneous fatty acid oxidation and synthesis [56].

The reducing equivalents NADH and $FADH_2$ generated by the TCA cycle have to be oxidized for the cycle to continue to function. To this aim, the first complex of the electron transport chain accepts electron from these reducing equivalents and transfer them sequentially to complex III and complex IV; at the end, complex IV passes them to molecular oxygen generating two molecules of water [56,57]. The transfer of electrons through the complexes is coupled with the pumping of protons from the mitochondrial matrix to the IMS [58].This proton pumping generates a proton motive force, composed by a chemical (ΔpH) and an electrical (Δψ) component. The major component of this force is the mitochondrial membrane potential derived from the separation of the charges between the matrix and the IMS. The proton motive force derived from the proton gradient is used by the F_1F_0-ATPsynthase, also known as complex V, to generate ATP from ADP and P_i [58]. Complex V is composed of two distinct multisubunit portions, a catalytic one (F_1-ATPase) and a hydrophobic proton-pumping one (F_0). In intact mitochondria, the protons accumulated in the IMS enter the F_0 complex and exit in the mitochondrial matrix. The energy dissipated in this way promotes the rotation of the F_0 in a clockwise direction, inducing conformational changes in the F_1-ATPase and enabling the production of ATP [59].

The efficiency of mitochondrial respiration depends on several factors, including cristae morphology, crucial to ensure the optimal efficiency of the electron transport, and the formation of supercomplexes, in which the complexes of the ETC are organized with different stoichiometries [14,57,60]. The most complete supercomplex described is the respirasome (CI-$CIII_2$-CIV); in mammals, two additional supercomplexes have been described, namely CI-$CIII_2$ and $CIII_2$-CIV (Fig. 1A) [61,62]. Several studies have proposed possible functions of the supercomplexes, including the maintenance of the structural organization of the individual complexes, the reduction of electron leakage and mtROS production , the facilitation of substrate channeling, and finally the prevention of protein aggregation [63–66]. The observation that the acute ablation of OPA1 leads to the loss of SCs assembly remarks the crucial role of OPA1-dependent cristae reshaping in the regulation of OXPHOS and energy homeostasis, emphasizing the central role of this protein at the interface between morphology and function [67].

Form follows function, function follows form

The first observation of cristae remodeling was made in 1966 by Hackenbrock, documenting the shift between an orthodox and a condensed state, induced by the decrease in ADP levels during mitochondrial respiration. The main difference between these morphologies consists in the relative states of expansion or contraction of the matrix and the cristae lumen [68]. Cristae in the orthodox state tend to be tubes or short flat lamellae, while mitochondria in the condensed state have larger internal compartments with multiple tubular connection. This shift in the mitochondrial ultrastructure has been linked to the increase in the efficiency of ATP production [69].

Since that observation, several other studies have unveiled the contribution of cristae morphology to mitochondrial bioenergetics and vice versa. Firstly, the complexes and supercomplexes of the OXPHOS machinery localize to this compartment of the IMM [70]. Mitochondrial cristae not only increase the surface available to harbor larger quantities of respiratory chain complexes, but their morphology is believed to provide optimal conditions for the electron flux. Indeed, supercomplexes assembly is enhanced by OPA1-dependent modulation of cristae morphology, and this mechanism increases the efficiency of mitochondrial respiration [13].

Furthermore, mitochondrial cristae reshaping has been shown to respond to different metabolic cues. Modifications in length and width of cristae and CJs can occur in response to changes in substrate availability, bioenergetic state or in response to different metabolic stresses that require mitochondrial adaptation, such as hypoxia, starvation, and increase in ROS levels [11,33–35,69,71]. Cristae remodeling in these conditions can regulate mitochondrial function by driving supercomplexes assembly and facilitating electron flux [13]. This mechanism can thus drive changes in ATP production in response to different cellular state and environmental cues to allow cellular adaptation.

Cristae remodeling has also been deeply studied during the apoptotic process, in which is fundamental to allow the release of pro-apoptotic molecules, such as cytochrome c, to trigger downstream effectors [72–75]. During apoptosis, “BH3-only” members of the BCL-2 family (such as t-Bid) induce a profound remodeling of cristae morphology associated with the widening of CJs up to 70 nm of diameter. These changes allow the release of cytochrome c from the cristae lumen and increase its amount in the IMS, from where it can be released in the cytosol after the mitochondrial outer membrane permeabilization [76,77]. In this context, it has been shown that OPA1 controls mitochondrial remodeling and cytochrome c mobilization, being OPA1 oligomers one of the early targets of t-Bid [32].

More broadly, the opposing processes of mitochondrial fusion and fission are key players in regulating mitochondrial adaptation to cellular stimuli.

Firstly, the reshaping of mitochondrial network is fundamental to ensure the maintenance of an intact and functional mitochondrial population. In this context, ensuring the proper elimination of

dysfunctional mitochondria is imperative for cell survival [11,78,79]. To subtend to this regulation, several quality control mechanisms have evolved, including mitophagy, a selective form of autophagy in which whole mitochondria are engulfed by autophagosomes. This process is heavily impacted by mitochondrial fission, primarily because a mitochondrion has to be physically separated from the network to undergo degradation. In fact, forcing hyperfusion of the mitochondrial network (through OPA1 overexpression or the expression of the dominant-negative form of DRP1) precludes the autophagic engulfment of mitochondria [80]. Additionally, during mitophagy MFN1 and MFN2 are ubiquitinated and degraded, inducing mitochondrial fission.

Secondly, mitochondrial network can be reshaped by different cellular metabolic states, as well can impact cellular adaptation to differential metabolic cues. Obesity and excessive lipid supplementation in several cell types has been shown to increase mitochondrial fragmentation [81–83]. Additionally, mitochondrial fission promotes the progression of nonalcoholic fatty liver disease and the effects of high-fat diet in mice are alleviated by the expression of the dominant-negative form of DRP1 through the alteration of mitochondrial respiration [84]. On the other hand, the induction of mitochondrial fragmentation via the deletion of MFN2 in brown adipose tissue is associated with improved insulin sensitivity and resistance to obesity in response to high-fat diet [85]. Finally, a recent study showed that mitochondrial fission reduces CPT1α sensitivity to malonyl-CoA inhibition, favoring fatty acid oxidation in mitochondria. In this context, the induced FAO has functional consequences that are specific for the cell type, such as increased hepatic gluconeogenesis or the induction of insulin secretion [86].

Mitochondria as signaling organelles

Mitochondria are crucial organelles in the determination of cell fate, as they are involved in a plethora of processes required for cellular function, proliferation, and differentiation [11,87]. In this context, the cell-mitochondria communication works both through indirect signaling pathways and direct contact sites [88].

Mitochondria can communicate indirectly with the rest of the cell through four main mechanisms: the release of cytochrome c to induce cell death, the release of mtDNA to activate immune responses, the production of ROS to impact protein homeostasis and overall cellular survival and the activation of AMPK to control mitochondrial fusion and fission [51,89–92]. Additionally, recent evidence indicates that mitochondrial metabolism, and in particular the abundance of TCA metabolites, can be considered as a fifth mechanism contributing to control cell fate and function [51].

A classic example of mitochondrial driven signaling is apoptosis, a conserved pathway of programmed cell death required for tissue homeostasis. In mammals, the intrinsic apoptotic pathway is characterized by the activation and oligomerization of the pro-apoptotic BCL2 homologs BAX and BAK. This oligomerization promotes the formation of pores in the OMM through which pro-apoptotic factors are released into the cytosol where they can trigger the downstream apoptotic pathway [93–95].

Other than pro-apoptotic factors, MOMP also mediates the release of mitochondrial DAMPs. One of them is the mtDNA, able to trigger in the cytosol pro-inflammatory responses activating the cGAS-STING-type I interferon pathway [96]. DAMPs can also be released during mitochondrial stress, as part of the evolution of pathways involved in the maintenance of mitochondrial homeostasis [96]. This necessity stems from the fact that mitochondrial proteome is principally encoded by nuclear genes. Thus, a precise coordination between mitochondria and the nucleus is required.

Other than apoptosis and mitophagy to cope with mitochondrial stress, these organelles are characterized by a specific unfolded protein response. The mtUPR is a stress signaling cascade between mitochondria and the nucleus that drives transcriptional changes promoting mitochondrial function. The activation of this cascade promotes glycolysis, limiting OXPHOS, to decrease the burden of energy production on mitochondria; additionally, also the mevalonate pathway, the mitochondrial network and the mtDNA maintenance are affected [96–100].

Mitochondria are a significant source of ROS, produced mainly as a by-product of mitochondrial respiration. In particular, complex I and complex III are major sites for the generation of O_2^- , that is immediately reduced to the more stable H_2O_2 [10]. Historically, ROS were thought to act exclusively as cellular damaging agents; however, recent evidence points out to their role as mediators of intracellular signaling. For example, H_2O_2 can act as a signaling molecule by directly oxidizing

specific sulfur-containing amino acid, impacting the function and stability of proteins [101]. Additionally, H_2O_2 in presence of Fe^{2+} can also generate $^{\bullet}OH$, that reacting with PUFAs initiates ferroptosis, a specific type of non-apoptotic cell death [102].

Lastly, AMPK is a highly conserved sensor of low intracellular ATP, which is activated in response to a plethora of mitochondrial stresses. Activated AMPK then phosphorylates downstream effectors to redirect metabolism towards increased catabolism [91]. Notably, the activation of AMPK also regulates mitophagy, induces mitochondrial biogenesis and promotes mitochondrial fission in response to the energetic stress [103–105]. Its central role in the regulation of these processes shows that AMPK constitutes a signal integration platform that is able to both reshape cellular metabolism and maintain mitochondria homeostasis [91].

Further, TCA cycle intermediates can control gene expression through posttranslational modifications of protein or epigenetic modifications [51,106.] Indeed, the majority of the chromatin modifying enzymes uses metabolic intermediates as co-factors for their activity. Thus, epigenetic reshaping is extremely dependent on the energetic status of the cell. For example, histone acetylation is heavily influenced by nucleo-cytoplasmic acetyl-CoA availability [107,108]. Acetyl-CoA can be produced from several carbon sources, like glucose, fatty acids, and amino acids. In mitochondria, acetyl-CoA it is converted into citrate by citrate synthase within the TCA cycle. Then citrate can be exported into the cytosol, where ACLY breaks it down into acetyl-CoA and oxalacetate. Cellular levels of acetyl-CoA are strictly connected with nutrient availability and the general energy status of the cell. When energy production is high, acetyl-CoA levels and histone acetylation increase promoting chromatin relaxation and gene expression [109]. Additionally, both histone and DNA methylation depend on TCA intermediate levels. The lysine-demethylases family is mainly composed of Jumonji C-domain demethylases (JmjC), that are activated by Fe^{2+} and α-ketoglutarate and inhibited by succinate and fumarate [51].

These multifaceted functions of mitochondria in normal physiology make them important cellular stress sensors and allow for cellular adaptation to the environment. Similarly, mitochondria are central to allow flexibility for cancer cell to proliferate in the tumor environment, characterized by low nutrient and oxygen levels [110].

Mitochondria and cancer

Cancer cells are characterized by the multistep acquisition of a series of specific hallmarks that ultimately lead to malignant transformation [5]. In this context, multiple evidence points to the involvement of mitochondria in all steps of carcinogenesis [4].

Nonetheless, the role of mitochondrial ultrastructure and network dynamics in cancer progression is poorly understood. By summarizing the main aspects of the reshaping of mitochondrial morphology during cancer growth, it appears evident that tumor cells are able to modify both mitochondrial ultrastructure and network according to the cancer stage and the changing environment [111].

Interestingly, OPA1 is overexpressed and a negative prognostic marker for several tumors. For example, in triple negative breast cancer, OPA1 expression correlates with a worst prognosis and its silencing is able to inhibit cancer proliferation by increasing the levels of miRNAs of the 148/152 family [112]. In KRAS-driven lung adenocarcinoma, OPA1 is crucial to induce cancer growth by promoting the ETC-mediated NAD^+ regeneration necessary for oxidative biosynthesis [113]. Venetoclax-resistant AML cells are characterized by narrow mitochondrial cristae and OPA1 overexpression. Additionally, some types of ovarian cancer are characterized by an increase in mitochondrial biogenesis and cristae remodeling, accompanied by an increased stability of OPA1 oligomers [114,115]. Lastly, HSP90 has been associated with unfavorable prognosis in PDAC. In this context, HSP90 interacts with OPA1 to regulate mitochondrial cristae structure and mitochondrial respiration efficiency [116].

On the other hand, the specific role of the fusion-fission balance is extremely dependent on the cancer type and stage [117,118]. Mitochondrial fission is often associated with mitophagy and apoptosis in cancer cells, while mitochondrial fusion seems to inversely correlate with tumor development. Oncogenes can directly dictate changes in mitochondrial dynamics. Oncogenic KRAS expression in pancreatic cancer can induce mitochondrial fragmentation through the ERK-dependent phosphorylation of DRP1 [119–121]. In addition, in breast cancer cell lines the inhibition of DRP1-driven mitochondrial fragmentation has been associated with increased genome instability and reduced invasiveness [122]. On the other hand, MYC has been suggested to induce mitochondrial fusion to promote the biosynthesis of metabolic precursor and favor MYC-driven cell growth [110,123].

One of the main features of cancer cells is the ability to evade cell death, which is tightly linked to mitochondria. In cancer cells the balance of BCL-2 proteins is deregulated to promote cell survival and the threshold of BH3-only proteins required to initiate apoptosis is higher [124,125]. Commonly, oncogenic signaling pathways can converge at the level of the BCL-2 family, leading to an imbalance in the BCL-2 rheostat and favoring cell survival. A classic example is represented by TP53, a tumor suppressor that, physiologically is activated in response to DNA damage or hypoxia and once

activated it can promote DNA repair or alternatively apoptosis. Loss-of-function mutations in TP53 result in apoptosis resistance and are frequently associated with advanced tumor stage and poor prognosis [5].

Moreover, some types of cancer are driven by mutation in genes of the TCA cycle. In particular, the accumulation of some oncometabolites, such as fumarate, succinate, and 2-hidroxyglutarate, modifies several processes including the induction of epigenetic changes, driving the tumorigenic process [126,127]. In the context of epigenetic regulation, the accumulation of succinate and fumarate is able to inhibit Jumonji C domain-containing histone demethylases and the Ten-eleven translocation (TET) protein family by competitively inhibit α-ketoglutarate usage as a substrate for dioxygenases [51,128]. Furthermore, citrate resides at a crucial intersection between catabolic and anabolic metabolism, and hence operates as a major node of flexibility [4]. Additionally, citrate is the main precursor for cytosolic acetyl-CoA, a central metabolite for fatty acid and cholesterol synthesis as well as for acetylation of proteins, including histones. Elevated histone acetylation as a consequence of an increase in the nucleo-cytoplasmatic pool of acetyl-CoA affects the expression of genes involved in cell growth and proliferation. The main acetyl-CoA generating enzyme in the cytosol, ACLY, is upregulated in different type of tumors, as for example in PDAC where its deletion or inhibition impairs tumorigenesis [51,129].

During tumor initiation and progression, cells undergo a metabolic reprogramming that involves glycolysis, lipid, and glutamine metabolism as well as mitochondrial function. Indeed, cancer cells need high levels of energy and building blocks for their uncontrolled proliferation and for their survival in the nutrient- and oxygen-poor tumor microenvironment.

Despite the Warburg effect, mitochondria are active in cancer cells that are highly heterogeneous in terms of metabolic pathways. Together with a hyper-activated oxidative phosphorylation, an increased mitochondrial mass and biogenesis has been associated with the altered proliferation, the increased invasiveness, and the drug-resistance characteristic of some cancer cells [4]. Consistently, cells surviving oncogenic KRAS withdrawal in a murine model of PDAC are characterized by a reshaped mitochondrial ultrastructure, as well as by an upregulation of mitochondrial biogenesis, OXPHOS activity, and membrane potential. These data suggest that the more aggressive tumor subpopulation relies on mitochondrial respiration for its survival and proliferation [130]. Additionally, the inhibition of complex I leads to the complete regression of the tumor in a PDX model of chemoresistant triple negative breast cancer supporting even more the suggestion that mitochondria and mitochondrial respiration are involved in cancer biology [131].

Furthermore, glutaminolysis and fatty acid oxidation are mitochondrial metabolic pathways commonly upregulated in tumors.

Glutamine is one of the most abundant circulating amino acids and it is highly consumed in different types of cancer, such as ovarian, pancreatic and breast cancer [132]. KRAS-dependent upregulation of GOT1 and GOT2 in PDAC boosts the production of aspartate for nucleotide synthesis as well the generation of NADPH by the malic enzyme 1. Notably, PDAC cells are extremely sensible to glutamine deprivation and the inhibition of glutaminolytic enzymes results in the suppression of tumor growth both *in vitro* and *in vivo* [133,134].

Regarding fatty acid oxidation, its contribution to cancer progression is less characterized and less straightforward. Nonetheless, some cancers like KRAS-mutant lung cancer, TNBC and AML overexpress and over activate key FAO enzymes [135–137]. Additionally, several tumors rely on FAO for their proliferation, as inhibition of CPT1α suppresses the growth of cell lines derived from ovarian cancer, prostate cancer, and multiple myeloma [138–142]. As a matter of fact, pharmacological inhibition of FAO decreases Ki-67 staining and delayed the appearance of glioma *in vivo* [143].

Lastly, ROS play a pleiotropic role during tumorigenesis; in several tumors, ROS levels are augmented, favoring mutagenesis and providing a survival advantage. On the other hand, it has also been reported that increased levels of mitochondrial ROS can have toxic effects in cancer cells[4]. For example, MFN2-induced decrease of ROS production reduces ovarian cancer cells proliferation and EMT [144]. Additionally, the reduction of ROS *in vivo* in a murine model of PDAC is able to reduce preneoplastic lesion formation [145]. In general, a key issue for cancer cells is to keep ROS levels high enough to be beneficial, but below the threshold of cell death induction, making the balance of ROS levels a possible therapeutic vulnerability.

In conclusion, mitochondria exert central bioenergetic functions, participate in transcriptional regulation, ROS production and homeostasis and cell death, thus constituting promising targets for the development of new strategies for both cancer diagnosis and therapy.

PANCREATIC DUCTAL ADENOCARCINOMA (PDAC)

The pancreas is a mixed organ, with both endocrine and exocrine functions. Its endocrine compartment is represented by the islets of Langerhans and secretes hormones involved in the regulation of glucose homeostasis [146]. On the other hand, the exocrine compartment constitutes the large majority of the whole organ and acts as an accessory digestive gland, secreting digestive enzymes that are released in the duodenum [147].

Pancreatic cancers can develop from endocrine or exocrine cells. Endocrine tumors arise from pancreatic islets cells and are uncommon, representing less than 5% of total pancreatic cancers. Conversely, pancreatic cancers derived from the exocrine compartment are more common and are classified in two subtypes according to histological features: mucinous tumors, which account for a minor fraction of the exocrine neoplastic formations, and pancreatic ductal adenocarcinoma (PDAC), which represents the 90% of all pancreatic cancers. PDAC manifests at very late stages, when surgical resection is not a therapeutic option [148].

Pancreatic ductal adenocarcinoma is one of the deadliest cancers worldwide, characterized by a median overall survival of less than 6 months from the diagnosis and a 5-year mortality of approximately 92% [149]. This dismal prognosis can be primarily addressed to the combination of late diagnosis and to the ineffectiveness of current therapeutic approaches. In fact, patients often remain asymptomatic until late stages of the disease, when the tumor has already compromised organ functions and disseminated throughout the body. There is urgent demand for strategies that allow earlier diagnosis and for new therapeutic targets that together might reduce the tremendous health burden of PDAC [149].

The main genetic driver of PDAC is the prototypical proto-oncogene *Kirsten Rat Sarcoma Virus* (*KRAS*). Gain-of-function *KRAS* mutations are reported in more than 90% of patients. These dramatically promote cellular proliferation and tumorigenesis, in part through the reprogramming of cellular metabolism [150]. Other frequent genetic alterations include mutations or deletions in *TP53*, *CDKN2A* and *SMAD4* genes that elicit several tumor-promoting effects, such as increase in genomic instability and rewiring of cellular metabolism [151].

These oncogenic insults are deeply intertwined and are ultimately able to promote tumorigenesis [7,152].

A very distinct hallmark of PDAC pathogenesis is the deposition of a dense and desmoplastic stroma, that critically contributes to tumor progression and imposes the rewiring of cancer cell metabolism in order to adapt to nutrients and oxygen scarcity. Most common metabolic rearrangements are the upregulation of both glycolysis and glutaminolysis and an extensive scavenging of non-canonical carbon sources [7].

Recently, the mapping of mutations across the genome of human cancers have unveiled that alterations in genes that organize, modulate, and maintain chromatin architecture are a distinctive feature of cancer [153]. In addition, accumulating evidence points to the existence of non-mutational epigenetic reprogramming as a mutation-less cancer evolution phenotype [154]. In this context, aberrant DNA methylation and post-translational histone modifications are main epigenetic alterations, also contributing to PDAC heterogeneity and progression [155,156].

The complex interaction between genetic and epigenetic landscapes and the metabolic rewiring of pancreatic cancer cells is not completely understood. Evidence suggests that KRAS-driven metabolic reshaping could impact pancreatic tumorigenesis also by affecting the epigenetic regulation of chromatin organization [129].

Anatomy and physiology of the pancreas

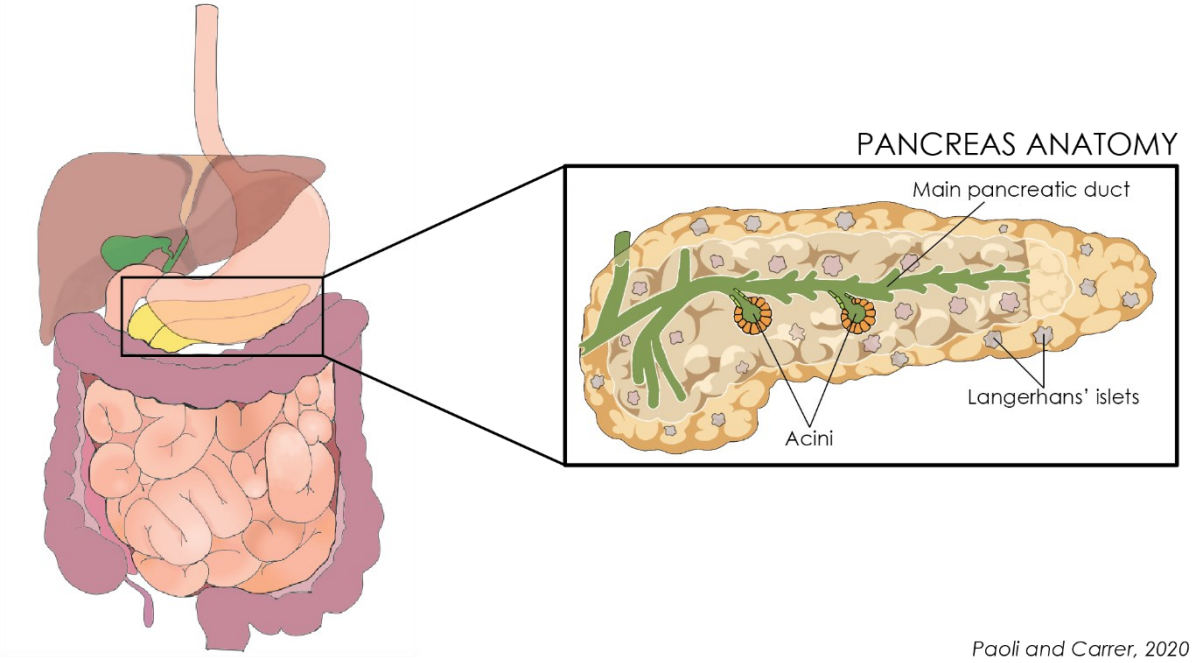

Fig. 3 Anatomic organization of the GI tract. The pancreas is magnified on the right, along few representative structures within the organ.

The pancreas develops from the dorsal and ventral pancreatic buds, during the fourth week of gastrulation. Initiation of pancreatic development is controlled by the timely expression of a wide set of molecular factors and pathways, including PDX1, PTF1, Notch, Hh and Wnt [157].

In adult organisms, the pancreas is a retroperitoneal organ located between the stomach and the first lumbar vertebra and it is an extremely heterogeneous tissue, composed by a mixed population of epithelial, glandular and stromal cells (Fig. 3) [158,159].

The pancreas can be roughly subdivided into four anatomical parts, with no clear demarcation amongst them: the head, the body, the neck and the tail.

The head of the pancreas is the portion curved by the duodenum, near which lies the common bile duct; thus, malignancies developing in this portion of the pancreas might obstruct the duct, with consequent retention of bile pigments and enlargement of the gallbladder. The body is the region that passes behind the stomach and the pancreas ends at the hilum of the spleen with its tail. Lastly, the neck is the narrower portion, that lays adjacent to the pylorus of the stomach (Fig. 3) [158]. From the tail of the pancreas starts the main pancreatic duct, also known as the duct of Wirsung, which runs longitudinally through the extension of the organ. This duct lies in the dorsal portion of the pancreatic parenchyma, receiving the intralobular ducts throughout its course. In the pancreatic head, the main pancreatic duct combines with the common bile duct, forming the hepatopancreatic ampulla (Ampulla of Vater). The latter, then, enters obliquely through the wall of the duodenum with the duodenal papilla. Additionally, the pancreas has an accessory pancreatic duct (duct of Santorini) that collects

short pancreatic ducts from the anterosuperior portion of the head and then connects with the main pancreatic duct at its initial part [147].

The pancreas is a heterogeneous organ, being composed of both endocrine and exocrine components. The islets of Langerhans represent the endocrine compartment, that is scattered across the tissue. This compartment accounts for the 2% of the whole organ and secretes insulin, somatostatin, and glucagon to regulate glucose utilization and levels in the blood [146].

However, the large majority of the pancreatic parenchyma is represented by the exocrine cells that produce the pancreatic juice, a mixture of digestive enzymes released into the duodenum through pancreatic ducts.

The core exocrine unit of the organ is the acinus, composed of post-mitotic epithelial cells, called acinar cells. Acinar cells (that represent approximately 85% of all pancreatic cells) are polarized, conical-shaped cells, with a basal nucleus and cytosolic zymogen granules. These store inactive proteases, which are released into the tubular network upon activation [146]. The enzymatic fluid drains from an acinus into the intralobular ducts. On the other hand, ductal cells secrete a bicarbonate-rich fluid that delivers digestive enzymes to the duodenum and allows the maintenance of the correct pH [159].

Pancreatic excretion can be divided in different phases. In the cephalic one, the secretion of digestive enzymes from acinar cells is stimulated by vagal input in response to the sight, smell, or taste of food. This kind of secretion continues also during the gastric phase, in which the gastric distention initiates vagal reflexes. During the intestinal phase, the acidification of the lumen of the duodenum stimulates the secretion of secretin from S cells. Finally, the presence of lipids, protein and carbohydrates into the duodenum causes the release of cholecystokinin (CCK), the main mediator of pancreatic enzyme secretion [146].

Epidemiology and risk factors of PDAC

The incidence and death rates of pancreatic cancers are increasing worldwide and little or no advances have been made to the clinical practice. Although the burden of other common cancer types, such as lung and breast cancer, have decreased over the last decades thanks to progress in both diagnosis and therapy, the incidence of PDAC is still growing by a rate of 0,5% to 1% every year while its prognosis remains steady, projecting pancreatic cancer to become the second leading cause of cancer-related death by 2030 in the US [149]. Despite low incidence (13 per 100,000 people per year), PDAC has one of the highest death rates of any solid tumor, with an overall 5-year survival of about 10%[148].

Nowadays, 50% of PDAC patients are diagnosed with metastatic disease, while only 10% to 15% of those have localized, surgically-resectable tumors; the remaining (30-35% of individuals with PDAC) is diagnosed with a locally advanced disease that is not operable. Age-standardized incidence of pancreatic cancer varies significantly between countries, but is consistently growing in areas with higher human development index [160–162]. Indeed, age and disordered lifestyle habits are associated with higher risk of developing PDAC [163].

A number of risk factors have been identified. Several environmental exposures and chronic diseases increase the incidence of PDAC but modifiable risk factors also contribute significantly. For example, cigarette smoking is strongly associated with PDAC onset through a multifactorial mechanism involving DNA damage, inflammation, and fibrosis [164]. A meta-analysis revealed that cigarette smoking increases the probability of developing PDAC, ranging from 2 to 3 times, depending on the number of cigarettes per day [165,166]. Others known risk factors linked to lifestyle are heavy alcohol drinking and obesity. In particular, unhealthy diet and obesity are associated to increased mortality [167]. Additionally, obesity is often associated with the onset of type 2 diabetes, known to be another risk factor of PDAC. Notably, the sudden appearance of diabetes can be a sign of PDAC, while chronic diabetes predisposes to pancreatic cancer, as a consequence of intrapancreatic hyperinsulinemia and insulin resistance [168]. Like diabetes, acute and chronic pancreatitis are risk factors for PDAC as cycles of inflammation and tissue damage can initiate tumorigenesis; at the same time, pancreatitis can also develop as a result of an underlying pancreatic cancer [169].

Pathogenesis of PDAC

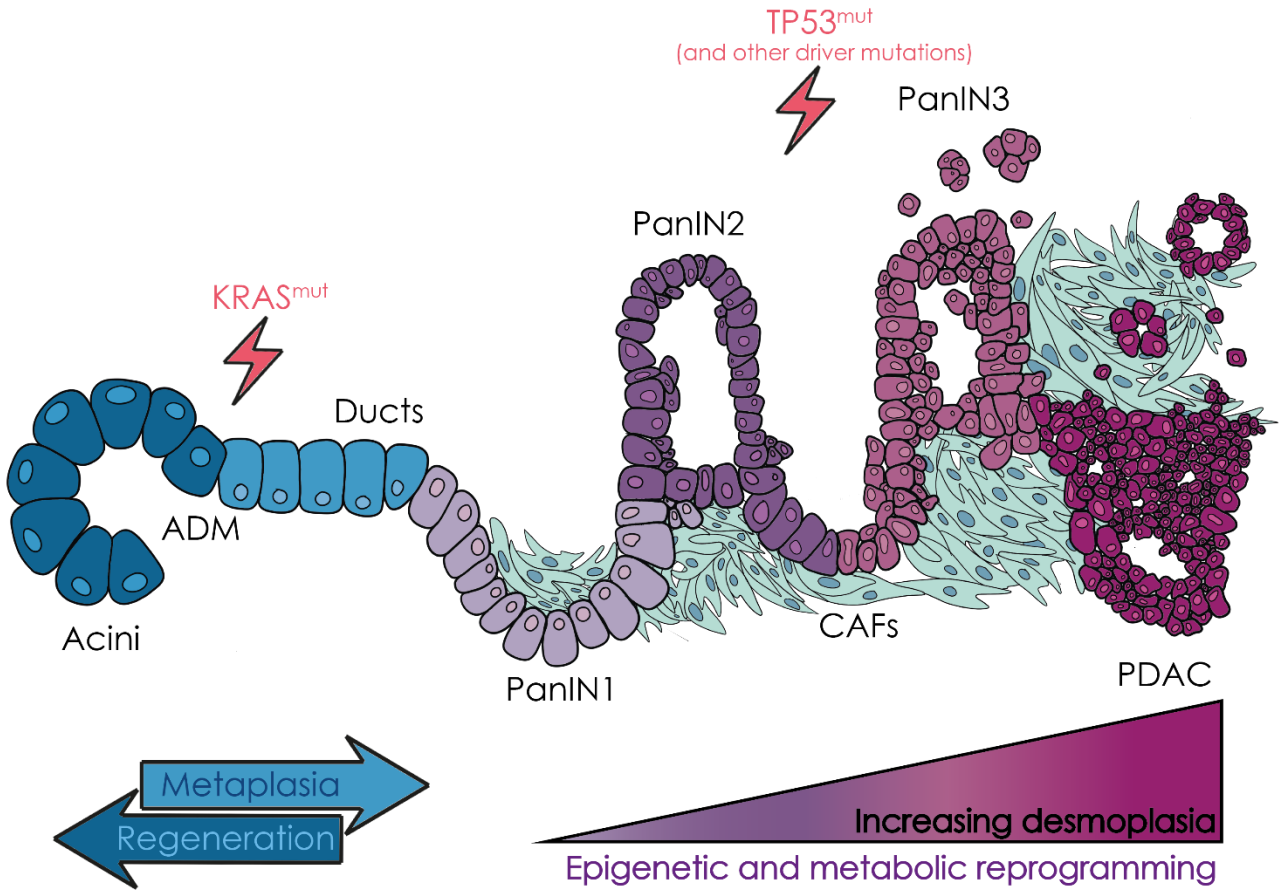

Fig. 4 Schematic representation of pancreatic ductal adenocarcinoma multi-step progression and its hallmarks. These include KRAS mutations and TP53 loss as well as the excessive desmoplastic reaction and the extensive reprogramming of both metabolism and epigenetics. ADM, acinar to ductal metaplasia; PanIN1-3, pancreatic intraepithelial neoplasia 1-3; CAFs, cancer associated fibroblast; PDAC, pancreatic ductal adenocarcinoma.

Carcinogenesis of PDAC is characterized by a well-defined multi-step progression, where tumor formation is preceded by the appearance of non-invasive (intra-epithelial) preneoplastic lesions (Fig. 4). Most common precursors are pancreatic intraepithelial neoplasia (PanIN; 85-95% of non-cancerous lesions in humans), followed by macroscopic cystic structures called intraductal papillary mucinous neoplasms (IPMN, 10-15%) [170]. Non-invasive PanIN lesions are commonly classified into three histological grades according to the extent of cytological and architectural atypia. PanIN1A (flat) and PanIN1B (papillary) show low grade dysplasia and minimal cytological and architectural atypia. PanIN2 exhibit minor loss of polarity, nuclear crowding and enlargement, pseudo-stratification and hyperchromasia with frequent papillary formation. While PanIN1 and PanIN2 are considered low-grade lesions that are not predictive for PDAC formation, PanIN3 are high-grade advanced lesions with severe nuclear atypia, luminal necrosis, and epithelial cell budding into the ductal lumen (Fig. 4) [171]. Although these lesions are characterized by a distinctive ductal-like morphology, recent lineage-tracing experiments combined with genomic analyses of human

specimens demonstrated that cancerous foci predominantly originate from acinar cells which can undergo acinar-to-ductal metaplasia (ADM) in response to environmental or oncogenic stimuli [172–174]. During this metaplastic event, acinar cells transdifferentiate into ductal-like cells, capable of giving rise to PanIN (Fig. 4). This tumor-initiating event is normally a physiologic, reversible process that supports tissue repair and pancreatic regeneration after injury. However, oncogenic inputs make ADM irreversible and resulting metaplastic cells engage in a multi-step progression with the formation of low- and high-grade lesions and eventually of carcinomas (Fig. 4) [172]. Among oncogenic stimuli, mutations in KRAS are believed to be the most common initiating event.

KRAS is a small GTPase, whose activity affects several pathways that control proliferation, differentiation, migration, and survival, such as the RAF-MEK-ERK and the PI3K-AKT-mTOR pathways. Inactive KRAS is bound to GDP; in response to multiple stimuli, including growth factors, GDP is replaced with GTP by GEFs, with a consequent conformational change in the G domain of the protein and its functional activation [175,176].

Oncogenic KRAS mutations typically results in a single amino acid substitution in codons G12 (91%), G13 (2%) or Q61(17%), with $KRAS^{G12D}$ being the more frequent and the one with the worst prognosis [176–179]. G12 and G13 mutations introduce a steric hindrance that inhibits the interaction between KRAS and GAPs; while Q61 mutations disrupt the coordination of a water molecule required for GTP hydrolysis [180]. In general, these mutations impair KRAS ability to hydrolyze GTP, locking KRAS in its GTP-bound active state.

One of the most characterized KRAS effectors is the MAPK pathway, a major driver of cell proliferation, inflammatory signaling, differentiation, and cell survival. KRAS can also activate the PI3K/AKT axis by associating with the p110 subunit of the PI3K complex, that suppresses apoptosis by promoting MDM2-dependent p53 proteolysis. Moreover, in the murine pancreas, KRAS mutation suppresses the expression of acinar genes, such as Mist1 and Cpa1, and promotes the induction of ductal genes, including Krt19 and Muc1. However, hyperactive KRAS *per se* is not able to promote the formation of carcinoma *in situ* (PanIN3) and PDAC; indeed, precancerous lesions progress to frank carcinoma only after the acquisition of additional mutations [172,181].

Other than KRAS mutations, PanIN1 are also characterized by telomere shortening, that predisposes cells to chromosomal instability. Moreover, PanIN2 are associated with the inactivation of CDKN2A (30% of PDAC patients). CDKN2A encodes for the p16 protein, a cyclin-dependent kinase inhibitor that regulates the entry into the S-phase of the cell cycle. CDKN2A loss is crucial for pancreatic carcinogenesis, as p16 is able to induce senescence in combination with oncogenic KRAS expression [177,180,182]. Finally, later stages of carcinogenesis (i.e., PanIN3 and PDAC) display mutations in TP53 (72% of PDAC patients) as well as inactivation of SMAD4 (30% of PDAC patients) [177]. Unlike

KRAS mutations and CDKN2A loss, TP53 and SMAD4 inactivation are relatively late events, normally in settings of high-grade lesions or cancer. SMAD4 is a mediator of the canonical TGFβ signaling and its loss leads to increased migratory behavior, immune evasion, and autocrine activation. SMAD4 loss has a deleterious effect on patients' prognosis and it is associated with increased metastatization [179,183,184]. Lastly, TP53 is the most commonly mutated tumor suppressor gene in PDAC, and it has a multitude of tumor-promoting effects, including increased genome instability, reprogrammed cellular metabolism and enhanced metastatic propensity. The majority of TP53 alterations in PDAC are gain-of-function missense mutation with effects on cell cycle activation, inhibition of apoptosis and metabolic changes in association with an increased genome instability to allow the survival of tumor cells [179,185]. Other than these four major driver mutations, PDAC is characterized by a large compendium of less frequently altered genes, involved in DNA maintenance and damage response, epigenetic regulation, and axon guidance [151,177].

In recent years, considerable effort has been invested to define transcriptional subtypes of human PDAC. Initial efforts utilized microarray analyses of gene expression profiles from microdissected pancreatic cancer to define three PDAC subtypes: "classical", "quasi-mesenchimal", and "exocrine-like", each exhibiting distinct prognoses and responses to therapies[186]. Subsequently, the employment of a "virtual dissection strategy" on bulk RNAseq data identified two tumor subtypes – "classical" and "basal-like" – and two stromal subtypes – "normal stroma" and "activated stroma" [187]. Furthermore, four additional subtypes – "squamous", "pancreatic progenitor", "immunogenic", and "aberrantly differentiated endocrine exocrine" – were characterized through RNA-seq analysis of 96 PDACs with high epithelial cellularity [188]. Despite these efforts, consensus has been reached on two main subtypes: the well-differentiated pancreatic progenitor/classical subtype and a quasi-mesenchymal, basal-like, squamous subtype, the latter characterized by low differentiation and poor prognosis [151,174,177,180]. These classification endeavors were challenged by PDAC's hallmark feature: a densely desmoplastic microenvironment and abundant stroma.

Indeed, histologically PDAC is characterized by a dense stromal compartment that consists of various cellular and acellular components. This desmoplastic reaction, which is characterized by the dramatic increase in the proliferation α-SMA positive fibroblasts and by the increased deposition of extracellular matrix components, starts to evolve early around PanIN lesions and, in frank carcinomas, up to the 90% of the tumor bulk is represented by the stroma [189].

Interestingly, the continuous interplay between malignant cells and their surrounding microenvironment influences the development of PDAC. In fact, the extreme fibrotic reaction leads to altered ECM composition, ultimately promoting the activation of resident fibroblasts and the recruitment of inflammatory cells and pericytes, favoring angiogenesis and tumor progression [190]. In

particular, type I, III and IV collagens are the main structural proteins that compose PDAC ECM. The large amount of ECM components, that also include proteoglycans, hyaluronic acid, and fibronectin, makes PDAC a physically stiff tumor with increased interstitial fluid pressure [191,192].

Moreover, early response to $KRAS^{G12D}$ mutation in mice is associated with the upregulation of Hedgehog signaling, leukocyte infiltration, and accumulation of a collagen rich matrix [193]. However, suppressing expression of mutant KRAS in established tumors leads to rapid remodeling of the stroma, with a reduction in activated fibroblasts and resolution of inflammation [193,194].

Other than the ECM, the TME is also characterized by cellular infiltration. Predominant cell types within the TME are cancer-associated fibroblasts (CAF), various classes of regulatory and cytotoxic immune cells and macrophages, neurons, and endothelial cells. Several studies focused on the active role of CAFs during cancer initiation and progression [190,195]. It has become increasingly evident that pancreatic tumors harbor multiple CAF subtypes forming a highly heterogeneous population with inter- and intra-tumoral variation [196]. Of them, pancreatic stellate cells (PSCs) are a specific fibroblast population located in the peri-acinar space; under physiological condition PSCs are quiescent and responsible for tissue homeostasis. It has been shown that tumor cells can activate PSCs and that PSCs, in their activated myofibroblast-like state, can promote tumor cell proliferation, migration and invasiveness [197,198].

Additionally, oncogenic KRAS drives pro-inflammatory signaling in precancerous neoplasia through multiple mechanisms, including the activation of STAT3 and NF-κB or the up-regulation of chemoattractants for inflammatory macrophages [199–203]. In turn, inflammatory macrophages secrete soluble mediators, such as TNF and CCL5, and inhibitors of metalloproteases that promote tumor-initiating ADM and preneoplastic lesions formation [204]. Moreover, PanIN lesions actively reshape the microenvironment by driving the switch of macrophages towards the activated M2 phenotype [203]. Lastly, in PDAC, TAMs regulate immunosuppression, fibrogenesis, and angiogenesis and promote EMT, invasiveness, and metastasis [174]. Notably, PDAC is traditionally considered a non-immunogenic *cold* tumor, which employs multiple mechanisms to evade immune checkpoints. These include the recruitment of regulatory immune cells, the secretion of immunosuppressive chemokines, and the expression of checkpoint inhibitor surface proteins [205].

Summarizing, PDAC is characterized by a dense fibrotic stromal compartment, characterized by heterogeneous cellular composition, which is dictated by tumor cells in order to promote their proliferation, immune evasion and aggressiveness.

Metabolic and epigenetic reprogramming in PDAC

Metabolic reprogramming is a classic hallmark of cancer largely because uncontrolled proliferation demands adjustments of anabolism/catabolism to support accelerated biomass growth and mitigate redox stress [5]. An intriguing line of thinking hypothesizes that severe nutrient and oxygen shortage could function as selective pressures favoring survival of aggressive tumor cells able to withstand the harsh environmental conditions [206]. As discussed above, PDAC is characterized by several distinctive histological features. These include a brisk cellular infiltration that co-evolves with tumor mass and an excessive desmoplastic reaction that hampers the delivery of oxygen and nutrients. However, PDAC cells survive and thrive in these harsh environmental conditions thanks to an extensive but well-orchestrated reprogramming of their metabolism [207].

Two key aspects dominate PDAC metabolic rewiring: changes in carbon flux directly mediated by oncogenic KRAS and adaptations to enhance nutrient uptake and/or scavenging pathways [206].

Oncogenic KRAS upregulates central carbon metabolism, promoting glycolysis but also diverting glycolytic intermediates into anabolic pathways crucial for cancer cells proliferation. These include the hexosamine biosynthesis pathway, which generates UDP-GlcNAc for protein and lipid glycosylation, and the non-oxidative arm of the pentose phosphate pathway, which generates NADPH and ribose-5-phosphate crucial for nucleotide biosynthesis. Notably, knockdown of key KRAS-regulated enzymes in the non-oxidative PPP or the HBP slows the growth of murine PDAC cell lines *in vitro* and suppresses tumorigenicity in ectopic models of pancreatic cancer [206,208]. Compelling studies demonstrated that KRAS-driven metabolic reprogramming is orchestrated by the RAF-MEK-ERK pathway that leads to transcriptional and (post-)translational upregulation of master regulators of cellular anabolism [7,171,209]. The list of mutant KRAS-regulated metabolic processes is ever growing and data clearly demonstrate that oncogenes actively reprogram cellular metabolism to support growth of biomass, which is required for accelerated proliferation, but also to support signaling events and promote functional plasticity of tumor cells [7,206,207,209,210]. For example, oncogenic KRAS promotes protein acetylation in pancreatic epithelial cells through the elevation of acetyl-CoA cytoplasmic levels [159,211].

On the other hand, the uptake of canonical and non-canonical carbon sources is extremely flexible in PDAC to allow cancer and tumor-associated cells to cope with limited nutrient availability. For example, significant intratumoral heterogeneity in glucose utilization exists in PDAC and is largely dictated by nutrient availability and oxygen concentration. As a matter of fact, hypoxic cancer cells preferentially metabolize glucose anaerobically and upregulate MCT4 to export lactate, which is taken up through MCT1 by normoxic cancer cells, that can use lactate as a carbon source for mitochondrial OXPHOS [206,208,212–214].

Other than glucose, PDAC cells rely on glutamine utilization for their survival. Glutamine is a nonessential amino acid that functions as a precursor for other amino acids as well as nucleotides and hexosamines. Additionally, glutamine is a carbon skeleton donor for the replenishment of TCA cycle intermediates. GLS is the first enzyme of glutaminolysis, in which glutamine is converted in glutamate in mitochondria, and then in α-KG, by GLUD1. Notably, most cancer cells are addicted to glutamine in culture [206]. Glutamine has been shown to be required for pancreatic tumorigenesis both *in vivo* and *in vitro*. In PDAC, knockdown of GLS impairs tumor growth and glutamate supplementation is able to rescue the growth of pancreatic cancer cells under glutamine-free culture conditions [133,215]. Interestingly, PDAC cells rely on glutaminolysis also to maintain redox homeostasis. In fact, mitochondrial glutamate can be used to produce aspartate in a reaction catalyzed by GOT2. The latter can then be exported to the cytoplasm and metabolized into pyruvate by a sequence of reactions involving GOT, MDH1, and ME1. This non-canonical pathway is able to increase the reducing power in the form of NADPH and glutathione, both important for redox balance [7,216]. Other than through glutamine metabolism, oncogenic KRAS signaling controls redox homeostasis through the induction of NRF2, a crucial TF for antioxidant genes. Notably, NRF2 also modulates several genes involved in glutamine metabolism, such as the malic enzyme 1 [217,218].

Aside from glutamine, PDAC metabolism is highly dependent on serine levels. Indeed, PDAC tissues are particularly low in serine, but oncogenic KRAS induces genes involved in serine biosynthesis making cancer cells autotrophs and critically dependent on *de novo* serine generation for survival [219]. Mechanistically, serine can be generated from the glycolysis intermediate 3-phosphoglycerate and is the precursor of glycine and cysteine. Both these non-essential amino acids are components of glutathione, critical for the regulation of cellular ROS levels. Oncogenic KRAS has been shown to cooperate with LKB1 loss to induce the serine-glycine-one-carbon pathway to fuel tumor growth. As a matter of fact, human PDAC cells with LKB1 mutations are more sensitive to the inhibition of the serine biosynthesis [220].

Additionally, PDAC cells relies on the use of lysosomal nutrient scavenging pathways such as autophagy and macropinocytosis. Autophagy is a highly conserved cellular catabolic process that mediates the degradation of macromolecules and whole organelles, through their digestion in lysosomes. Products of the autophagic degradation are then recycled back to fuel biosynthetic and bioenergetic processes [7,221]. While in other cancer types autophagy seems to be triggered in response to various stressors, including DNA damage and ROS, basal autophagy levels are unusually high in PDAC. Cancer cells upregulate transcriptional programs that orchestrate lysosomal biogenesis and autophagy induction through the function of the MiT-TFE family of TFs, despite sustained anabolic metabolism and almost universal activation of mTORC1 pathway. In human PDAC, MiT-TFE

transcription factors are constitutively active in the nucleus and inhibition of MiT-TFE impairs tumor growth [222]. Notably, targeting autophagy, either by RNA interference or using chloroquine, decreases PDAC cell proliferation and tumor growth *in vivo* [223,224].

Macropinocytosis is a non-selective endocytic program by which cells uptake content from the extracellular fluid through large vesicles. KRAS activation induces macropinocytosis, through which PDAC cells uptake extracellular albumin that is degraded and amino acids ultimately fuel the central carbon metabolism [225]. Accordingly, the inhibition of macropinocytosis in a xenograft model of PDAC significantly impairs tumor growth [225]. Despite the limited abundance of lipid species in the PDAC TME, the scavenging of extracellular fatty acids is also upregulated. Scavenged lipids are hydrolyzed to produce fatty acids and glycerol; the former fuel the TCA cycle, while glycerol can be converted into dihydroxyacetone and enter the glycolytic pathway [226]. In this context, LDLR that facilitates cholesterol uptake, is associated with an increased risk of PDAC recurrence and its inhibition sensitizes PDACs to chemotherapy [227].

Cancer cells derived from the same tumor can display markedly diverse metabolic profiles. As a matter of fact, pancreatic cancer cells that survive to oncogene extinction in a KRAS-driven mouse model show stem-like features and rely on OXPHOS rather than on glycolysis for their survival [130]. This different metabolic profile was also confirmed in a human PDAC PDX model [228]. Additionally, genomic and transcriptomic analysis coupled with clinical data, shows the existence of different metabolic subgroups of PDAC cells – "quiescent", "glycolytic", "cholesterogenic", and "mixed" – that could predict different prognoses and responses to therapy [229]. Compared to the previously mentioned molecular subtypes of PDAC, the glycolytic subgroup is associated with the quasi-mesenchymal, basal-like, squamous subtype. This indicates that unique metabolic pathways may play a role in the prognostic impacts of established PDAC subtypes, suggesting potential opportunities to address diverse metabolic vulnerabilities across these subtypes.[186–188,229].

The contribution of metabolic rewiring to PDAC progression is multifaceted. While cancer cells need to adapt their metabolism to satisfy specific energetic and anabolic demands, they exploit changes in metabolite levels to support signaling and functional plasticity, which are critical for tumor evolution. Several studies have shown that metabolic alterations can promote pancreatic tumorigenesis and metastasis through epigenetic regulation [230]. Indeed, several metabolic intermediates act as cofactors for chromatin modifying enzymes and their levels critically dictate epigenetic marks, chromatin organization and, in turn, gene expression. Epigenetic marks are post-translational modification of DNA or histones that regulate higher order chromatin organization to control DNA accessibility and transcription factor positioning, affecting cell transcriptome. Ultimately, the epigenetic organization is able to impose cell identity [51,230].

For example, during ADM and PanIN formation both nucleo-cytosolic levels of acetyl-CoA and histone acetylation are increased. Notably, genetic ablation of ACLY, the main generator of acetyl-CoA in the cytosol, is able to significantly decrease tumor formation in a KRAS-driven mouse model of spontaneous carcinogenesis [129]. Additionally, a retrospective clinicopathologic analysis of 119 patients showed a positive relationship between tumor differentiation and acetylation in H4K12 and a worse prognosis for patients with high levels of H3K18 and H4K12 acetylation [231].

The impact of histone methylation on gene expression is more complex and vary according to lysine position. For example, H3K4me3 is generally associated with enhanced gene transcription and its loss enhances ADM; on the other hand, H3K27me3 suppresses gene transcription and its gain favors ADM and PDAC progression [232]. Additionally, aberrant DNA methylation of functional relevant genes is a hallmark of PDAC and DNA methyltransferases, that mediate this process, are frequently upregulated [233,234]. Histone methylation in PDAC is critically influenced by metabolic reprogramming. Indeed p53 loss decreases both S-adenosylmethionine (SAM) and α-ketoglutarate (α-KG) levels, two methylation-altering metabolites. Reduced SAM levels causes hypomethylation of H3K9 that results in loss of heterochromatin stability and satellite RNAs correct transcription. Notably, supplementation of SAM restores genomic integrity in p53 deficient cells [235]. Decrease α-KG instead determines lower DNA methylation, while its accumulation increases 5-hydroxymethylcytosine (5-hmC) and restricts cancer cell plasticity [236].

Other than the frequent mutations in the main four driver oncogenes of PDAC, discussed above, there is a range of less frequent genetic mutations, comprising mutations in genes related to DNA repair pathways as well as in epigenetic regulators, such as DNMT3A, TET2 and ASXL1 [177]. Notably, somatic mutations in SWI/SNF complex regulators and inactivation of histone modifying enzymes frequently occurs in conjunction with oncogenic KRAS, suggesting that alterations in the epigenome are important for driving PDAC progression [237,238]. The SWI/SNF complex is a multisubunit complex mediating ATP-dependent chromatin remodeling involved in transcriptional regulation and DNA repair [171].

In conclusion, both mutations in genes that regulate chromatin organization and alteration in the epigenome can affect tumorigenesis. In this context, nutrient availability and the rewiring of metabolism can reshape the epigenome dynamically during PDAC progression.

Understanding the metabolism-epigenetic cross-talk in pancreatic cancer and how this axis can be influenced by nutrient availability and the TME may help to identify targetable vulnerabilities.

AIM

Mitochondria are crucial organelles in cell physiology and pathology. Master regulators of cellular bioenergetic homeostasis, mitochondria are also central players in signal transduction and impact cell fate. In this context, mitochondrial circuits can adapt to favor several aspects of carcinogenesis and cancer progression. Compelling evidence demonstrates that mitochondria remodeling favors cancer cell survival and aggressiveness. Notwithstanding, our knowledge on how oncogene-driven pathways affect mitochondrial function and morphology and on how alterations in mitochondrial biology impact tumor progression is still limited. In particular, few studies dissect these aspects in PDAC, one of the deadliest cancers worldwide. Aim of this project is to dissect the rewiring of mitochondrial metabolism during the progression of PDAC, to identify possible targetable mechanisms at the basis of the aggressiveness of this tumor.

RESULTS

PDAC PROGRESSION IMPACTS THE MITOCHONDRIAL PROTEOME AND FOSTERS MITOCHONDRIAL RESPIRATION

Mounting evidence points out that mitochondria-associated pathways are crucial for tumor initiation and progression[4]. Nevertheless, our knowledge on how mitochondrial function changes during PDAC progression and how alterations in mitochondrial biology can affect this multi-step process is still incomplete.

To address this issue, I investigated alterations in the mitochondrial proteome across various stages of disease advancement. Human ductal cells expressing an oncogenic KRAS isoform (HPDE-KRAS^{G12D}) served as a model for pre-neoplastic cells ("early carcinogenesis", epithelial cells after the metaplasia (Fig. 4)). On the other hand, two distinct pancreatic cancer cell lines (PANC1 and MiaPaCa2) were employed to recapitulate the aggressive stages of PDAC progression ("late carcinogenesis"). Notably, these cell lines belong to the "quasi-mesenchymal" subtype of PDAC, which in patients is associated with a poor prognosis [186]. All the considered cell lines were stably transfected with constructs that allow the HA-tagging of mitochondrial for their efficient isolation [239]. Subsequently, we analyzed the proteome of immunoprecipitated mitochondria to seek stage-associated protein alterations. The proteomic datasets were manually filtered to exclude non-mitochondrial proteins, employing Uniprot subcellular localization, Mitocarta 3.0, and TargetP 2.0, which predict the presence of a canonical MTS (Fig. 5A). After this filtration step, I focused on protein that were significantly deregulated in both PDAC cell lines compared to non-transformed ductal cells. Of note, HPDE-KRAS^{G12D} expresses oncogenic KRAS; hence, dysregulated proteins are likely not altered at tumor initiation, but possibly in some stage during PDAC carcinogenesis. We found 80 proteins significantly downregulated in both PANC1 and MiaPaCa2, while 85 proteins were significantly upregulated. Gene ontology analyses of these commonly upregulated and downregulated proteins are respectively shown in Fig. 5B and 5C.

Among the downregulated pathways, the more significant resulted the ones involved in fatty acyl-CoA biosynthesis, arginine and lysine degradation, and apoptosis (Fig.5C).

On the other hand, significantly upregulated pathways include TCA cycle and ETC, protein import into mitochondria and fatty acid oxidation (Fig. 5B). Protein association map of consistently upregulated pathway also includes proteins involved in mitochondrial translation (Fig. 5D). It is also clear that the majority of proteins upregulated in both pancreatic cancer cell lines are either components or assembly factors of the ETC complexes and subunits of the ATP synthase. This underscores the critical role of OXPHOS pathway in "late carcinogenesis" cells.

In order to functionally validate the increase in mitochondrial respiration in PDAC cells, I performed 10 hours-long respirometry analysis in basal conditions in PANC1 and HPDE-KRAS^{G12D} cells (Fig. 5E). PANC1 cells have a significantly higher oxygen consumption rate than HPDE-KRAS^{G12D}, confirming the results of the mitochondrial proteomic analysis (Fig. 5B and Fig. 5D).

The increase in protein composing the ETC and the ATP synthase, as well as the increase in mitochondrial respiration, could be linked to a reshape in mitochondrial ultrastructure, and in particular in the number and tightness of mitochondrial cristae [13]. To evaluate if PDAC progression affects mitochondrial ultrastructure we firstly superimposed a curated list of proteins involved in mitochondrial morphology and protein import derived from MitoCarta 3.0 on the mitochondrial proteomic analysis.

Protein involved in the apoptotic pathway are downregulated in both PANC1 and MiaPaCa2 cells (Fig. 5F-G). In both cell lines, volcano plots show a clear upregulation of the components of the TIMM complex, that mediates the import and translocation of protein in the IMM. Additionally, some regulators of cristae morphology such as AIFM1 in PANC1 cells and OPA1 and IMMT (part of the MICOS complex) in MiaPaCa2 cells, are overexpressed in cancer cells (Fig. 5F-G).

In conclusion, “late carcinogenesis” PDAC cell lines show a rewired proteome compared to “early carcinogenesis” HPDE-KRAS^{G12D} cells, with a significant upregulation of protein of OXPHOS proteins and a consequent increase in oxygen consumption rate. In line with the functional relationship between mitochondrial respiration and the morphology of cristae, proteins involved in the regulation of mitochondrial ultrastructure are overexpressed in PDAC cell lines.

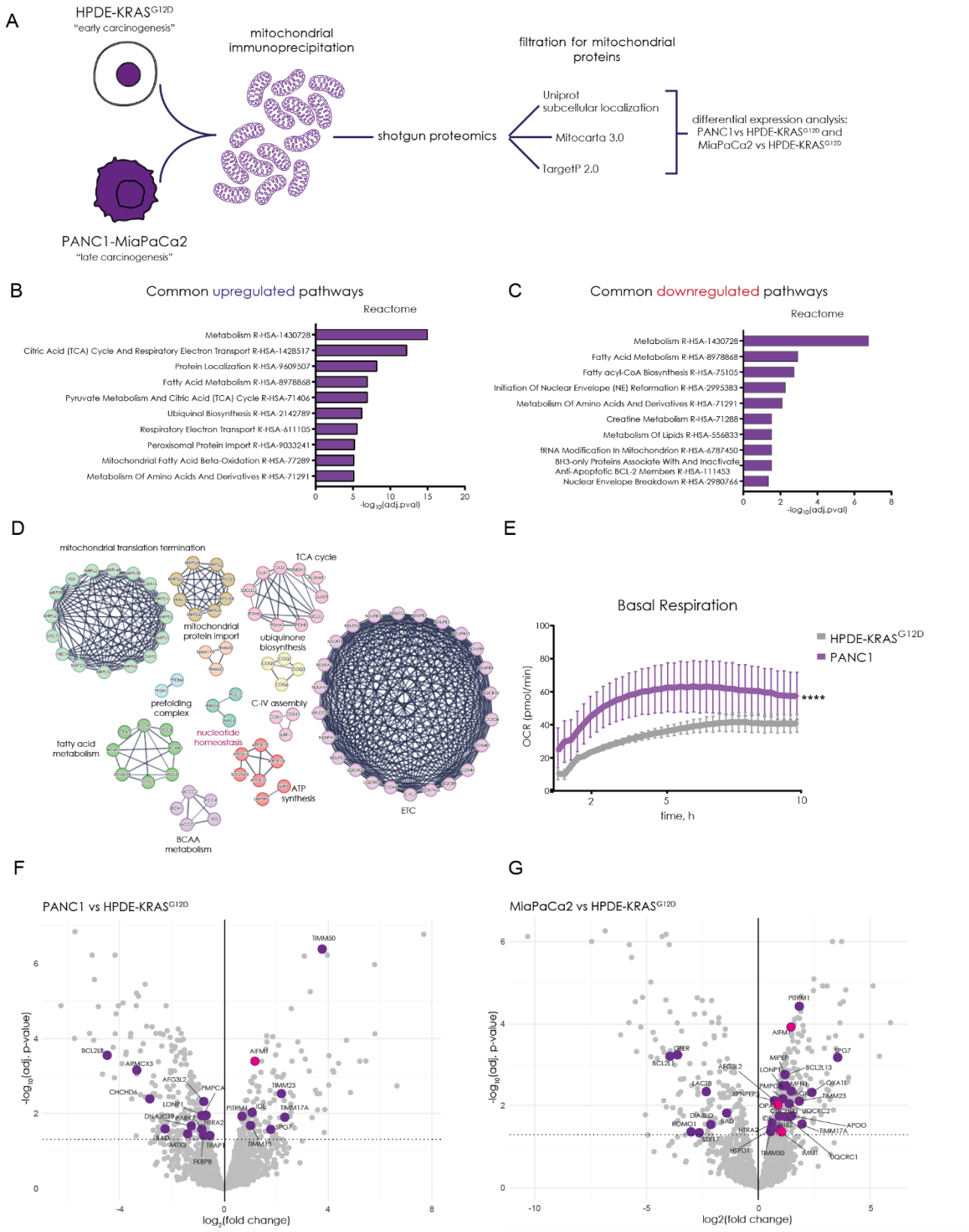

Fig. 5. Mitochondrial proteome is reshaped during PDAC progression. A) Experimental workflow of the mitochondrial proteomic analysis. B) Reactome GO analysis of commonly upregulated pathways on PDAC cells compared to HPDE-KRAS^{G12D} cells. Purple bars indicate significant pathways. C) Reactome GO analysis of commonly downregulated pathways on PDAC cells compared to HPDE-KRAS^{G12D} cells. Purple bars indicate significant pathways. D) String DB protein association map of commonly upregulated proteins in PDAC cells compared to HPDE-KRAS cells. E) 10 hours long respirometry performed using Resipher in basal conditions in PANC1 and HPDE-KRAS^{G12D}. Two way Anova. F) Volcano plot of the mitochondrial proteomic analysis on PANC1vsHPDE-KRAS^{G12D} cells. Purple dots indicate proteins involved in mitochondrial morphology and mitochondrial protein localization; pink dots indicate protein involved in cristae morphology. G) Volcano plot of the mitochondrial proteomic analysis on MiaPaCa2vsHPDE-KRAS^{G12D} cells. Purple dots indicate proteins involved in mitochondrial morphology and mitochondrial protein localization; pink dots indicate protein involved in cristae morphology.
**** p< 0,00001

MITOCHONDRIAL ULTRASTRUCTURE IS RESHAPED DURING PDAC PROGRESSION *in vitro* AND *in vivo*

Mitochondrial respiration and mitochondrial ultrastructure are deeply intertwined. Several studies have described that alterations in the number and morphology of mitochondrial cristae can impact the assembly of the complexes of the ETC and can regulate the efficiency of the electron transport [13,17]. Nonetheless, the status of mitochondrial ultrastructure across PDAC stages and is impact on progression are still unknown.

To this aim, I performed a morphometric analysis on transmission electron microscopy (TEM) images of mitochondria from HPDE-KRAS^{G12D}, PANC1 and MiaPaCa2 cells. I found that mitochondrial ultrastructure is markedly reshaped in pancreatic ductal adenocarcinoma cells compared to non-transformed cells (Fig. 6A-B). I focused on cristae density and cristae width, which have both been associated with mitochondrial respiration [17]. I observed an increase of cristae density, denoted by the number of mitochondrial cristae normalized on the area of the mitochondrion, in both PDAC cell lines although statistically significant only in MiaPaCa2 cells (Fig. 6B). Additionally, both PANC1 and MiaPaCa2 display a significant decrease in cristae width (Fig. 6C). These results suggest that mitochondrial cristae tighten as tumor cells evolve.

To confirm these findings *in vivo*, I evaluated the mitochondrial ultrastructural parameters in the pancreas of mice expressing mutant KRAS in the pancreatic epithelium (*Pdx1-Cre;LSL-Kras^{G12D}*, "KC" hereafter). KC mice spontaneously develop preneoplastic lesions, mostly PanIN which are also found in humans. These can be considered as an intermediate step in PDAC progression. As shown in the representative images in Fig. 6D and in the quantifications in Fig. 6E and Fig. 6F, mitochondria in KC pancreata display significantly higher cristae density and decreased cristae width compared to wildtype mice. These modifications in mitochondrial ultrastructure are not associated with modifications in mitochondrial content, as evident from the quantification of mtDNA levels (Fig. 6G).

Using the same mouse model, I also evaluate the morphology of mitochondrial network. To this end, I performed an immunofluorescence for TOMM20, localized in the OMM, in WT and KC pancreata (Fig. 6H). Mitochondrial network in KC mice is significantly more fragmented in KC pancreata compared with WT, as shown by the measurement of the fusion index (Fig. 6I). This result is in accordance with the existing literature, showing that DRP1 phosphorylation and mitochondrial fragmentation lie downstream KRAS activation [240].

Summarizing, mitochondrial cristae stability and morphology are reshaped in cancer cell lines and during PDAC progression *in vivo*.

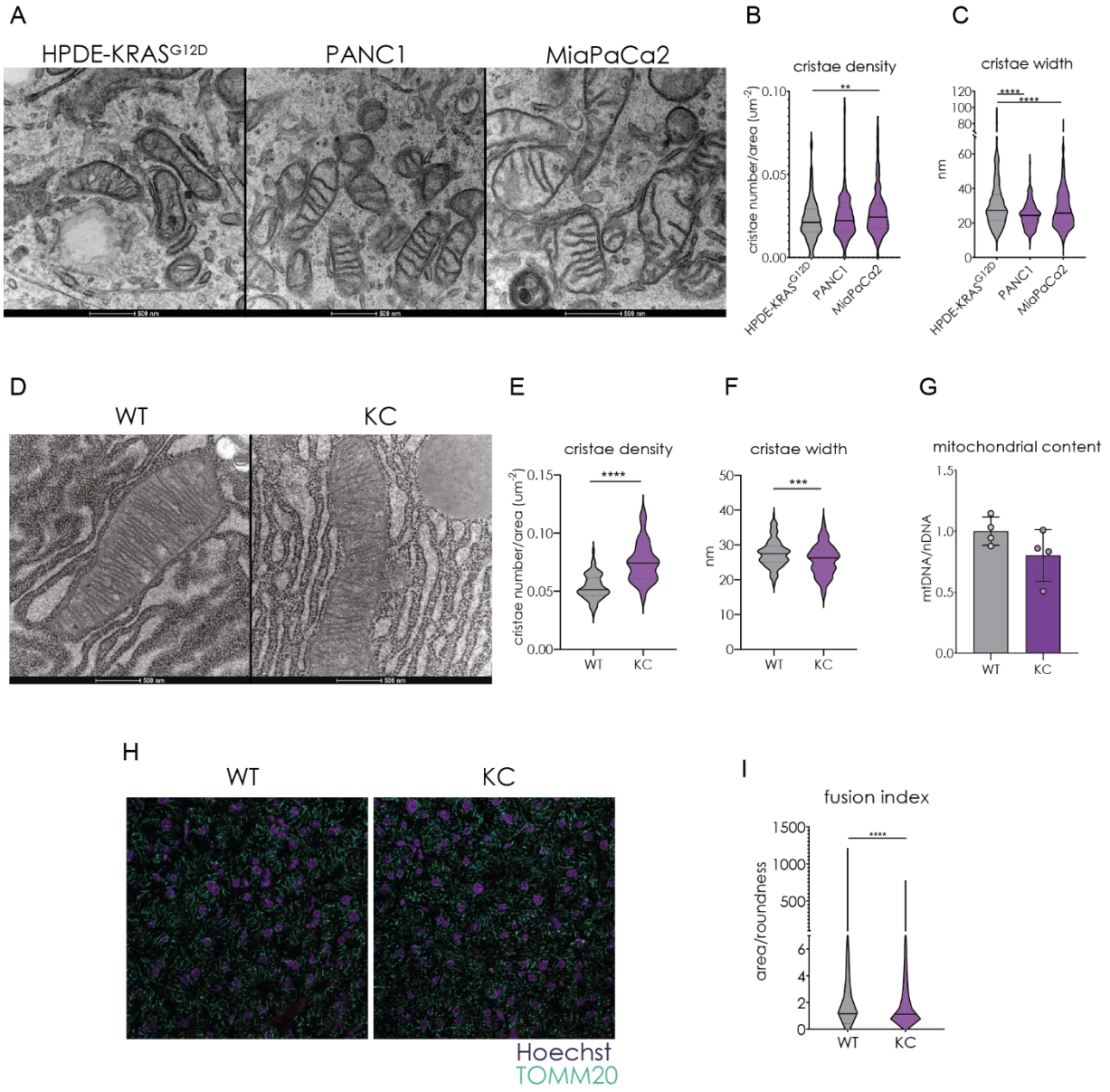

Fig. 6. Pancreatic ductal adenocarcinoma progression reshape mitochondrial morphology *in vitro* and *in vivo*. A) Representative TEM images of mitochondria of HPDE-KRAS^{G12D}, PANC1 and MiaPaCa2 cells showing the alterations in mitochondrial ultrastructure during PDAC progression. B) Quantification of mitochondrial cristae density in HPDE-KRAS^{G12D}, PANC1 and MiaPaCa2 cells. Mann-Whitney t-test. C) Quantification of mitochondrial cristae width in HPDE-KRAS^{G12D}, PANC1 and MiaPaCa2 cells. Mann-Whitney t-test. D) Representative TEM images of mitochondria of pancreatic tissues from WT or KC (Pdx-Cre; KRAS^{G12D}) mice at 8 weeks of age. E) Quantification of mitochondrial cristae density in pancreatic tissues from WT or KC mice. Mann-Whitney t-test. F) Quantification of mitochondrial cristae width in pancreatic tissues from WT or KC mice. Mann-Whitney t-test. G) Quantification of the ratio between mitochondrial and nuclear DNA on acinar cells isolated from WT and KC mice at 8 weeks of age. Nuclear DNA was detected with primers for β2microglobulin and mtDNA with primer for mt-CytB. H) Representative images of immunofluorescence of TOMM20 (turquoise) and Hoechst (purple) in pancreatic tissues from WT and KC mice at 8 weeks of age. I) Quantification of the fusion index (area of the mitochondrion/roundness of the mitochondrion) of mitochondrial network in pancreatic tissues from WT and KC mice. Mann-Whitney t-test.
** p< 0.001; *** p<0.0001; **** p< 0,00001

OPA1 AND NME4 ARE OVEREXPRESSED IN PDAC *in vitro* AND *in vivo*

To identify the players that dictate these alterations in the mitochondrial ultrastructure, I evaluated again the results of mitochondrial proteomic, focusing in particular on the protein association map (Fig. 5C). Both pancreatic cancer cell lines overexpress a set of proteins that are involved in the regulation and homeostasis of nucleotides. This cluster include NME4, NME6 and RCC1L. NME4 and NME6 are two nucleotide diphosphate kinases (NDPKs) and RCC1L is a mitochondrial guanidine nucleotide exchange factor (GEF) [241,242]. Notably, converging evidence reveal that these three proteins interact with OPA1 and regulates its activity[38,39,243]. In particular, NME4 resulted to be particularly interesting, as is sufficient to trigger OPA1's GTPase activity and its silencing phenocopies the loss of cristae typical of OPA1 loss in HeLa cells [38,244].

Notably, NME4 protein levels are higher in mitochondria isolated from PANC1 cells compared to the ones isolated from HPDE-KRAS^{G12D} (Fig.7A). These data were confirmed by the evaluation of mRNA levels in the same cellular models (Fig. 7B). These results indicate that NME4 levels increase regardless of oncogenic KRAS expression during pancreatic cancer progression *in vitro*. Additionally, immunohistochemistry analysis on WT and KC mice showed high levels of NME4 staining specifically in PanIN lesions of KC mice, contrary to normal parenchyma of both WT and KC mice, in which NME4 staining was considerably lower (Fig. 7C). We reasoned that NME4 might promote tumor progression and associate with poorer outcomes.

Mining of the TCGA dataset showed that NME4 mRNA levels in tumor samples from human patients are significantly higher compared to the normal tissue (Fig. 7D). Building from these evidences, we evaluated the protein expression of NME4 in a cohort of PDAC patients using a tissue microarray (TMA) approach. Immunohistochemistry analysis revealed that 36 patients on 76 have medium-strong staining for NME4 (Fig. 7E). Notably, the medium-strong NME4 group has a significantly lower cumulative survival, which aligns with our hypothesis that it promotes PDAC aggressiveness (Fig. 7F). In the same cohort, tumor grading significantly correlates with NME4 levels. Specifically, among the 41 tumors classified as high grade, 32 exhibit medium-strong staining for NME4, suggesting a crucial role for NME4 in PDAC progression (Fig. 7G).

NME4 is a poorly annotated and little studied protein. One of its few described role so far is the regulation of OPA1 activity. Building from this notion, I examined the expression of OPA1 in PDAC cell line to understand whether OPA1 might be differentially regulated across tumor stages, similar to NME4. In accordance, OPA1 protein levels are higher in mitochondria isolated from PANC1 than in HPDE-KRAS^{G12D} (Fig. 7A). OPA1 mRNA levels also tend to increase in PANC1 compared to normal ductal cells (Fig. 7H). Furthermore, OPA1 protein levels are elevated in the pancreas from

KC mice respect to WT mice (Fig. 7I). Lastly, in the TCGA dataset, OPA1 mRNA expression is significantly higher in tumor samples compared to normal parenchyma from patients (Fig. 7J). Interestingly, patients displaying high OPA1 mRNA levels have a significantly worst prognosis compared with patients with low mRNA levels, suggesting a role of OPA1 in the aggressiveness of PDAC (Fig. 7K).

These promising results indicate that, during PDAC progression, proteins involved in the regulation of mitochondrial cristae morphology are upregulated both *in vitro* and *in vivo*. We hypothesize that NME4 (alone or in concert with NME6 and RCC1L) might enhance OPA1 activity to reshape mitochondria and promote tumor evolution.

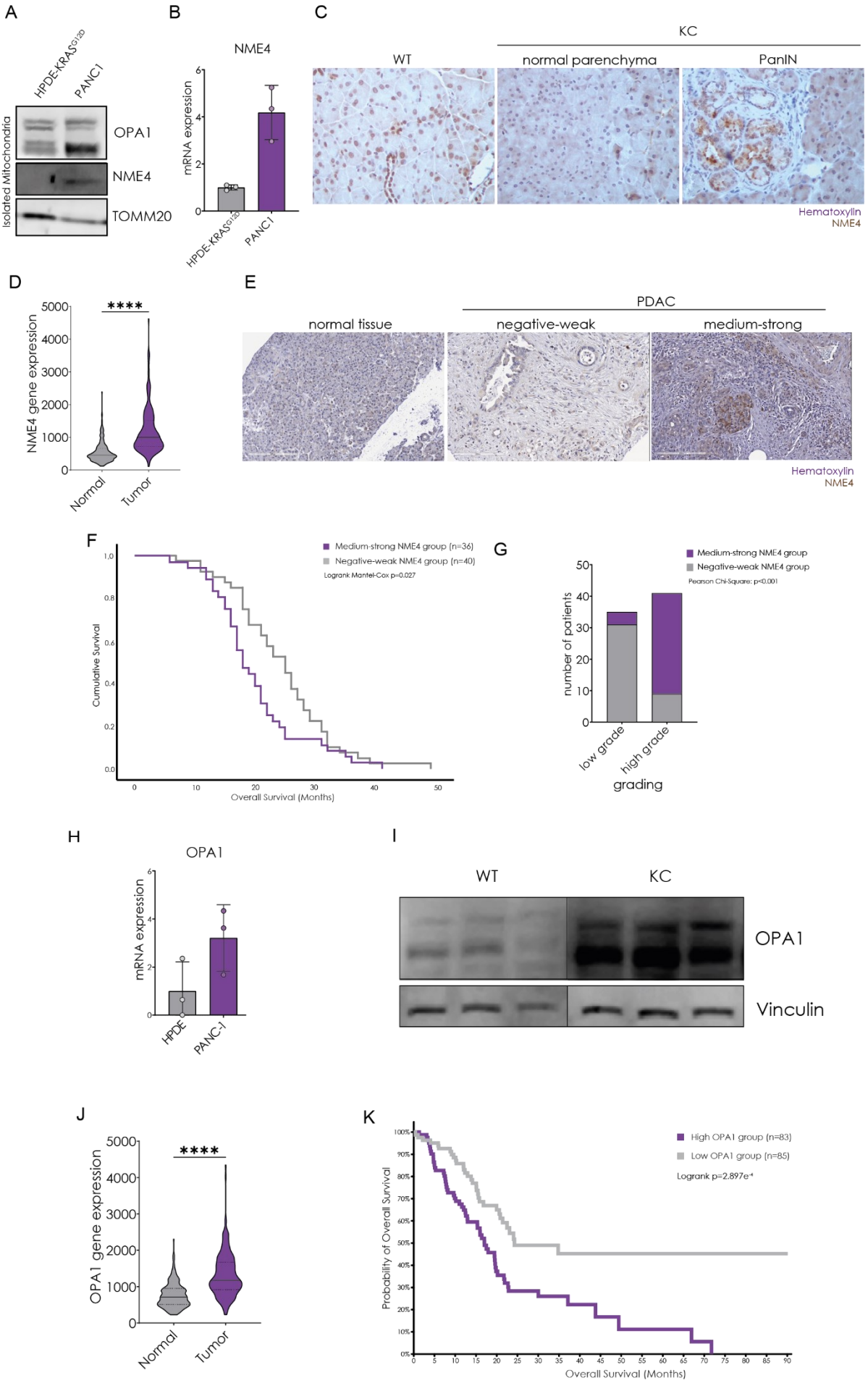
A
HPDE-KRASG12D
PANC1
Isolated Mitochondria
OPA1
NME4
TOMM20
B
NME4
mRNA expression
HPDE-KRASG12D
PANC1
C
KC
WT
normal parenchyma
PanIN
Hematoxylin
NME4
D
****
NME4 gene expression
Normal
Tumor
E
PDAC
normal tissue
negative-weak
medium-strong
Hematoxylin
NME4
F
Medium-strong NME4 group (n=36)
Negative-weak NME4 group (n=40)
Logrank Mantel-Cox p=0.027
Cumulative Survival
Overall Survival (Months)
G
Medium-strong NME4 group
Negative-weak NME4 group
Pearson Chi-Square: p<0.001
number of patients
low grade
high grade
grading
H
OPA1
mRNA expression
HPDE
PANC-1
I
WT
KC
OPA1
Vinculin
J
****
OPA1 gene expression
Normal
Tumor
K
High OPA1 group (n=83)
Low OPA1 group (n=85)
Logrank p=2.897e-4
Probability of Overall Survival
Overall Survival (Months)

Fig. 7 NME4 and OPA1 are overexpressed during PDAC and negative prognostic marker for patients. A) Immunoblot analysis of NME4, OPA1 (all isoforms) and TOMM20 levels in mitochondria isolated from HPDE-KRAS^{G12D} and PANC1 cells. B) qPCR analysis for NME4 mRNA levels in HPDE-KRAS^{G12D} and PANC1. NME4 levels were normalized on actin mRNA levels and data are shown as fold-change over HPDE-KRAS^{G12D}. C) Representative images of immunohistochemistry for NME4 in pancreata section of WT and KC mice at 4 months of age. Nuclei are stained with hematoxylin. D) Data from TCGA dataset of PDAC patients showing NME4 mRNA expression. Mann-Whitney t-test. E) Representative images of immunohistochemistry for NME4 in a tissue array of a cohort of 76 PDAC patients. Nuclei are stained with hematoxylin. F) Cumulative survival of PDAC patients stratified for NME4 levels. Patients with medium-strong staining for NME4 are represented by the purple line, while the ones with negative-weak staining are represented by the grey line. Logrank Mantel-Cox. G) Correlation analysis between tumor grading (low/high) and NME4 staining (negative-weak/medium-strong) in a cohort of 76 PDAC patients. Pearson Chi-Square. H) qPCR analysis for OPA1 mRNA levels in HPDE and PANC1. OPA1 levels were normalized on actin mRNA levels and data are shown as fold-change over HPDE. I) Immunoblot analysis of OPA1 and vinculin levels in total lysates from whole pancreas of 3 WT mice and 3 KC mice at 8 weeks of age. J) Data from TCGA dataset of PDAC patients showing OPA1 mRNA expression. Mann-Whitney t-test. K) Overall survival of PDAC patients from the TCGA dataset stratified for OPA1 mRNA levels. Patients with OPA1 high mRNA levels are represented by the purple line, while the ones with low OPA1 mRNA levels are represented by the grey line. Logrank.
**** $p < 0{,}00001$

NME4 DOWNREGULATION RESHAPES MITOCHONDRIAL MORPHOLOGY AND IMPAIRS MITOCHONDRIAL FUNCTION

NME4 was described to impact mitochondrial morphology through the regulation of OPA1 activity [38,244]. To validate the role of NME4 in the regulation of mitochondrial homeostasis in PDAC cells, I silenced NME4 in both human pancreatic cancer cell lines (PANC1 and KP4). The analysis of mRNA levels shows that the silencing of NME4 in both cell lines was effective, as mRNA levels are significantly decreased in silenced samples (Fig. 8A and Fig. 8E).

NME4 loss in PDAC cells significantly reshapes mitochondrial cristae morphology (Fig. 8B-D). In particular, cristae density is significantly decreased, indicating a lower number of mitochondrial cristae per mitochondrion in siNME4 cells (Fig. 8C). This decrease in cristae number is concurrent with a significant widening of their lumen (Fig. 8D). Both these phenotypes could be an indication of OPA1 loss of activity, as several studies report a consistent reshaping in response to OPA1 knockdown [244,245].

I then evaluated whether in cristae stability and morphology could also affect OXPHOS efficiency. To this aim, I performed a respirometry analysis on PANC1 upon silencing of NME4. NME4 loss is able to decrease oxygen consumption rate (OCR) of PANC1 cells at all levels (Fig. 8F-G). In particular, basal and maximal respiration are dampened by NME4 loss (Fig. 8G). Notably, this decrease in the OCR is not due to a change in mitochondrial content, as shown by the ratio between mtDNA and nuclear DNA, indicating that NME4 loss is able to dampen mitochondrial respiration (Fig. 8H).

Lastly, I also evaluated the contribution of NME4 knockdown to mitochondrial network dynamics, as OPA1 is one of the crucial players in mitochondrial fusion.

Silencing NME4 in KP4 cells is able induce mitochondrial network fragmentation, as evident from both the immunofluorescence for TOMM20 and its quantification (Fig. 8I-J).

These results validate the previously described role of NME4 in the regulation of both mitochondrial morphology and function also in models of PDAC [38,246]. Indeed, it has been already shown that NME4 regenerates mainly GTP in the IMS, for local use by the interacting GTPase OPA1. Additionally, NME4 also channels ADP via ANT into the matrix space for stimulation of respiration and ATP regeneration (Fig. 8K) [246]. I surprisingly found that PDAC cells heavily rely on NME4 activity to sustain elevated mitochondrial function.

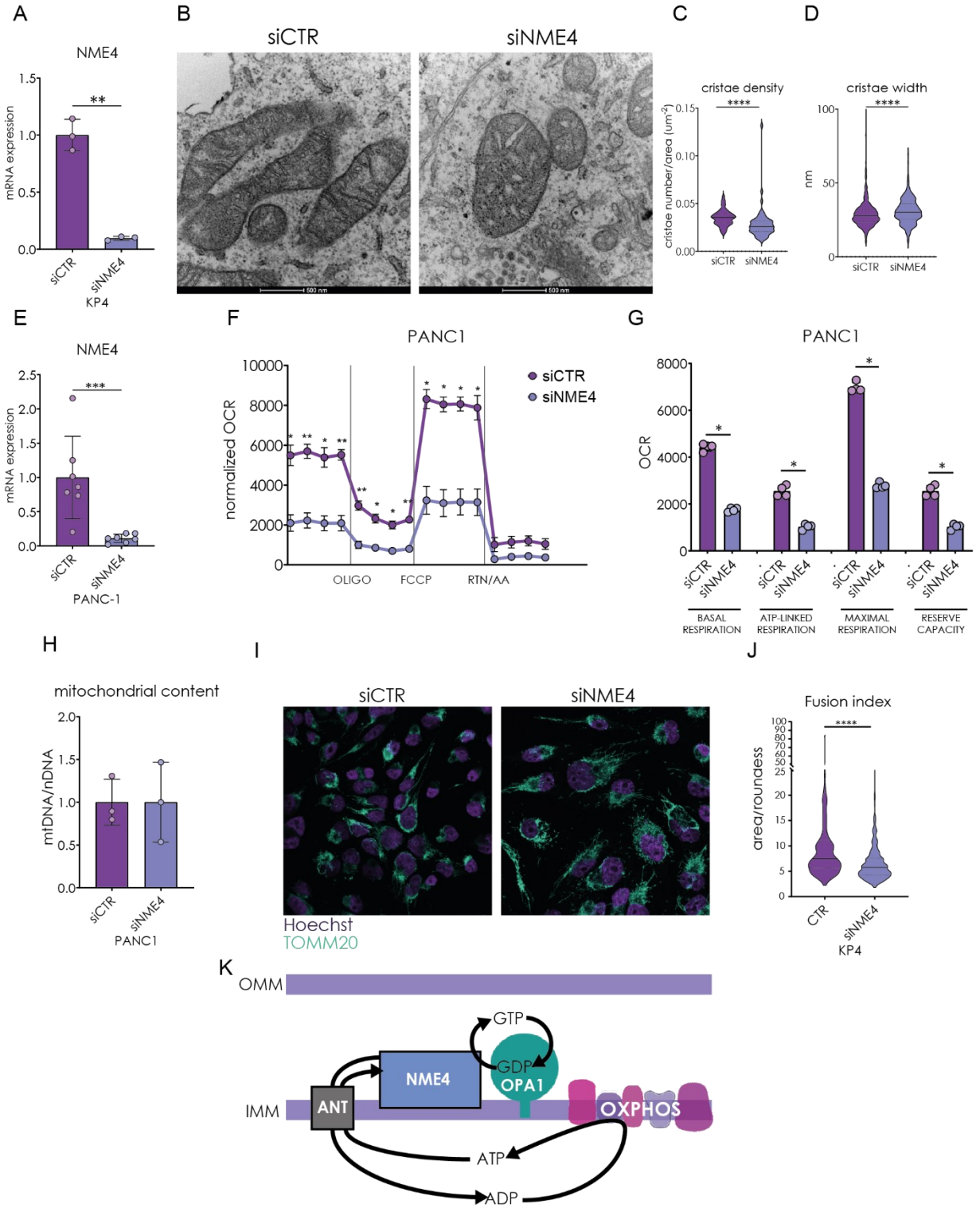

Fig. 8. NME4 downregulation reshape mitochondrial morphology and impairs mitochondrial respiration. A) qPCR analysis for NME4 mRNA levels in KP4 cells silenced for NME4 or for a control. NME4 levels were normalized on 18S mRNA levels and data are shown as fold-change over the control. B) Representative TEM images of mitochondria of KP4 cells silenced for NME4 or for a control showing the alterations in mitochondrial ultrastructure in response to NME4 loss. C) Quantification of mitochondrial cristae density in KP4-siCTR or KP4-siNME4 cells. Mann-Whitney t-test. D) Quantification of mitochondrial cristae width in KP4-siCTR or KP4-siNME4 cells. Mann-Whitney t-test. E) qPCR analysis for NME4 mRNA levels in PANC1 cells silenced for NME4 or for a control. NME4 levels were normalized on 18S mRNA levels and data are shown as fold-change over the control. Mann-Whitney t-test. F) Seahorse respirometric analysis on PANC1-siCTR and PANC1-siNME4 using the Seahorse XF Cell Mito Stress Test Kit. Data were normalized on the absorbance of Bradford reagent for each well. Two-way Anova. G) Basal respiration, ATP-linked respiration, maximal respiration and reserve capacity of the ETC in PANC1-siCTR and PANC1-siNME4. Mann-Whitney t-test. H) Quantification of the ratio between mitochondrial and nuclear DNA in PANC1-siCTR and PANC1-siNME4. Nuclear DNA was detected with primers for β2microglobulin and mtDNA with primers for mt-tRNA-Leu. I) Representative images of immunofluorescence of TOMM20 (turquoise) and Hoechst (purple) in PANC1-siCTR and PANC1-siNME4. J) Quantification of the fusion index (area of the mitochondrion/roundness of the mitochondrion) of mitochondrial network in PANC1-siCTR and PANC1-siNME4. Mann-Whitney t-test. K) Working model of NME4 activity in the regulation of OPA1 and OXPHOS.

* p< 0.05; ** p< 0.001; *** p<0.0001; **** p< 0,00001

OPA1 OVEREXPRESSION REPROGRAMS CELLULAR METABOLISM AND SIGNALS TO THE NUCLEUS IN THE NORMAL PARENCHYMA

Our findings so far suggest OPA1's possible involvement in fostering tumorigenesis. I therefore decided to directly evaluate the contribution of OPA1 to pancreatic carcinogenesis. I leveraged a previously described mouse model that slightly overexpresses OPA1 in the whole body ($OPA1^{TG}$) [37]. $OPA1^{TG}$ mice were generated by targeting a single copy of murine Opa1 isoform 1 driven by human β-actin promoter immediately upstream of the mouse X chromosome Hprt locus [13]. The pancreatic parenchyma of $OPA1^{TG}$ mice does not show major histological differences compared to WT mice (data not shown).

To examine the role of OPA1 in PDAC progression, I evaluated tumor-associated phenotypes caused by OPA1 overexpression in the normal pancreatic epithelium. Notably, OPA1 overexpressing mice display signs of active proliferation in the pancreas, as shown by the significant increase in number of nuclei positive for Ki67, a marker of DNA duplication (Fig. 9A-B). Interestingly, nuclei are also significantly enlarged possibly suggesting the intriguing possibility that cristae remodeling in mitochondria induces reprogramming of chromatin organization in the nucleus (Fig. 9C).

Chromatin architecture is controlled by epigenetic modifications, including post-translational histone modifications [247–249]. It has been shown that mitochondria-derived citrate promotes elevated histone acetylation at pre-neoplastic acinar cells to facilitate PDAC progression[129,211,250]. I therefore interrogated the status of histone acetylation in the pancreatic epithelium of $OPA1^{TG}$ mice. Immunohistochemistry analysis revealed that histone acetylation, in particular tetra-acetylated histone H4 (acetylated on all four lysines of H4 tail), is elevated in the parenchyma of OPA1-overexpressing mice compared to WT mice (Fig. 9D). Incidentally, nuclei appear again significantly enlarged in $OPA1^{TG}$ pancreata (Fig. 9D). These data reveal that the nuclear epigenome is sensitive to mitochondrial remodeling, in a mechanism that is independent from oncogenic KRAS, but that can possibly impact pancreatic carcinogenesis.

I set out to understand the mechanisms responsible for OPA1-associated histone hyperacetylation. I first evaluated the possible contribution of sirtuins, a class of protein deacetylases that use nicotinamide (NAD^+) as co-factor. I measured the levels of NAD^+ in OPA1-overexpressing acinar cells: no change was observed (Fig. 9E), which was surprising considering the positive effect of OPA1 on ETC (that regenerates NAD^+ from NADH) and the global increase in the OCR in OPA1-overexpressing acinar cells (Fig. 9G). Regardless, this rules out the contribution of sirtuin-mediated histone deacetylation. Of note, I observed a significant increase in NADH levels in OPA1-overexpressing acinar cells (Fig. 9F).

Histone acetylation is particularly sensible to fluctuations of nucleo-cytoplasmatic levels of acetyl-CoA, a central metabolite that in the cytosol can be produced from either mitochondrial citrate by ACLY or from acetate by ACCS2 [251]. I speculate that OPA1 might induce changes in acetyl-CoA availability that could ultimately impact the epigenome. To address the mechanism of this OPA1-dependent increase in histone acetylation, I tested whether OPA1 overexpression induced extensive metabolic reprogramming in acinar cells focusing on TCA cycle intermediates. Citrate levels are unimpacted by OPA1 overexpression; on the other hand, levels of downstream TCA metabolites were slightly decreased in OPA1-overexpressing acinar cells (Fig. 9H). This phenotype has been linked to the cataplerotic efflux of citrate from mitochondria and its conversion into acetyl-CoA, which is therefore available for either histone acetylation or *de novo* lipid biosynthesis [252]. To test this hypothesis, we performed a ^{13}C-glucose tracing in acinar cells from WT and OPA1^{TG} mice. Acinar cells were extracted from mice of either genotypes and cultured with isotopically-labeled glucose for 6 hours. At endpoint, metabolites were extracted with a solution of cold trichloro-acetic acid for targeted mass spectrometry quantification of acyl-CoA species. Surprisingly, glucose flux toward acetyl-CoA resulted to be reduced upon OPA1 overexpression (Fig. 9G). This indicates that enhanced glycolytic flux does not contribute to OPA1-elevated histone acetylation. At the same time, these data open an interesting discussion about the mechanisms by which OPA1-promoted reprogramming of mitochondrial function influence nuclear histone acetylation. While this issue remain unclear, hypotheses are debated in the Discussion session. In sum, OPA1 overexpression in normal pancreas favors active DNA duplication, fosters histone acetylation and reprograms cellular metabolism. I asked how the three can possible be linked and whether OPA1 ultimately impacts pancreatic carcinogenesis.

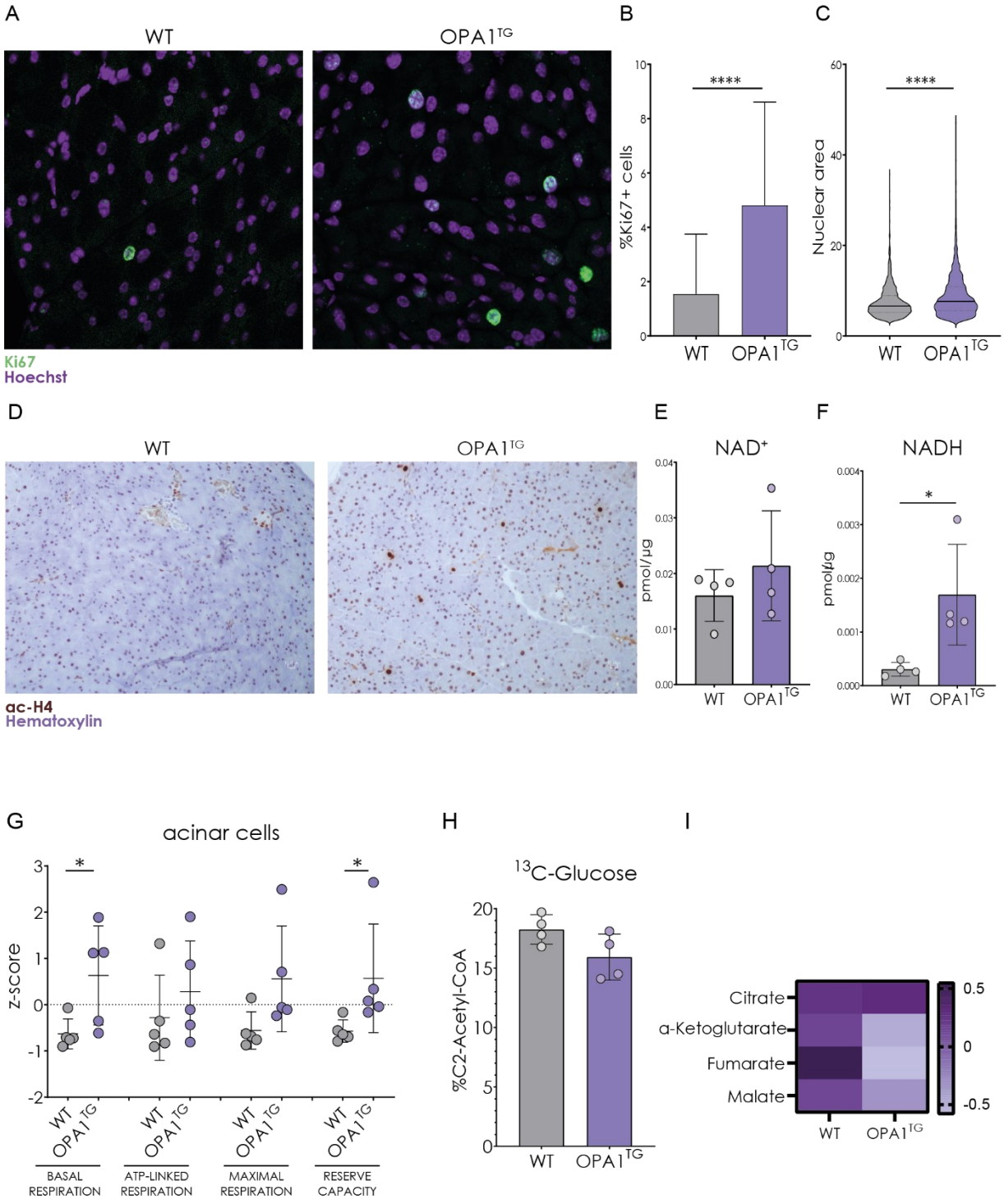

Fig. 9 OPA1 overexpression impact DNA duplication, histone acetylation and cellular metabolism in the pancreas in physiological conditions. A) Representative images of immunofluorescence of Ki67 (green) and Hoechst (purple) in pancreas from WT and OPA1^{TG} mice at 8 weeks of age. B) Quantification of the percentage of Ki67 positive cells for field in pancreas from WT and OPA1^{TG} mice at 8 weeks of age. Mann-Whitney t-test. C) Quantification of nuclear dimension in pancreas from WT and OPA1^{TG} mice at 8 weeks of age. Mann-Whitney t-test. D) Representative images of immunohistochemistry for highly acetylated histone H4 (ac-H4) in pancreas from WT and OPA1^{TG} mice at 8 months of age. Nuclei are stained using Hematoxylin. E-F) Quantification of NAD^+ and NADH in acinar cells extracted from pancreas of WT and OPA1^{TG} mice at 8 weeks of age. Data are normalized on ug of proteins. Mann-Whitney t-test G) z-score of basal respiration, ATP-linked respiration, maximal respiration and reserve capacity of the ETC measured using Orobors from acinar cells extracted from pancreas of WT and OPA1^{TG} mice at 8 weeks of age. Mann-Whitney t-test. H) Quantification of the percentage of labeled acetyl-Coa determined by LC-MS on acinar cells extracted from pancreas of WT and OPA1^{TG} mice at 8 weeks of age cultured for 6 hours in the presence of ^{13}C-Glucose. I) Heat-map of z-scores of TCA cycle metabolites determined by LC-MS in acinar cells extracted from pancreas of WT and OPA1^{TG} mice at 8 weeks.
* $p< 0.05$; **** $p< 0,00001$.

OPA1 OVEREXPRESSION ACCELERATES PDAC PROGRESSION *in vivo*

Considering the results obtained WT mice and that elevated histone acetylation and cellular proliferation can support pancreatic carcinogenesis, we anticipated that OPA1 overexpression could accelerate tumor formation [129].

To tackle this hypothesis, we bred *Pdx1-Cre;LSL-KRAS^{G12D}* with *OPA1^{TG}* mice generating mice expressing KRAS^{G12D} in the pancreas and overexpressing OPA1 (KCO^{TG}) [37,253]. We then examined pancreatic histology in KC and KCO^{TG} mice at 4 months of age. Both KC and KCO^{TG} mice display widespread preneoplastic lesions in the pancreas, without significant differences in their number and overall area (Fig. 10 A-C). These observations suggest that OPA1 overexpression does not impact the initiation or the first phases of pancreatic ductal adenocarcinoma *in vivo*.

Carcinogenesis in KC mice has been widely documented and follows a robust multi-step model. At four months of age, mice exhibit exclusively low grade pancreatic intraepithelial neoplasia (PanIN grade 1 or 2); this was obvious also in our cohort [253,254]. On the other hand, 3/8 KCO^{TG} mice develop high grade dysplastic lesions (Fig. 10A), indicating that OPA1 overexpression is able to accelerate PDAC progression.

To confirm the tumor-promoting role of OPA1, we employed both pharmacological and genetic targeting of OPA1. OPA1 silencing is able to inhibit cell growth both in PANC1 cells and in a primary line of murine PDAC (Fig. 10E-F). The latter is derived from KPC mice (*Pdx1-Cre;LSL-Kras^{G12D};LSL-Trp53^{R172H}*), which develop invasive and widely metastatic pancreatic ductal adenocarcinoma[255]. Notably, treatment with an OPA1 inhibitor impairs the growth of both human and murine PDAC cells in a dose-dependent manner, without affecting non-transformed ductal cells - HPDE cells (Fig. 10D) [256].

OPA1 overexpression *in vivo* has been shown to prevent cytochrome c release through the stabilization of mitochondrial cristae, thus inhibiting apoptosis[37]. Considering that resisting cell death is one of the classical hallmarks of cancer, I evaluated whether OPA1 could impact this sensitivity to apoptosis in our moue model of PDAC progression[257]. Immunohistochemistry analysis of pancreata from both KC and KCO^{TG} mice showed extremely low levels of cleaved-caspase3, marker of apoptotic activation, ruling out the evasion from cell death as a mechanism for the accelerated progression in KCO^{TG} mice (Fig. 10 G-H).

Building from the observation that OPA1 overexpression in normal pancreas fosters histone acetylation and that metabolically-sensitive histone hyperacetylation supports pancreatic carcinogenesis, I stained tissue slides from either KC or KCO^{TG} mice highly acetylated histone H4 [129]. Immunohistochemistry revealed that during pancreatic carcinogenesis OPA1 fosters histone

acetylation, both in neoplastic lesions and in the surrounding normal parenchyma. On the other hand, histone acetylation is elevated specifically in neoplastic lesions in KC mice, as expected (Fig. 10 I). In conclusion, OPA1 overexpression is able to accelerate PDAC tumorigenesis and its inhibition specifically impairs pancreatic cancer cells growth, while normal ductal cells remain insensitive. These phenotypes are not caused by limited activation of apoptosis but likely involves a deregulation of the epigenetic landscape of pancreatic exocrine cells.

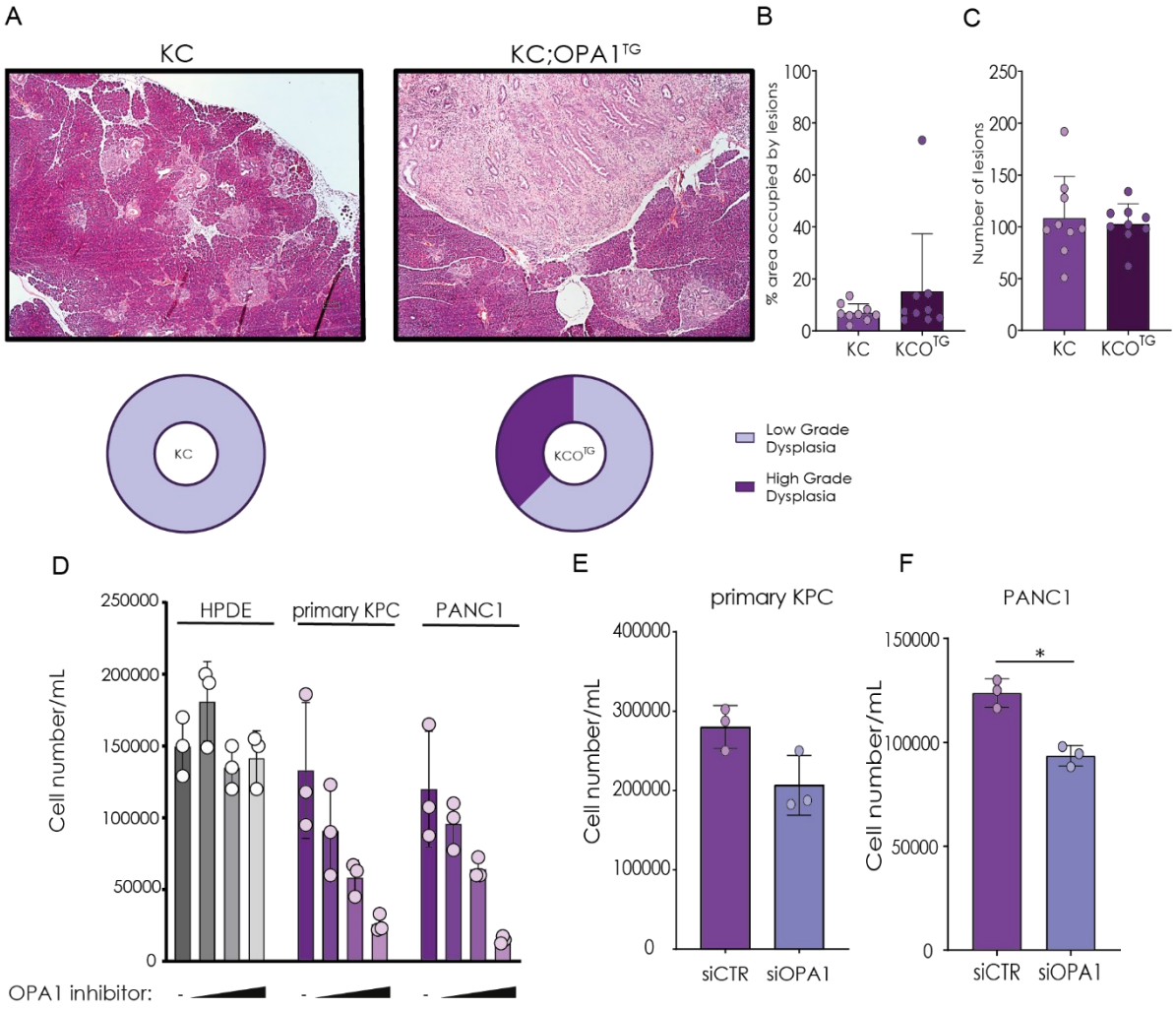
A
KC
KC;OPA1TG
B
% area occupied by lesions
KC
KCOTG
C
Number of lesions
KC
KCOTG
KC
KCOTG
Low Grade Dysplasia
High Grade Dysplasia
D
HPDE
primary KPC
PANC1
Cell number/mL
OPA1 inhibitor:
E
primary KPC
Cell number/mL
siCTR
siOPA1
F
PANC1
*
Cell number/mL
siCTR
siOPA1

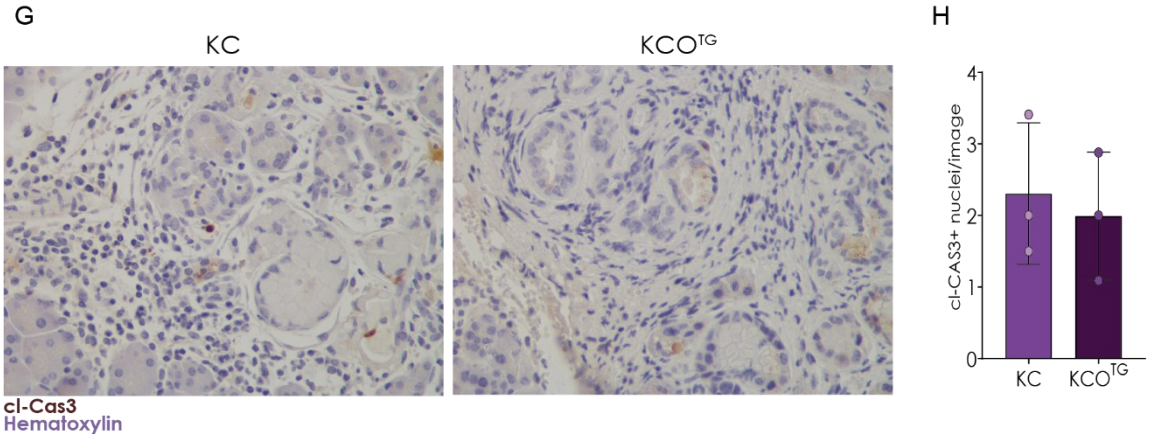
G
KC
KCOTG
cl-Cas3
Hematoxylin
H
cl-CAS3+ nuclei/image
KC
KCOTG

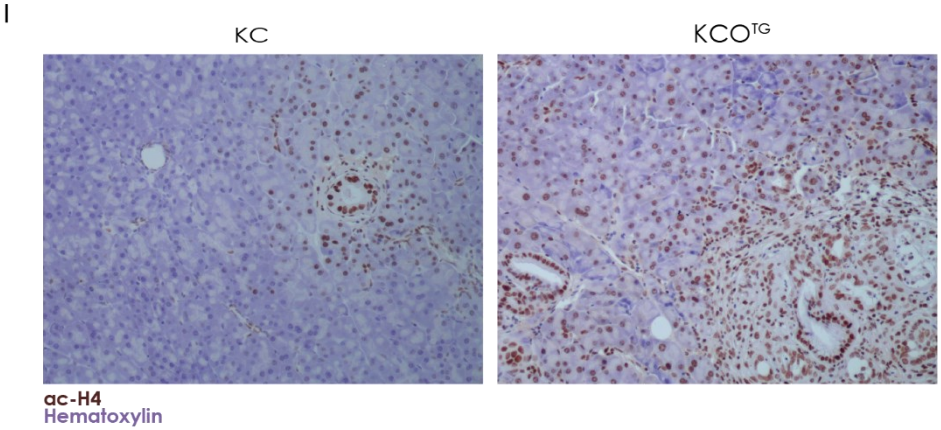
I
KC
KCOTG
ac-H4
Hematoxylin

Fig. 10 OPA1 overexpression accelerate PDAC progression. A) Representative images of Hematoxylin and Eosin staining of section of pancreas from KC and KCO^{TG} mice at 4 months of age. Grading of neoplastic lesions in the mice is shown in the graphs underneath the images. B-C) Quantification of the number and area of preneoplastic lesions in pancreas from KC and KCO^{TG} mice at 4 months of age. D) Determination of cellular growth in response to increasing doses (0 uM; 12,5 uM; 25 uM;50 uM) of an OPA1 inhibitor in HPDE, KPC primary and PANC1 cells, quantified as number of cells for mL after 48 hours of treatment. E-F) Determination of cellular growth in response to OPA1 loss KPC primary and PANC1 cells, quantified as number of cells for mL after 48 hours from the silencing of OPA1. Mann-Whitney t-test. G) Representative images of immunohistochemistry analysis of cl-caspase 3 in pancreas from KC and KCO^{TG} mice at 4 months of age. H) Quantification of the percentage of cl-caspase 3 positive cells for field for mice in KC and KCO^{TG} mice at 4 months of age. I) Representative images of immunohistochemistry for highly acetylated histone H4 (ac-H4) in pancreas from KC and KCO^{TG} mice at 4 months of age. Nuclei are stained using Hematoxylin.
* $p < 0.05$

OPA1 AFFECTS DNA DUPLICATION AND DAMAGE DURING PDAC PROGRESSION

Building from the obtained results, I investigated the mechanism through which OPA1-driven cristae remodeling could accelerate PDAC progression. Of note, I already ruled out truncated sensitivity to apoptosis.

OPA1 overexpression fosters DNA duplication in $KRAS^{WT}$ background (Fig. 9A-B), so I hypothesized that could contribute to accelerated tumor growth. In KCO^{TG} pancreata, the percentage of Ki67 positive cells is significantly higher compared to KC pancreata, both in pancreatic lesions and in the normal parenchyma (Fig. 11 A-B). In the same context, we observed also a significant increase in nuclear area (Fig. 11 C), that could be a sign of more relaxed, decondensed chromatin, due to the increased histone acetylation (Fig. 10 I) or linked to frequent DNA replication (Fig. 11 B) [258,259].

Both increased histone acetylation and fastened DNA duplication contribute to the establishment of replication stress, a long-known yet nonspecific and poorly characterized phenomenon that leads to genomic instability [260]. I speculated that OPA1 overexpression might determine a replication stress phenotype with the accrual of damaged DNA. To tackle this hypothesis, I performed several immune-stainings for the double strand break marker γH2AX and counted the number of positive foci per nucleus as a readout for genomic instability. The number of γH2AX foci for nucleus was significantly higher in pancreas of KCO^{TG} in both neoplastic lesions and in the normal parenchyma (Fig. 11D-E). Additionally, the silencing of OPA1 in PANC1 significantly decreases DNA damage, as indicated by the increase in the percentage of cells with less than 10 foci for nucleus (Fig. 11F-G). Considering the increase in both DNA duplication and DNA damage in response to OPA1 overexpression (Fig. 11A-E) and the fact that DNA damage could be a consequence of replication stress in cancer, we wonder if OPA1 could impact cell cycle progression [261]. Notably, OPA1 silencing causes an accumulation of PANC1 cells in the G0/G1 phases and a consequent decreases in the percentage of cells in S and M/G2 phases, confirming the role of OPA1 in the progression of the cell cycle (Fig. 11H). Additionally, silencing NME4 in the same cell line has a milder effect on cell cycle, decreasing only the percentage of cells in the S phase (Fig. 11I). These striking results indicate the crucial role of OPA1 in the regulation of genome integrity and the progression of cell cycle, suggesting a mechanism for the accelerated PDAC progression and aggressiveness *in vivo*.

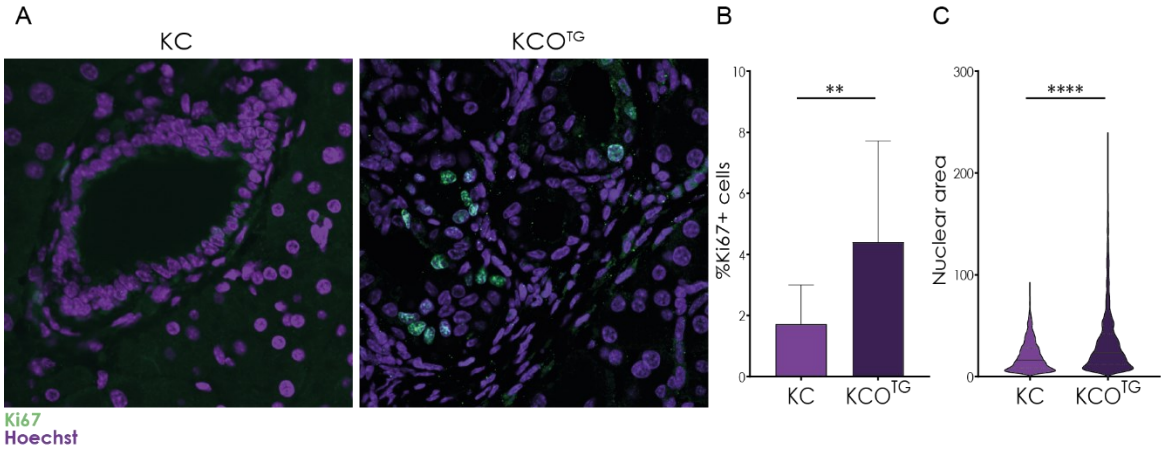
A
KC
KCO^TG
Ki67
Hoechst
B
%Ki67+ cells
**
KC
KCO^TG
C
Nuclear area
****
KC
KCO^TG

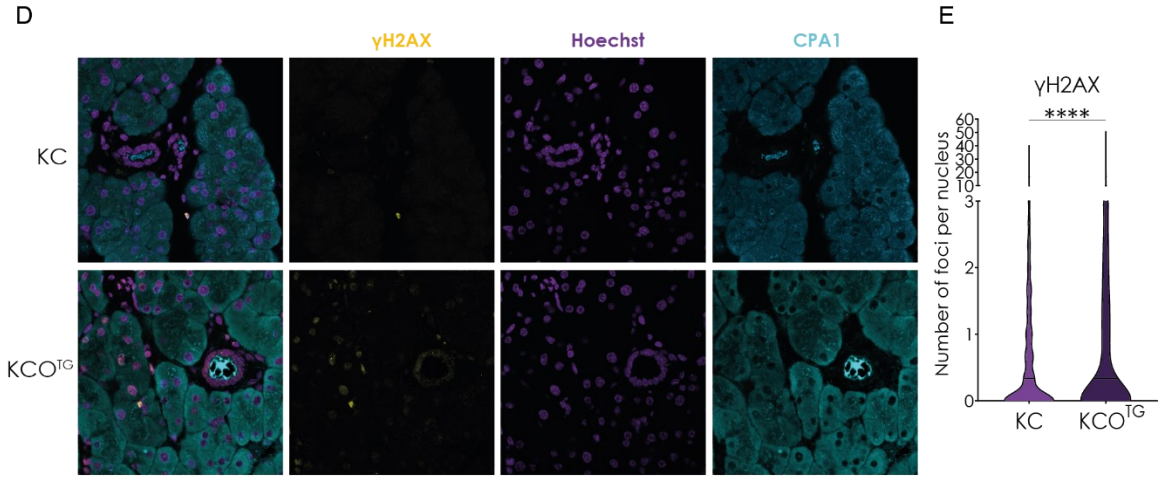
D
γH2AX
Hoechst
CPA1
KC
KCO^TG
E
γH2AX
****
Number of foci per nucleus
KC
KCO^TG

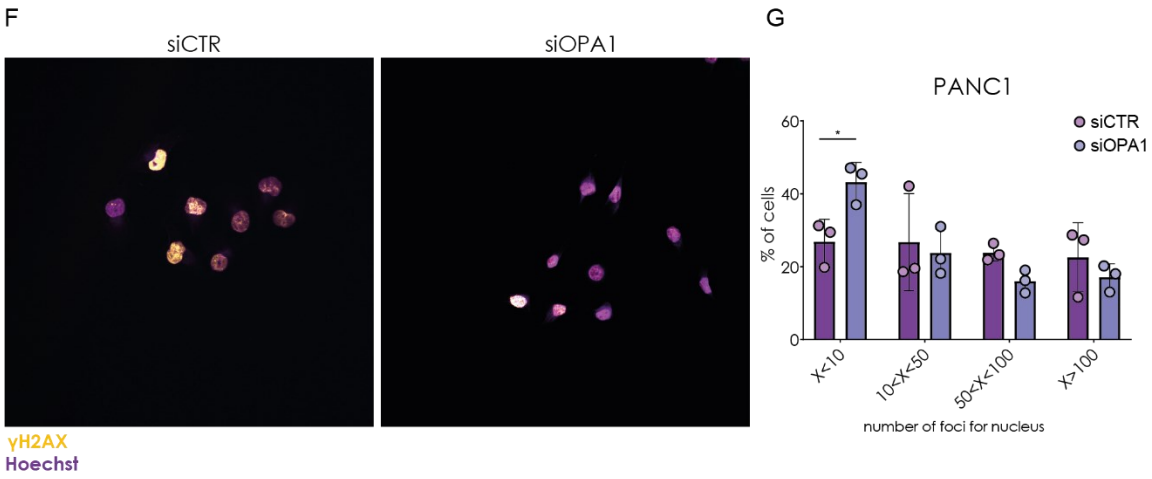
F
siCTR
siOPA1
γH2AX
Hoechst
G
PANC1
siCTR
siOPA1
% of cells
X<10
10<X<50
50<X<100
X>100
number of foci for nucleus

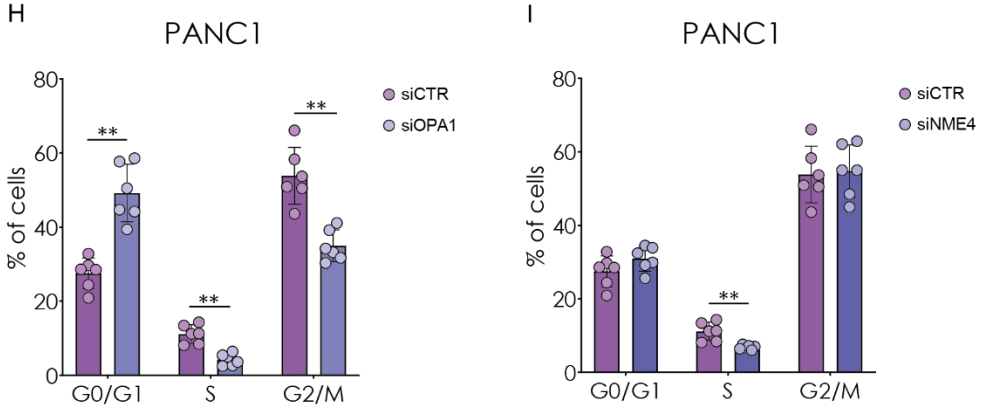
H
PANC1
siCTR
siOPA1
% of cells
G0/G1
S
G2/M
I
PANC1
siCTR
siNME4
% of cells
G0/G1
S
G2/M

Fig. 11 OPA1 regulates cell cycle progression and impact genome stability. A) Representative images of immunofluorescence of Ki67 (green) and Hoechst (purple) in pancreas from KC and KCO^{TG} mice at 4 months of age. B) Quantification of the percentage of Ki67 positive cells for field in pancreas from KC and KCO^{TG} mice at 4 months of age. Mann-Whitney t-test. C) Quantification of nuclear dimension in pancreas from KC and KCO^{TG} mice at 4 months of age. Mann-Whitney t-test. D) Representative images of immunofluorescence of γH2AX (yellow), CPA1 (turquoise) and Hoechst (purple) in pancreas from KC and KCO^{TG} mice at 4 months of age. E) Quantification of the number of γH2AX for nucleus in pancreas from KC and KCO^{TG} mice at 4 months of age. Mann-Whitney t-test. F) Representative images of immunofluorescence of γH2AX (yellow) and Hoechst (purple) in PANC1-siCTR and PANC1-siOPA1. G) Quantification of the percentage of cells with less than 10 foci per nucleus ($x<10$), with a number of foci for nucleus between 10 and 50 ($10<x<50$), with a number of foci for nucleus between 50 and 100 ($50<x<100$), or with more than 100 foci per nucleus ($x>100$) in PANC1-siCTR and PANC1-siOPA1. Mann-Whitney t-test. H-I) Percentage of cells in G1/G2, S and G2/M phases of the cell cycle in PANC1-siCTR and PANC1-siOPA1 and PANC1-siCTR and PANC1-siNME4, respectively. Phases of the cell cycle were determined through the evaluation of propidium iodide intensity by FACS. Two-way Anova.
** $p< 0.001$; **** $p< 0,00001$

DISCUSSION

In 1927, Otto Warburg's pioneering work highlighted cancer cells' inclination towards glycolysis over oxidative phosphorylation [1]. Warburg concluded that cancer universally arose from the demise of mitochondria. However, subsequent studies spanning a century have painted a more nuanced picture of metabolic reprogramming in cancer, also emphasizing the role of mitochondria in this complex and dynamic process [4]. Beyond maintaining the bioenergetic homeostasis of the cell, mitochondria play pivotal roles in signaling cascades, redox state regulation, epigenetic organization and cellular homeostasis in general, influencing cell fate [10,87,88,96,110]. The variety of mitochondrial bioenergetic and signaling functions is mirrored by the dynamic change in their morphology, which in turn regulates mitochondrial responses to cellular and environmental cues [262].

The understanding of the mechanisms behind metabolic rewiring and their relevance as potential therapeutic options is particularly relevant in the study of pancreatic ductal adenocarcinoma. PDAC is an extremely deadly malignancy, characterized by a late diagnosis and few therapeutic options [148,151,174,180,263]. Additionally, the majority of patients harbor mutations in the proto-oncogene KRAS, that is one of the first events of pancreatic carcinogenesis, and eventually leads to the reprogramming of various metabolic pathways [121,133,150,171,176,207,209,264–267]. Recent evidence clearly shows that both KRAS mutations and early dysplastic lesions are prevalent in the healthy population [268]. It is likely that most pre-neoplastic lesions will never acquire sever dysplastic features and will never progress to carcinoma. This leaves the field with a critical unresolved question: What promotes (and inhibits) the evolution of metaplastic cells into highly dysplastic lesions? A better understanding of the molecular mechanisms responsible for metaplasia-to-dysplasia switch is critical to intersect the disease early and improve the existing prevention strategies to curtain cancer incidence.

In this intricate context, our study seeks to dissect the mitochondrial rewiring occurring during pancreatic ductal adenocarcinoma progression, aiming to identify potential targetable mechanisms underpinning its aggressiveness.

To examine the contribution of mitochondrial biology to PDAC progression, we started evaluating the changes in the mitochondrial proteome during pancreatic carcinogenesis. Utilizing cellular models mimicking different stages of PDAC, we identified a significant reshaping of the mitochondrial proteome, including a consistent increase in the levels of proteins involved in several metabolic pathways, such as the TCA cycle and fatty acid oxidation, proteins involved in protein import into mitochondria, and several components of the mitochondrial translation machinery. Noteworthy and unexpected alterations included the upregulation of components associated with the oxidative phosphorylation pathway, particularly the electron transport chain and ATP synthase

subunits. The overexpression of both protein involved in the translation of protein encoded by the mtDNA and protein involved in the import of nuclear encoded mitochondrial proteins further confirm the crucial role of the coordination between mitochondria and the rest of the cells and is coherent with the increase of the OXPHOS pathway, being composed by both nuclear and mitochondrial encoded proteins.

The increase in the majority of the complexes of the ETC and in the subunits of the ATP synthase was confirmed by the augmented mitochondrial respiration in PDAC cells compared to non-transformed counterparts. While these results collide with Warburg initial working hypothesis, compelling evidence now aligns with our findings showing the complex contribution of functional mitochondria to tumorigenesis [1,4,110,130,213]. Many suggest the targeting of mitochondria as a viable anti-cancer strategy [4,269]. Indeed, complex I and III-deficient cells do not develop tumors when injected in immunocompetent mice [270–272]. Of note, an elegant study recently deployed artificial test components to parse the individual contribution of different mitochondrial functions to tumor growth *in vivo* and identified the electron transport chain as the most essential for its ability to oxidize ubiquinol [272]. Several evidences in literature point out that changes in mitochondrial respiration are often associated with modifications in mitochondrial ultrastructure and in particular in the biogenesis and stability of mitochondrial cristae [11,13,17,36,71,262]. Consistently, we uncovered modifications in mitochondrial ultrastructure both in human cell lines and *in vivo* during pancreatic carcinogenesis. In particular, PDAC progression is associated with increased cristae density and decreased cristae width, both consistent with the increase in respiration[13,37,68,71,262].

We identified NME4, a nucleotide diphosphate kinase, as a candidate for these changes in mitochondrial ultrastructure. Indeed, NME4 has been associated with the regulation of the GTPase activity of OPA1, a crucial regulator of cristae stability and then mitochondrial respiration [37,38,242,243,273]. Notably, NME4 is in a complex with OPA1 and has a crucial role in the regulation of mitochondrial ultrastructure, as its silencing in HeLa cells disrupt mitochondrial cristae [38,243]. Intrigued by this interaction, we validated the role of NME4 in pancreatic cancer cell lines, finding that NME4 loss in KP4 cells reshape mitochondrial ultrastructure by decreasing the number of mitochondrial cristae and increasing their width. Additionally, these changes are associated with a significant decrease in the overall mitochondrial respiration in PANC1. These results suggest that NME4 and OPA1 functionally overlap in the regulation of mitochondrial morphology and respiration in pancreatic cancer cells [13,262,274] .

Notably, elevated NME4 levels were observed in PDAC cell lines and validated in clinical samples from PDAC patients. Our data revealed a correlation between high NME4 expression and poorer survival outcomes. These findings link for the first time a nucleotide diphosphate kinase – exclusively

mitochondrial – to pro-oncogenic effects. In fact, NME4 is a little studied protein that belongs to the multifunctional NDPK protein family, localized mainly in the mitochondrial intermembrane space, bound to the inner membrane by anionic phospholipids like cardiolipin [40,243,246]. At mitochondria. NME4 has two crucial functions: (i) phosphotransfer from oxidatively generated ATP to different nucleoside diphosphates, mainly GDP to generate the GTP for local fueling of mitochondrial GTPases like OPA1, a driver of mitochondrial fusion at the IMM level and (ii) cardiolipin transfer from the inner to the outer membrane, where it serves as a pro-mitophagic or pro-apoptotic signal [40,243,246]. However, the role of NME family members in cancer is almost completely elusive. Yet, very recent evidence suggest that mito-cytoplasmatic isoforms (i.e.: NME6) might be involved in nucleotide sensing to the nucleus [275–277].

We also found elevated OPA1 levels in PDAC cells and a correlation with poorer patient prognosis. These data highlight the crucial role of the reshaping of mitochondrial ultrastructure in pancreatic carcinogenesis, pinging us to investigate the mechanisms underlying this axis between mitochondrial morphology and PDAC. While the promoting role of OPA1 has been documented, our research shows the ability of OPA1 to influence nuclear events. This provides an exciting novel mechanistic insight that unfortunately remains incompletely understood. OPA1 overexpression in normal pancreatic tissue led to active DNA duplication, histone acetylation, and cellular proliferation. This observation prompted further investigation into the impact of OPA1 on pancreatic cancer progression *in vivo*. Our results revealed that OPA1 slight overexpression accelerates PDAC progression, fostering high-grade dysplastic lesions. Importantly, pharmacological and genetic targeting of OPA1 hinders pancreatic cancer cell growth, presenting OPA1 as a potential therapeutic target.

Mechanistically, OPA1 silencing induces a cell cycle shift, accumulating cells in the G0/G1 phases and reducing the percentage in the S and M/G2 phases. These results were also obtained silencing NME4 in PANC1 cells, again linking NME4 activity with OPA1 function.

We posit a model where the mitochondrial upregulation of the protein complex formed by NME4, NME6 and RCC1L is a critical event for the evolution of early metaplastic cells into dysplastic carcinogenic cells. This complex enhances OPA1 activity driving cristae remodeling. This is associated with stabilization of respiratory complexes and elevated oxygen consumption.

We reason that augmented ETC activity might explain the tumor-promoting role of OPA1. Increased genomic instability might suggest toxic accumulation of reactive oxygen species. However, preliminary data show that ROS levels are not altered in OPA1- or NME4-silenced cells.

In contrast, we hypothesize a mechanism involving a dysregulation of nucleotide synthesis. In fact, nucleotide imbalance has been recently proposed as a cause of replication stress and has been shown to impact cell fate decision but also tumor growth and differentiation [278–282]. Alterations in the ETC

limit ubiquinol oxidation and reverberate onto the biosynthesis of pyrimidines [272]. On the other hand, OPA1 overexpression could accelerate ubiquinol oxidation and elevate its availability for cytoplasmatic enzymes, such as dihydroorotate dehydrogenase (DHODH), the rate-limiting enzyme in the *de novo* synthesis of pyrimidines. Hence, OPA1 overexpression would determine a nucleotide imbalance with consequences for check point controls and fork progression. This intriguing link between mitochondrial dysfunction and nucleotide synthesis could be a pivotal contributor to the observed DNA damage, active DNA replication, and altered cell cycle progression. The dysregulated nucleotide synthesis pathway could serve as a nexus where mitochondrial dynamics, cellular metabolism, and genomic stability converge, painting a more comprehensive picture of PDAC pathogenesis.

The findings presented in this thesis not only advance our understanding of mitochondrial dynamics in PDAC but also unveil potential therapeutic targets. NME4 and OPA1, identified as key players in mitochondrial remodeling, offer promising avenues for intervention. The correlation between their expression levels and patient prognosis underscores their clinical relevance. Future research could delve deeper into the molecular intricacies of NME4 and OPA1 function, explore in more details their interaction during pancreatic carcinogenesis, and investigate targeted therapies to modulate their activities.

In conclusion, this research contributes significantly to the evolving landscape of PDAC biology, shedding light on the intricate interplay between mitochondrial dynamics, cell cycle regulation, and tumor progression.

METHODS

CELL LINES AND CULTURE

All PDA cell lines were cultured in DMEM (Biowest, L0101) supplemented with 10 % Fetal Bovine Serum (FBS) (Biowest, S1810) supplemented with 0.3 mg/mL glutamine (Biowest, X0550), 100 IU/ml penicillin G, and 100 µg/µL streptomycin (Biowest, L0022). Human pancreatic duct epithelial cells (HPDE) were kindly donated by R. Perera (UCSF, USA) and cultured in Keratinocyte Serum Free medium (Gibco, 17005-034) and RPMI 1640 (Biowest, L0501) supplemented with 10% FBS, 100 IU/ml penicillin G, 100 µg/µL streptomycin, 2.5 µg epidermal growth factor (EGF) (Gibco, 37000015), and 25 µg/mL bovine pituitary extract (BPE) (Gibco, 37000015). PANC1 were kindly provided by I. Szabó (University of Padova); MiaPaca-2 were kindly provided by V. Corbo (University of Verona); KP4 were kindly donated by R. Zoncu (UC Berkeley, USA). HPDE-KRAS^{G12D}-OMP25-GFP, PANC1-OMP25-GFP and MiaPaCa2-OMP25-GFP cells used for the mitochondrial proteomic analysis were kindly provided by R. Perera (UCSF, USA).

KPC cells are in-house generated cell lines derived from the clonal expansion of cells isolated from pancreatic neoplastic lesions in KPC mice (Pdx-Cre; [LSL-p53$^{fl/fl}$; LSL-Kras^{G12D}]). KPC mice rapidly develop PDA tumors and KPC-derived cell lines were used as de facto tumor cell lines. Progression is accelerated in KPC mice which simultaneously harbor P53 mutations or deficiency.

Negative mycoplasma contamination status of all cell lines and primary cells used in the study was established using either visual inspection of Hoechst staining or with a mycoplasma detection kit (Invivogen, MYSNC-100).

The assessment of cell growth *in vitro* was performed by manual counting of live cells with Burker chamber.

Silencing was performed using Lipofectamine RNAiMax (Life Technologies, 56532) following the indications of the manufacturer. The used siRNAs are the following: siNC4 (Life Technologies, AM641), siNME4 (Life Technologies, s9594), siOPA1 (Life Technologies, 144409).

MITOCHONDRIAL IMMUNOPRECIPITATION AND PROTEOMICS

HPDE-KRAS^{G12D}, PANC1 and MiaPaCa2 stably expressing OMP25-GFP-3xHA, tagging specifically mitochondria, were scraped in ice-cold KPBS buffer (136 mmol/L KCl, 10 mmol/L KH_2PO_4 pH 7.25) supplemented with Pierce protease inhibitor and were collected by centrifugation. The pellets were resuspended in KPBS buffer supplemented with 50 mmol/L sucrose and 0.5 µmol/L TCEP and mechanically lysed, followed by centrifugation at 2,700 rpm for 10 minutes. The supernatant containing the organelles was incubated with 50 µL of anti-HA–conjugated Dynabeads

(Thermo Scientific, 88837) for 30 minutes with rotation. Lysosome-bound beads were washed 3 times and eluted overnight at 4°C using KPBS buffer containing 0.1% NP-40 detergent. Protein concentration was measured using the Pierce BCA Protein Assay Kit. Equal amounts of protein from each condition were used for mass spectrometry–based proteomics or immunoblotting.

Mass spectrometry analysis was performed as follows. A trichloroacetic acid precipitation was performed to remove detergents by adding 1 volume of 6.1N trichloroacetic acid to 4 volume of sample and incubated on ice for 10 minutes. The samples were centrifuged at 14,000 rpm at 4°C for 5 minutes, and the supernatant was removed. The pellet was then washed twice with 200 μL of cold acetone at 14,000 rpm at 4°C for 5 minutes, and the residual acetone was allowed to evaporate.

The precipitated protein was resuspended in 100 μL of 6 mol/L urea in 100 mmol/L Tris pH 7.8 and treated with 5 μL of 200 mmol/L DTT in 100 mmol/L Tris pH 7.8 for 60 minutes to reduce the disulfide bonds. The resulting free cysteine residues were subjected to an alkylation reaction. The samples were subjected to tryptic digestion at 37°C overnight with gentle shaking. Urea, Tris, and other nonvolatile reagents in the sample were removed by solid-phase extraction using Sep-Pak Plus C18 Cartridges (Waters Corp; WAT020515) according to the manufacturer's specifications.

The peptide solutions were manually injected on a Shimadzu microflow high-performance liquid chromatography (HPLC) system consisting of two LC20AD pumps, a CBM20A controller, and a FRC10A fraction collector. Fractions were analyzed by reversed-phase HPLC using Waters NanoAcquity pumps and autosampler and a Thermo Fisher Orbitrap Elite mass spectrometer using a nano flow configuration. Peptides were identified from the MS data using SEQUEST algorithms. A species-specific database was generated from NCBI's nonredundant (nr.fasta) database and concatenated to a database of common contaminants (keratin, trypsin, etc.). The resulting data were then loaded into Scaffold (Proteome Software), and a minimum of two peptides and a peptide threshold of 95% and protein threshold of 99% were used for identification of peptides and protein-positive identifications.

Then proteins were filtered manually for mitochondrial protein using MitoCarta 3.0, the subcellular localization of UniProt, and TargetP 2.0 (MTS predictor). For the comparative analysis, LFQ analyst was used.

GeneOntology analysis of the mitochondrial proteomic analysis was performed using Enrichr on a curated list of commonly upregulated or downregulated proteins. The protein association map of the commonly upregulated proteins was made using StringDB, with a confidence of 0.7 and eliminating the disconnected dot.

CELL CYCLE ANALYSIS

PANC1-siCTR, PANC1-siOPA1 and PANC1-siNME4 cells were trypsinized and washed in cold PBS. Cells were then resuspended in cold 70% EtOH in PBS and incubated 1h at 4°C and then moved at -20°C for 24h. The day after, cells were centrifuged at 3000 rpm for 3 minutes and washed in PBS. Cells were incubated with 50 mg/mL of Propidium Iodide (Life Technologies, P3566) and 200 µg/mL of RNAse (Sigma-Aldrich, R4875) for 1h at RT.

Samples were acquired and analyzed using the BD Canto-CALIBUR. Cells were gated based on SSC-A or FSC-A to eliminate cell debris. The median fluorescence intensity was measured for each independent biological sample based on at least 3×10^4 gated events. Cell cycle phases were determined by the morphology of the PI peaks and percentage of cells in each phase was measured.

ANIMAL STUDIES

$OPA1^{TG}$ mice were previously described [37]. To generate KCO^{TG} mice, $OPA1^{TG}$ mice were bred to Pdx1-Cre; LSL-$Kras^{G12D}$ transgenic mice. Mice were largely born according to the Mendelian ratios. Genotyping was performed by PCR amplification of ear snips digested with Proteinase K, using primers listed in Table 1. Unless otherwise stated, all experimental mice were a mix of male and female.

Mice were sacrificed at 8 weeks or 4 months of age, depending on the specific experiment and in any case before the humane end point was reached.

Table 1 Primers used for genotyping of transgenic mice used in the study

Target	*Sequence*
Pdx1-Cre FW	TGCCACGACCAAGTGACAGC
Pdx1-Cre RV	CCAGGTTACGGATATAGTTCATG
$KRAS^{WT}$	TGTCTTTCCCCAGCACAGT
$KRAS^{G12D}$	GCAGGTCGAGGGACCTAATA
$KRAS^{COMMON}$	CTGCATAGTACGCTATACCCTGT
$OPA1^{WT}$ *FW*	GAG GGA GAA AAA TGC GGA GTG
$OPA1^{WT}$ *RV*	CTC CGG AAA GCA GTG AGG TAA G
$OPA1^{TG}$ *FW*	GCA ATG ACG TGG TCC TGT TTTG
$OPA1^{TG}$ *RV*	GAT AGG TCA GGT AAG CAA GCA AC

PRIMARY MURINE PANCREATIC ACINAR CELLS ISOLATION

Primary pancreatic acinar cells were isolated from 6-8-week-old mice pancreata collected upon sacrifice. Resected pancreata were washed twice in cold hank's balanced salt solution (HBSS, Biowest, L0607) and subsequently minced on a sterile petri dish using sterile blades. 20mL of HBSS were added to the minced tissue and centrifugated for 4 minutes at 720g 4°C. Tissue was then digested with 1 mg of collagenase P (Roche, 11215809103) in 5mL HBSS at 37°C for 30 min, inverting the tubes every 2 mins and interrupting digestion every 10 min to mechanically disrupt the clogs by pipetting with progressively smaller pipette tubes. The reaction was stopped, and tissue homogenate was washed twice with HBSS containing 5% calf serum (CS, Biowest, S0400) and then filtered through a 500µm mesh and a 100µm strainer. The flow-through was carefully laid onto an HBSS solution containing 30% of CS and centrifugated for 3mins at 200g 4°C. This gradient sedimentation step enriches the preparation for acini, although does not impede the accidental co-isolation of other cell populations. The pellet was resuspended in Waymouth's medium containing 10% CS and supplemented with 0.2mg/mL soybean trypsin inhibitor (Sigma-Aldrich, T9253). Trypsin inhibitor is added to prevent autodigestion of the explants due to stress-induced release of proteases from acinar cells themselves. Isolated primary pancreatic acinar cells were resuspended in Waymouth's complete medium and plated in low-adhesion dishes for a maximum of 4 days.

For glucose tracing, suspension-plated cells were allowed to recover overnight in Waymouth's medium supplemented with 10% CS and 0.1 mg/mL Soybean Trypsin Inhibitor. In the morning, cells were collected and rapidly spun down and resuspended in glucose- DMEM +10% dialyzed FBS (Voden, S181D) supplemented with either 10 mM [U-13C]-glucose (Cambridge Isotope Laboratories, CLM-1396–1), plated in low-adhesion petri dishes and incubated at 37°C for 6 hours.

ACYL-COA QUANTIFICATION AND ISOTOPOLOGUE ANALYSIS

Acyl-CoA analyses were performed by liquid chromatography-mass spectrometry/high-resolution mass spectrometry (LC-MS/HRMS) as previously described [283]. Briefly, approximately 100 $\times 10^6$ acinar cells were cultured in suspension in low adhesion 6 mm petri dishes. At harvest, cells were placed on ice, transferred to 15 ml falcon tubes and centrifuged at 600 xg for 2 minutes at 4 °C. Medium was aspirated and the cell pellet resuspended in 1 mL 10% (w/v) trichloroacetic acid (Sigma-Aldrich, T6399) for acyl-CoA extraction. For quantification, an equal amount (100 µL) of $^{13}C_3$-labeled acyl-CoA internal standard was added to each sample [283]. Samples were pulse sonicated, centrifugated and the supernatant was purified by solid-phase extraction using Oasis HLB 1cc (30 mg) SPE columns (Waters). Eluate was evaporated to dryness under nitrogen gas and re-suspended

in 50 µL of 5 % 5- sulfosalicylic acid (w/v) for injection. Samples were analyzed by an Ultimate 3000 autosampler coupled to a Thermo Q-Exactive Plus instrument in positive electrospray ionization mode. For isotopic tracer analysis, isotopic enrichment from [U-13C]glucose was calculated to compensate for the non-linearity of isotopic enrichment using the FluxFix calculator.

METABOLITES QUANTIFICATION

To extract polar metabolites for mass spectrometry analysis, acinar cells derived from a whole pancreas were lysed in 80% methanol. Subsequently, the samples were centrifuged and dried using a vacuum concentrator and stored at −80 °C. The measurements of the metabolites were obtained with an Acquity UPLC system interfaced with a Quattro Premier mass spectrometer (Waters, Milford, MA, USA) [64]. The calibration curves were established using standards and processed under the same conditions as the samples, at five concentrations [65, 66]. The best fit was determined using a regression analysis of the peak analyte area.

NAD^+ and NADH levels were measured using the NAD/NADH quantitation kit (Sigma-Aldrich, MAK037), following the indication of the manufacturer.

PROTEIN EXTRACTION AND WESTERN BLOT

For the validation of the mitochondrial proteomic, mitochondria were extracted as previously described [284]. In brief, cells were scraped in PBS and centrifuged at 600 rcf at 4°C for 10 minutes. Pellet was resuspended into IBc (10 mM Tris-MOPS, 1 mM EGTA/Tris, 200 mM Sucrose) and homogenized using a Teflon pestle in a glass potter. After a series of high-speed centrifugations, a mitochondrial suspension was obtained. Both mitochondria and pancreas harvested from mice were lysed using NP-40 lysis buffer (25 mM Tris-HCl pH7.4, 150 mM NaCl, 1 mM EDTA, 1 % NP-40), supplemented with PhosSTOP phosphatase inhibitor cocktail (Roche,) and protease inhibitor cocktail (Roche,) and protein concentration was measured using the Bradford Reagent (Sigma-Aldrich, B6916). 25 µg of protein per sample were resolved on 8%, 4-12% or 4-20%, depending on the proteins of interest, SDS-Urea PAGE gel and transferred to PVDF membranes. Membranes were blocked in 5 % milk for 1h at room temperature. Incubation with the appropriate dilution of primary antibody was carried out at 4 °C o/n. NME4 (Gentex, GTX121931), OPA1 (Cell Signaling technology, 80471S), TOMM20 (Gentex, GTX133756), Vinculin (Sigma-Aldrich, V4505). Fluorescent-conjugated secondary antibody were used at a dilution of 1:2000 for 1h at RT.

QUANTITATIVE PCR (qPCR)

Total RNA was isolated from triplicate cell cultures under each condition using TRIzol Reagent (Invitrogen, 15596026). Briefly, cells were washed in PBS, lysed with TRIzol and after homogenizing the sample, transferred to microfuge tubes. Then chloroform was added and the homogenate was allowed to separate into a clear upper aqueous layer (containing RNA), an interphase and a red lower organic layer (containing proteins and DNA). The aqueous phase with RNA was transferred to a new tube and the process was repeated twice. Isopropanol was added to the aqueous phase and the homogenate was left for 1h on ice to allow RNA precipitation. Finally, the RNA was precipitated through centrifugation (20 mins at 13.000g 4°C) and the resulting white gel-like pellet was washed twice in Et-OH 75%, then air dried and finally resuspended in 20-50μL of RNase-free water.

Reverse transcription was performed using the High-Capacity cDNA Reverse Transcription Kits (Applied Biosystem, 4387406). Generally, 500ng-1μg of RNA was used. cDNA was diluted 1:20 (or 1:10) and used as a template in the CAPITAL qPCR Green master mix (Biotech Rabbit, BR0501701). Transcript levels are provided as fold change, calculated using ΔΔCt. For the quantification of mtDNA, DNA was extracted from human cell lines or acinar cells extracted from mice using *Quick*-DNA™ extraction kit (Zymo Research, D4075) and the DNA was diluted to 5 ng/μL and used as a template in the CAPITAL qPCR Green master mix. Used primers are listed in Table 2.

Table 2 Primers used for qPCR

Target	*Sequence*
h-NME4 FW	AGGGTACAATGTCGTCCGC
h-NME4 RV	GACGCTGAAGTCACCCCTTAT
h-OPA1 FW	AGCCTCGCAGGAATTTTTGG
h-OPA1 RV	AGCCGATCCTAGTATGAGATAGC
h-Actin FW	CGCCGCCAGCTCACCATG
h-Actin RV	CACGATGGAGGGGAAGACGG
h-18S FW	GTTCAGCCACCCGAGATTGA
h-18S RV	CCCATCACGAATGGGGTTCA
h-β2MG FW	TGCTGTCTCCATGTTTGATGTATCT
h-β2MG RV	TCTCTGCTCCCCACCTCTAAGT
h-mt-tRNA-Leu FW	CACCCAAGAACAGGGTTTGT
h-mt-tRNA-Leu RV	TGGCCATGGGTATGTTGTTA
m- β2MG FW	ATGGGAAGCCGAACATACTG
m- β2MG FW	CAGTCTCAGTGGGGGTGAAT
m-mt-CytB FW	CTAGAAACCCCGAAACCAAA
m-mt-CytB FW	CCAGCTATCACCAAGCTCGT

TRANSMISSION ELECTRON MICROSCOPY (TEM)

Cells or pancreatic tissue from mice were fixed one hour at 4 °C in 2.5% glutaraldehyde in sodium cacodylate buffer 0.1M pH 7.4 and washed using sodium cacodylate 0.1M pH 7.4. Cells were incubated with osmium tetroxide 1% + potassium ferrocyanide 1% in sodium cacodylate buffer 0.1M pH 7.4 for 1h at 4° C, embedded in epoxy resin and sectioned. Ultrafine (60-80 nm) dissections were performed with Ultratome V (Leica) ultramicrotome and contrasted with 1% of Uranyl acetate and 1% of Lead citrate. Thin sections were imaged on a transmission electron microscope FEI Tecnai G2 with OSIS Veleta cameras and visualized at a magnification of 37000 X.

For the morphometric analysis of mitochondria, mitochondrial area, mitochondrial perimeter, mitochondrial aspect ratio, mitochondrial cristae length and mitochondrial cristae width was manually measured using ImageJ. Cristae width was measured on the widest portion in completely visible cristae. Cristae density was calculated as the number of mitochondrial cristae normalized for the area of the mitochondria.

For HPDE-KRAS^{G12D}, PANC1 and MiaPaCa2 were measured at least 150 mitochondria from at least 10 different cells. For WT and KC pancreatic tissues, 50 mitochondria per mouse from 3 mice for genotype were analyzed. For KP4-siCTR and KP4-siNME4 50 mitochondria per biological replicates from 3 different biological replicates were analyzed.

IMMUNOFLUORESCENCE, IMMUNOHISTOCHEMISTRY AND ANALYSIS OF MURINE PANCREATIC TISSUE

For histological evaluation, the whole pancreas was harvested from mice and laid on a planar surface for overnight formalin fixation. After the fixation step, tissues were paraffine-embedded and sectioned at 4 μm.

Tumor evaluation was performed on hematoxylin and eosin dyed sections and whole pancreata were reconstructed through software guided tile merging using the DM6B Leica microscope. Image J software was used for quantification of the area of the entire pancreata as well as of individual neoplastic foci.

Immunohistochemistry was performed on paraffin-embedded sections. Tissue sections were dewaxed and rehydrated. Antigen retrieval was performed by boiling samples in citrate buffer for 20 min and the immunohistochemistry was performed using the Mouse to mouse HRP Staining kit (Histoline, MTM001). Primary antibodies against pan-acetylated histone H4 (acH4, Invitrogen, PA5-40083), cleaved caspase 3 (cl-cas3, Cell Signaling Technology, 9661T) were incubated overnight at 4 °C. Quantification of cleaved caspase 3 was performed counting the number of positive cells per field.

Immunofluorescence was performed on paraffine-embedded sections. Tissue sections were dewaxed and rehydrated. Antigen retrieval was performed by boiling samples in citrate buffer for 20 min. Samples were blocked in PBS-FBS 2,5% and primary antibodies against TOMM20 (Gentex, GTX133756), Ki67 (Invitrogen, PA5-19462), γH2AX (Cell Signaling, 2577S), CPA1 (R&D Systems, AF2765) were incubated overnight at 4 °C. Fluorescent-conjugated secondary antibodies were incubated 1h at RT. Nuclei were stained using Hoechst 33342 (Invitrogen, H3570).

For immunofluorescence analysis *in vitro,* cells were seeded on 13 mm coverslips (Life Technologies, 174950). Cells were fixed using 4% PFA and permeabilized in 0,1% Triton X-100. Cells were blocked in PBS-FBS 2,5% and primary antibody against TOMM20 (Gentex, GTX133756) and γH2AX (Cell Signaling, 2577S) were incubated overnight at 4 °C. Fluorescent-conjugated secondary antibodies were incubated 1h at RT. Nuclei were stained using Hoechst 33342 (Invitrogen, H3570).

Immunofluorescence were visualized using Zeiss LSM900 upright confocal microscope with a magnification of 40X.

γH2AX was quantified manually counting the number of foci per nucleus. *In vitro* cells data are represented classifying cells for the number of foci per nucleus. Ki67 was quantified as the percentage of positive nuclei on the total number of nuclei per field. Nuclear area was measured using a MatLab tool (Mitochondrial Analyzer), kindly donated by M. Bortolozzi (VIMM).

Mitochondrial network morphology was evaluated on images stained with the TOMM20 antibody using a MatLab tool (Mitochondrial Analyzer), kindly donated by M. Bortolozzi (VIMM). In particular, the fusion index is calculated as the ratio between the area of a single fluorescent object (mitochondria) and the roundness of the same object.

TISSUE MICROARRAYS, IMMUNOHISTOCHEMISTRY AND CORRELATION WITH CLINICAL OUTCOME ON HUMAN SAMPLES

To assess NME4 as a potential prognostic biomarker, we assembled a cohort comprising early-stage patients (stage I–IIb, n = 76) undergoing adjuvant gemcitabine treatment. We selected representative cores from individual primary pancreatic ductal adenocarcinoma formalin-fixed paraffin-embedded or normal pancreas adjacent tissues, before treatment, and combined them into tissue microarrays, following established protocols. Immunohistochemical staining of NME4 was conducted according to the manufacturer guidelines. Negative control slides, stained without the primary antibody, were utilized. The BenchMark Special Stain Automation system (Ventana Medical Systems, Export, USA) was employed for visualization. Evaluation of staining involved an assessment of tumor and tissue loss, background, and overall interpretability. Immunostaining intensity was categorized into two grades—low and high expression—based on a scoring system considering staining intensity (graded

as 0: absent, 1: weak, 2: moderate, 3: strong) and the number of stained cells. All patients provided written informed consent for the storage and analysis of their tumor material and survival data. This study received approval from the Local Ethics Committee of the University of Pisa (Ethics approval #3909, 3 July 2013). Correlation with clinicopathological characteristics, including progression-free survival (PFS) and overall survival (OS), was analyzed using Kaplan–Meier curves and the log-rank test. Univariate analysis was conducted, and factors with a P value below 0.1 were assessed in the multivariate analysis following the Wald model, utilizing SPSS software version 26 (IBM Corp, Armonk, NY). Statistical significance was set at P values below 0.05.

RESPIROMETRIC ANALYSES

Long term respirometric analysis on HPDE-KRAS^{G12D} and PANC1 cells were performed using the Resipher System (Lucid Scientific). Briefly, cells was seeded into a 96-well in complete medium and maintained for 24 h at 37 °C, 5% CO_2. The day after, the medium was changed with complete DMED w/o phenol red and the Resipher System was attached to the plate and maintained at 37°C, 5% CO_2 for 10 hours.

Metabolic parameters of PANC1-siCTR and PANC1-siNME4 were calculated using the Seahorse XFe24. Briefly, PANC1-siCTR and PANC1-siNME4 were seeded in a 24-well Seahorse XF24 cell culture microplate in complete medium and maintained for 24 h at 37 °C, 5% CO_2. To evaluate the OCR and ECAR, one hour previous to the experiment the medium was replaced with Seahorse medium (Dulbecco's Modified Eagle Medium, Agilent, 103335-100) supplemented with 1 mM sodium pyruvate (Biowest, L0642), 2 mM glutamine (Biowest, X0550) and 10 mM glucose (Sigma-Aldrich, G8270) and sequentially injecting the following reagents: Oligomycin A (0,5 µM), Carbonyl cyanide-4-(trifluoromethoxy)phenylhydrazone (FCCP) (1 µM), Antimycin and Rotenone (0,5 µM). Data were analyzed with Agilent Seahorse Wave software.

Oxygen consumption rate of acinar cells extracted from WT or OPA1^{TG} mice was performed using Oroboros O2k. Briefly, acinar cells were extracted as previously described and cultured in Waymouth's complete medium for 24 h at 37°C, 5% CO_2. The day after, medium was replaced with Mir05 buffer (0,5 mM EGTA, 3 mM $MgCl_2$, 60 mM Lactobionic acid, 20 mM Taurine, 10 mM KH2PO4, 20 mM HEPES, 110 mM D-Sucrose, 1 g/L fatty acid free BSA) and cells were transferred into the chamber of the Oroboros O2K system, after its calibration. Oxygen consumption rate was measured following the addition of pyruvate (5 mM), Oligomycin A (10 nM), Carbonyl cyanide m-chlorophenyl hydrazone (CCCP) (titration- 0,5 µM per step), Antimycin A (2,5 µM) and Rotenone (0,5 µM). Data were normalized on protein quantity, calculated using the Bradford Reagent.

STATISTICAL ANALYSIS

Data are presented as the means of experimental replicates with their respective standard deviations, unless otherwise indicated. For data derived from mice every dot represented a biological replicates. Graphs and statistical analysis was performed using GraphPad Prism. Repeated-measures ANOVA with Tukey-Kramer adjustment for multiple comparisons was used to evaluate significant differences in the 10 hours long respirometric analysis. For survival, log-rank test was performed using GraphPad Prism. The other data, if not differently specified, were analyzed using non-parametric t-test (Mann-Whitney).

Significance was defined as follows: *, $P < 0.05$; **, $P < 0.01$; ***, $P < 0.001$; ****,$P<0.0001$

REFERENCES

1. Warburg, O., Wind, F. & Negelein, E. THE METABOLISM OF TUMORS IN THE BODY. *Journal of General Physiology* **8**, 519–530 (1927).
2. Vazquez, A. *et al.* Cancer metabolism at a glance. *J Cell Sci* **129**, 3367–3373 (2016).
3. Schiliro, C. & Firestein, B. L. Mechanisms of Metabolic Reprogramming in Cancer Cells Supporting Enhanced Growth and Proliferation. *Cells* **10**, 1056 (2021).
4. Porporato, P. E., Filigheddu, N., Pedro, J. M. B.-S., Kroemer, G. & Galluzzi, L. Mitochondrial metabolism and cancer. *Cell Res* **28**, 265–280 (2018).
5. Hanahan, D. & Weinberg, R. A. Hallmarks of Cancer: The Next Generation. *Cell* **144**, 646–674 (2011).
6. Mizrahi, J. D., Surana, R., Valle, J. W. & Shroff, R. T. Pancreatic cancer. *The Lancet* **395**, 2008–2020 (2020).
7. Encarnación-Rosado, J. & Kimmelman, A. C. Harnessing metabolic dependencies in pancreatic cancers. *Nat Rev Gastroenterol Hepatol* **18**, 482–492 (2021).
8. Halbrook, C. J., Lyssiotis, C. A., Pasca di Magliano, M. & Maitra, A. Pancreatic cancer: Advances and challenges. *Cell* **186**, 1729–1754 (2023).
9. Chandel, N. S. Mitochondria as signaling organelles. *BMC Biol* **12**, 34 (2014).
10. Chakrabarty, R. P. & Chandel, N. S. Mitochondria as Signaling Organelles Control Mammalian Stem Cell Fate. *Cell Stem Cell* **28**, 394–408 (2021).
11. Pernas, L. & Scorrano, L. Mito-Morphosis: Mitochondrial Fusion, Fission, and Cristae Remodeling as Key Mediators of Cellular Function. *Annu Rev Physiol* **78**, 505–531 (2016).
12. Vogel, F., Bornhövd, C., Neupert, W. & Reichert, A. S. Dynamic subcompartmentalization of the mitochondrial inner membrane. *J Cell Biol* **175**, 237–247 (2006).
13. Cogliati, S. *et al.* Mitochondrial cristae shape determines respiratory chain supercomplexes assembly and respiratory efficiency. *Cell* **155**, 160–171 (2013).
14. Giacomello, M., Pyakurel, A., Glytsou, C. & Scorrano, L. The cell biology of mitochondrial membrane dynamics. *Nat Rev Mol Cell Biol* **21**, 204–224 (2020).
15. Ikon, N. & Ryan, R. O. Cardiolipin and mitochondrial cristae organization. *Biochimica et Biophysica Acta (BBA) - Biomembranes* **1859**, 1156–1163 (2017).
16. Jiang, Z. *et al.* Cardiolipin Regulates Mitochondrial Ultrastructure and Function in Mammalian Cells. *Genes (Basel)* **13**, 1889 (2022).
17. Quintana-Cabrera, R., Mehrotra, A., Rigoni, G. & Soriano, M. E. Who and how in the regulation of mitochondrial cristae shape and function. *Biochem Biophys Res Commun* **500**, 94–101 (2018).
18. Arselin, G. *et al.* The Modulation in Subunits e and g Amounts of Yeast ATP Synthase Modifies Mitochondrial Cristae Morphology. *Journal of Biological Chemistry* **279**, 40392–40399 (2004).
19. Quintana-Cabrera, R. & Scorrano, L. Determinants and outcomes of mitochondrial dynamics. *Mol Cell* **83**, 857–876 (2023).
20. Tarasenko, D. *et al.* The MICOS component Mic60 displays a conserved membrane-bending activity that is necessary for normal cristae morphology. *Journal of Cell Biology* **216**, 889–899 (2017).
21. Friedman, J. R., Mourier, A., Yamada, J., McCaffery, J. M. & Nunnari, J. MICOS coordinates with respiratory complexes and lipids to establish mitochondrial inner membrane architecture. *Elife* **4**, (2015).
22. Zerbes, R. M. *et al.* Mitofilin complexes: conserved organizers of mitochondrial membrane architecture. *bchm* **393**, 1247–1261 (2012).

23. Rabl, R. *et al.* Formation of cristae and crista junctions in mitochondria depends on antagonism between Fcj1 and Su *e* / *g*. *Journal of Cell Biology* **185**, 1047–1063 (2009).
24. Anand, R., Reichert, A. S. & Kondadi, A. K. Emerging Roles of the MICOS Complex in Cristae Dynamics and Biogenesis. *Biology (Basel)* **10**, 600 (2021).
25. Olichon, A. *et al.* Loss of OPA1 Perturbates the Mitochondrial Inner Membrane Structure and Integrity, Leading to Cytochrome c Release and Apoptosis. *Journal of Biological Chemistry* **278**, 7743–7746 (2003).
26. Lee, H., Smith, S. B. & Yoon, Y. The short variant of the mitochondrial dynamin OPA1 maintains mitochondrial energetics and cristae structure. *Journal of Biological Chemistry* **292**, 7115–7130 (2017).
27. MacVicar, T. & Langer, T. OPA1 processing in cell death and disease – the long and short of it. *J Cell Sci* (2016) doi:10.1242/jcs.159186.
28. Jiang, X., Jiang, H., Shen, Z. & Wang, X. Activation of mitochondrial protease OMA1 by Bax and Bak promotes cytochrome c release during apoptosis. *Proceedings of the National Academy of Sciences* **111**, 14782–14787 (2014).
29. Anand, R. *et al.* The *i* -AAA protease YME1L and OMA1 cleave OPA1 to balance mitochondrial fusion and fission. *Journal of Cell Biology* **204**, 919–929 (2014).
30. Del Dotto, V. *et al.* OPA1 Isoforms in the Hierarchical Organization of Mitochondrial Functions. *Cell Rep* **19**, 2557–2571 (2017).
31. Song, Z., Chen, H., Fiket, M., Alexander, C. & Chan, D. C. OPA1 processing controls mitochondrial fusion and is regulated by mRNA splicing, membrane potential, and Yme1L. *J Cell Biol* **178**, 749–755 (2007).
32. Frezza, C. *et al.* OPA1 Controls Apoptotic Cristae Remodeling Independently from Mitochondrial Fusion. *Cell* **126**, 177–189 (2006).
33. Patten, D. A. *et al.* OPA1-dependent cristae modulation is essential for cellular adaptation to metabolic demand. *EMBO J* **33**, 2676–2691 (2014).
34. Khacho, M. *et al.* Acidosis overrides oxygen deprivation to maintain mitochondrial function and cell survival. *Nat Commun* **5**, 3550 (2014).
35. Gomes, L. C. & Scorrano, L. Mitochondrial elongation during autophagy. *Autophagy* **7**, 1251–1253 (2011).
36. Kondadi, A. K., Anand, R. & Reichert, A. S. Cristae Membrane Dynamics – A Paradigm Change. *Trends Cell Biol* **30**, 923–936 (2020).
37. Varanita, T. *et al.* The Opa1-Dependent Mitochondrial Cristae Remodeling Pathway Controls Atrophic, Apoptotic, and Ischemic Tissue Damage. *Cell Metab* **21**, (2015).
38. Boissan, M. *et al.* Nucleoside diphosphate kinases fuel dynamin superfamily proteins with GTP for membrane remodeling. *Science (1979)* **344**, 1510–1515 (2014).
39. Huang, G. *et al.* WBSCR16 Is a Guanine Nucleotide Exchange Factor Important for Mitochondrial Fusion. *Cell Rep* **20**, 923–934 (2017).
40. Milon, L. *et al.* The Human nm23-H4 Gene Product Is a Mitochondrial Nucleoside Diphosphate Kinase. *Journal of Biological Chemistry* **275**, 14264–14272 (2000).
41. Agarwal, R. P., Robison, B. & Parks, R. E. [49] Nucleoside diphosphokinase from human erythrocytes. in 376–386 (1978). doi:10.1016/S0076-6879(78)51051-3.
42. Arroyo, J. D. *et al.* A Genome-wide CRISPR Death Screen Identifies Genes Essential for Oxidative Phosphorylation. *Cell Metab* **24**, 875–885 (2016).
43. DeVay, R. M. *et al.* Coassembly of Mgm1 isoforms requires cardiolipin and mediates mitochondrial inner membrane fusion. *Journal of Cell Biology* **186**, 793–803 (2009).
44. Mishra, P. & Chan, D. C. Metabolic regulation of mitochondrial dynamics. *Journal of Cell Biology* **212**, 379–387 (2016).
45. Chan, D. C. Fusion and Fission: Interlinked Processes Critical for Mitochondrial Health. *Annu Rev Genet* **46**, 265–287 (2012).

46. Labbé, K., Murley, A. & Nunnari, J. Determinants and Functions of Mitochondrial Behavior. *Annu Rev Cell Dev Biol* **30**, 357–391 (2014).
47. Ban, T. *et al.* Molecular basis of selective mitochondrial fusion by heterotypic action between OPA1 and cardiolipin. *Nat Cell Biol* **19**, 856–863 (2017).
48. Cipolat, S., de Brito, O. M., Dal Zilio, B. & Scorrano, L. OPA1 requires mitofusin 1 to promote mitochondrial fusion. *Proceedings of the National Academy of Sciences* **101**, 15927–15932 (2004).
49. Naylor, K. *et al.* Mdv1 Interacts with Assembled Dnm1 to Promote Mitochondrial Division. *Journal of Biological Chemistry* **281**, 2177–2183 (2006).
50. Tilokani, L., Nagashima, S., Paupe, V. & Prudent, J. Mitochondrial dynamics: Overview of molecular mechanisms. *Essays Biochem* **62**, 341–360 (2018).
51. Martínez-Reyes, I. & Chandel, N. S. Mitochondrial TCA cycle metabolites control physiology and disease. *Nat Commun* **11**, 102 (2020).
52. Meléndez-Hevia, E., Waddell, T. G. & Cascante, M. The puzzle of the Krebs citric acid cycle: Assembling the pieces of chemically feasible reactions, and opportunism in the design of metabolic pathways during evolution. *J Mol Evol* **43**, 293–303 (1996).
53. Krebs, H. A. & Eggleston, L. V. The oxidation of pyruvate in pigeon breast muscle. *Biochemical Journal* **34**, 442–459 (1940).
54. Arnold, P. K. & Finley, L. W. S. Regulation and function of the mammalian tricarboxylic acid cycle. *Journal of Biological Chemistry* **299**, 102838 (2023).
55. Baldwin, J. E. & Krebs, H. The evolution of metabolic cycles. *Nature* **291**, 381–382 (1981).
56. Navdeep Singh Chandel. *Navigating Metabolism*. (Cold Spring Harbor Laboratory Press, 2015).
57. Cogliati, S., Cabrera-Alarcón, J. L. & Enriquez, J. A. Regulation and functional role of the electron transport chain supercomplexes. *Biochem Soc Trans* **49**, 2655–2668 (2021).
58. Erich Et Al -Mitoeagle, G. & Group, T. Mitochondrial physiology Extended resource of Mitochondrial respiratory states and rates. *Bioenerg Commun* **2020**,.
59. Dimroth, P., Matthey, U. & Kaim, G. Critical evaluation of the one- versus the two-channel model for the operation of the ATP synthase's Fo motor. *Biochimica et Biophysica Acta (BBA) - Bioenergetics* **1459**, 506–513 (2000).
60. Protasoni, M. *et al.* Respiratory supercomplexes act as a platform for complex <scp>III</scp> -mediated maturation of human mitochondrial complexes I and <scp>IV</scp>. *EMBO J* **39**, (2020).
61. Acín-Pérez, R., Fernández-Silva, P., Peleato, M. L., Pérez-Martos, A. & Enriquez, J. A. Respiratory Active Mitochondrial Supercomplexes. *Mol Cell* **32**, 529–539 (2008).
62. Letts, J. A. & Sazanov, L. A. Clarifying the supercomplex: the higher-order organization of the mitochondrial electron transport chain. *Nat Struct Mol Biol* **24**, 800–808 (2017).
63. Maranzana, E., Barbero, G., Falasca, A. I., Lenaz, G. & Genova, M. L. Mitochondrial Respiratory Supercomplex Association Limits Production of Reactive Oxygen Species from Complex I. *Antioxid Redox Signal* **19**, 1469–1480 (2013).
64. Lopez-Fabuel, I. *et al.* Complex I assembly into supercomplexes determines differential mitochondrial ROS production in neurons and astrocytes. *Proceedings of the National Academy of Sciences* **113**, 13063–13068 (2016).
65. Lapuente-Brun, E. *et al.* Supercomplex Assembly Determines Electron Flux in the Mitochondrial Electron Transport Chain. *Science (1979)* **340**, 1567–1570 (2013).
66. Hirst, J. Open questions: respiratory chain supercomplexes—why are they there and what do they do? *BMC Biol* **16**, 111 (2018).

67. Javadov, S., Jang, S., Chapa-Dubocq, X. R., Khuchua, Z. & Camara, A. K. Mitochondrial respiratory supercomplexes in mammalian cells: structural versus functional role. *J Mol Med* **99**, 57–73 (2021).
68. Hackenbrock, C. R. ULTRASTRUCTURAL BASES FOR METABOLICALLY LINKED MECHANICAL ACTIVITY IN MITOCHONDRIA. *J Cell Biol* **30**, 269–297 (1966).
69. Mannella, C. A. The relevance of mitochondrial membrane topology to mitochondrial function. *Biochimica et Biophysica Acta (BBA) - Molecular Basis of Disease* **1762**, 140–147 (2006).
70. Gilkerson, R. W., Selker, J. M. L. & Capaldi, R. A. The cristal membrane of mitochondria is the principal site of oxidative phosphorylation. *FEBS Lett* **546**, 355–358 (2003).
71. Mannella, C. A. Structure and dynamics of the mitochondrial inner membrane cristae. *Biochimica et Biophysica Acta (BBA) - Molecular Cell Research* **1763**, 542–548 (2006).
72. Martinou, J.-C. & Youle, R. J. Mitochondria in Apoptosis: Bcl-2 Family Members and Mitochondrial Dynamics. *Dev Cell* **21**, 92–101 (2011).
73. Lee, Y., Jeong, S.-Y., Karbowski, M., Smith, C. L. & Youle, R. J. Roles of the Mammalian Mitochondrial Fission and Fusion Mediators Fis1, Drp1, and Opa1 in Apoptosis. *Mol Biol Cell* **15**, 5001–5011 (2004).
74. Otera, H. *et al.* Mff is an essential factor for mitochondrial recruitment of Drp1 during mitochondrial fission in mammalian cells. *Journal of Cell Biology* **191**, 1141–1158 (2010).
75. Frank, S. *et al.* The Role of Dynamin-Related Protein 1, a Mediator of Mitochondrial Fission, in Apoptosis. *Dev Cell* **1**, 515–525 (2001).
76. Scorrano, L. *et al.* A Distinct Pathway Remodels Mitochondrial Cristae and Mobilizes Cytochrome c during Apoptosis. *Dev Cell* **2**, 55–67 (2002).
77. Germain, M., Mathai, J. P., McBride, H. M. & Shore, G. C. Endoplasmic reticulum BIK initiates DRP1-regulated remodelling of mitochondrial cristae during apoptosis. *EMBO J* **24**, 1546–1556 (2005).
78. Ashrafi, G. & Schwarz, T. L. The pathways of mitophagy for quality control and clearance of mitochondria. *Cell Death Differ* **20**, 31–42 (2013).
79. Kleele, T. *et al.* Distinct fission signatures predict mitochondrial degradation or biogenesis. *Nature* **593**, 435–439 (2021).
80. Twig, G. & Shirihai, O. S. The Interplay Between Mitochondrial Dynamics and Mitophagy. *Antioxid Redox Signal* **14**, 1939–1951 (2011).
81. Molina, A. J. A. *et al.* Mitochondrial Networking Protects β-Cells From Nutrient-Induced Apoptosis. *Diabetes* **58**, 2303–2315 (2009).
82. Bach, D. *et al.* Mitofusin-2 Determines Mitochondrial Network Architecture and Mitochondrial Metabolism. *Journal of Biological Chemistry* **278**, 17190–17197 (2003).
83. Gao, A. W., Cantó, C. & Houtkooper, R. H. Mitochondrial response to nutrient availability and its role in metabolic disease. *EMBO Mol Med* **6**, 580–589 (2014).
84. Galloway, C. A., Lee, H., Brookes, P. S. & Yoon, Y. Decreasing mitochondrial fission alleviates hepatic steatosis in a murine model of nonalcoholic fatty liver disease. *American Journal of Physiology-Gastrointestinal and Liver Physiology* **307**, G632–G641 (2014).
85. Mahdaviani, K. *et al.* Mfn2 deletion in brown adipose tissue protects from insulin resistance and impairs thermogenesis. *EMBO Rep* **18**, 1123–1138 (2017).
86. Ngo, J. *et al.* Mitochondrial morphology controls fatty acid utilization by changing <scp>CPT1</scp> sensitivity to <scp>malonyl-CoA</scp>. *EMBO J* **42**, (2023).
87. Chandel, N. S. Mitochondria as signaling organelles. *BMC Biol* **12**, 34 (2014).

88. Kasahara, A. & Scorrano, L. Mitochondria: from cell death executioners to regulators of cell differentiation. *Trends Cell Biol* **24**, 761–770 (2014).
89. Liu, X., Kim, C. N., Yang, J., Jemmerson, R. & Wang, X. Induction of Apoptotic Program in Cell-Free Extracts: Requirement for dATP and Cytochrome c. *Cell* **86**, 147–157 (1996).
90. Chandel, N. S. *et al.* Mitochondrial reactive oxygen species trigger hypoxia-induced transcription. *Proceedings of the National Academy of Sciences* **95**, 11715–11720 (1998).
91. Herzig, S. & Shaw, R. J. AMPK: guardian of metabolism and mitochondrial homeostasis. *Nat Rev Mol Cell Biol* **19**, 121–135 (2018).
92. West, A. P. & Shadel, G. S. Mitochondrial DNA in innate immune responses and inflammatory pathology. *Nat Rev Immunol* **17**, 363–375 (2017).
93. Antonsson, B., Montessuit, S., Sanchez, B. & Martinou, J.-C. Bax Is Present as a High Molecular Weight Oligomer/Complex in the Mitochondrial Membrane of Apoptotic Cells. *Journal of Biological Chemistry* **276**, 11615–11623 (2001).
94. Nechushtan, A., Smith, C. L., Lamensdorf, I., Yoon, S.-H. & Youle, R. J. Bax and Bak Coalesce into Novel Mitochondria-Associated Clusters during Apoptosis. *J Cell Biol* **153**, 1265–1276 (2001).
95. Tait, S. W. G. & Green, D. R. Mitochondria and cell death: outer membrane permeabilization and beyond. *Nat Rev Mol Cell Biol* **11**, 621–632 (2010).
96. Shen, K. *et al.* Mitochondria as Cellular and Organismal Signaling Hubs. *Annu Rev Cell Dev Biol* **38**, 179–218 (2022).
97. Nargund, A. M., Pellegrino, M. W., Fiorese, C. J., Baker, B. M. & Haynes, C. M. Mitochondrial Import Efficiency of ATFS-1 Regulates Mitochondrial UPR Activation. *Science (1979)* **337**, 587–590 (2012).
98. Nargund, A. M., Fiorese, C. J., Pellegrino, M. W., Deng, P. & Haynes, C. M. Mitochondrial and Nuclear Accumulation of the Transcription Factor ATFS-1 Promotes OXPHOS Recovery during the UPRmt. *Mol Cell* **58**, 123–133 (2015).
99. Lin, Y.-F. *et al.* Maintenance and propagation of a deleterious mitochondrial genome by the mitochondrial unfolded protein response. *Nature* **533**, 416–419 (2016).
100. Rauthan, M., Ranji, P., Aguilera Pradenas, N., Pitot, C. & Pilon, M. The mitochondrial unfolded protein response activator ATFS-1 protects cells from inhibition of the mevalonate pathway. *Proceedings of the National Academy of Sciences* **110**, 5981–5986 (2013).
101. Tan, D. Q. & Suda, T. Reactive Oxygen Species and Mitochondrial Homeostasis as Regulators of Stem Cell Fate and Function. *Antioxid Redox Signal* **29**, 149–168 (2018).
102. Stockwell, B. R. & Jiang, X. The Chemistry and Biology of Ferroptosis. *Cell Chem Biol* **27**, 365–375 (2020).
103. Liang, J. *et al.* Myristoylation confers noncanonical AMPK functions in autophagy selectivity and mitochondrial surveillance. *Nat Commun* **6**, 7926 (2015).
104. Zong, H. *et al.* AMP kinase is required for mitochondrial biogenesis in skeletal muscle in response to chronic energy deprivation. *Proceedings of the National Academy of Sciences* **99**, 15983–15987 (2002).
105. Toyama, E. Q. *et al.* AMP-activated protein kinase mediates mitochondrial fission in response to energy stress. *Science (1979)* **351**, 275–281 (2016).
106. Ryan, D. G. *et al.* Coupling Krebs cycle metabolites to signalling in immunity and cancer. *Nat Metab* **1**, 16–33 (2018).
107. Moussaieff, A. *et al.* Glycolysis-Mediated Changes in Acetyl-CoA and Histone Acetylation Control the Early Differentiation of Embryonic Stem Cells. *Cell Metab* **21**, 392–402 (2015).

108. Lee, J. V. *et al.* Akt-Dependent Metabolic Reprogramming Regulates Tumor Cell Histone Acetylation. *Cell Metab* **20**, 306–319 (2014).
109. Wellen, K. E. *et al.* ATP-Citrate Lyase Links Cellular Metabolism to Histone Acetylation. *Science (1979)* **324**, 1076–1080 (2009).
110. Vyas, S., Zaganjor, E. & Haigis, M. C. Mitochondria and Cancer. *Cell* **166**, 555–566 (2016).
111. Simula, L., Nazio, F. & Campello, S. The mitochondrial dynamics in cancer and immune-surveillance. *Semin Cancer Biol* **47**, 29–42 (2017).
112. Zamberlan, M. *et al.* Inhibition of the mitochondrial protein Opa1 curtails breast cancer growth. *Journal of Experimental & Clinical Cancer Research* **41**, 95 (2022).
113. Sessions, D. T. *et al.* Opa1 and Drp1 reciprocally regulate cristae morphology, ETC function, and NAD+ regeneration in KRas-mutant lung adenocarcinoma. *Cell Rep* **41**, 111818 (2022).
114. Chen, X. *et al.* Targeting Mitochondrial Structure Sensitizes Acute Myeloid Leukemia to Venetoclax Treatment. *Cancer Discov* **9**, 890–909 (2019).
115. Signorile, A. *et al.* Human Ovarian Cancer Tissue Exhibits Increase of Mitochondrial Biogenesis and Cristae Remodeling. *Cancers (Basel)* **11**, 1350 (2019).
116. Hu, L.-P. *et al.* Single-cell RNA sequencing reveals that targeting HSP90 suppresses PDAC progression by restraining mitochondrial bioenergetics. *Oncogenesis* **10**, 22 (2021).
117. Maycotte, P. *et al.* Mitochondrial dynamics and cancer. *Tumor Biology* **39**, 101042831769839 (2017).
118. Srinivasan, S., Guha, M., Kashina, A. & Avadhani, N. G. Mitochondrial dysfunction and mitochondrial dynamics-The cancer connection. *Biochimica et Biophysica Acta (BBA) - Bioenergetics* **1858**, 602–614 (2017).
119. Serasinghe, M. N. *et al.* Mitochondrial Division Is Requisite to RAS-Induced Transformation and Targeted by Oncogenic MAPK Pathway Inhibitors. *Mol Cell* **57**, 521–536 (2015).
120. Kashatus, J. A. *et al.* Erk2 Phosphorylation of Drp1 Promotes Mitochondrial Fission and MAPK-Driven Tumor Growth. *Mol Cell* **57**, 537–551 (2015).
121. Nagdas, S. *et al.* Drp1 Promotes KRas-Driven Metabolic Changes to Drive Pancreatic Tumor Growth. *Cell Rep* **28**, 1845-1859.e5 (2019).
122. Zhao, J. *et al.* Mitochondrial dynamics regulates migration and invasion of breast cancer cells. *Oncogene* **32**, 4814–4824 (2013).
123. Graves, J. A. *et al.* Mitochondrial Structure, Function and Dynamics Are Temporally Controlled by c-Myc. *PLoS One* **7**, e37699 (2012).
124. Campbell, K. J. & Leung, H. Y. Evasion of cell death: A contributory factor in prostate cancer development and treatment resistance. *Cancer Lett* **520**, 213–221 (2021).
125. Fontana, F. & Limonta, P. Dissecting the Hormonal Signaling Landscape in Castration-Resistant Prostate Cancer. *Cells* **10**, 1133 (2021).
126. Fu, Y., Yu, J., Li, F. & Ge, S. Oncometabolites drive tumorigenesis by enhancing protein acylation: from chromosomal remodelling to nonhistone modification. *Journal of Experimental & Clinical Cancer Research* **41**, 144 (2022).
127. Dalla Pozza, E. *et al.* Regulation of succinate dehydrogenase and role of succinate in cancer. *Semin Cell Dev Biol* **98**, 4–14 (2020).
128. Huang, S., Wang, Z. & Zhao, L. The Crucial Roles of Intermediate Metabolites in Cancer. *Cancer Manag Res* **Volume 13**, 6291–6307 (2021).
129. Carrer, A. *et al.* Acetyl-CoA metabolism supports multistep pancreatic tumorigenesis. *Cancer Discov* **9**, 416–435 (2019).
130. Viale, A. *et al.* Oncogene ablation-resistant pancreatic cancer cells depend on mitochondrial function. *Nature* **514**, 628–632 (2014).

131. Evans, K. W. *et al.* Oxidative Phosphorylation Is a Metabolic Vulnerability in Chemotherapy-Resistant Triple-Negative Breast Cancer. *Cancer Res* **81**, 5572–5581 (2021).
132. Cluntun, A. A., Lukey, M. J., Cerione, R. A. & Locasale, J. W. Glutamine Metabolism in Cancer: Understanding the Heterogeneity. *Trends Cancer* **3**, 169–180 (2017).
133. Son, J. *et al.* Glutamine supports pancreatic cancer growth through a KRAS-regulated metabolic pathway. *Nature* **496**, 101–105 (2013).
134. Mukhopadhyay, S., Vander Heiden, M. G. & McCormick, F. The metabolic landscape of RAS-driven cancers from biology to therapy. *Nat Cancer* **2**, 271–283 (2021).
135. Padanad, M. S. *et al.* Fatty Acid Oxidation Mediated by Acyl-CoA Synthetase Long Chain 3 Is Required for Mutant KRAS Lung Tumorigenesis. *Cell Rep* **16**, 1614–1628 (2016).
136. Linher-Melville, K. *et al.* Establishing a relationship between prolactin and altered fatty acid β-Oxidation via carnitine palmitoyl transferase 1 in breast cancer cells. *BMC Cancer* **11**, 56 (2011).
137. Mao, S. *et al.* Inhibition of CPT1a as a prognostic marker can synergistically enhance the antileukemic activity of ABT199. *J Transl Med* **19**, 181 (2021).
138. Shao, H. *et al.* Carnitine palmitoyltransferase 1A functions to repress FoxO transcription factors to allow cell cycle progression in ovarian cancer. *Oncotarget* **7**, 3832–3846 (2016).
139. Qu, Q., Zeng, F., Liu, X., Wang, Q. J. & Deng, F. Fatty acid oxidation and carnitine palmitoyltransferase I: emerging therapeutic targets in cancer. *Cell Death Dis* **7**, e2226–e2226 (2016).
140. Schlaepfer, I. R. & Joshi, M. CPT1A-mediated Fat Oxidation, Mechanisms, and Therapeutic Potential. *Endocrinology* **161**, (2020).
141. Tirado-Vélez, J. M., Joumady, I., Sáez-Benito, A., Cózar-Castellano, I. & Perdomo, G. Inhibition of Fatty Acid Metabolism Reduces Human Myeloma Cells Proliferation. *PLoS One* **7**, e46484 (2012).
142. Ma, Y. *et al.* Fatty acid oxidation: An emerging facet of metabolic transformation in cancer. *Cancer Lett* **435**, 92–100 (2018).
143. Lin, H. *et al.* Fatty acid oxidation is required for the respiration and proliferation of malignant glioma cells. *Neuro Oncol* **19**, 43–54 (2017).
144. Ashraf, R. & Kumar, S. Mfn2-mediated mitochondrial fusion promotes autophagy and suppresses ovarian cancer progression by reducing ROS through AMPK/mTOR/ERK signaling. *Cellular and Molecular Life Sciences* **79**, 573 (2022).
145. Liou, G.-Y. *et al.* Mutant KRas-Induced Mitochondrial Oxidative Stress in Acinar Cells Upregulates EGFR Signaling to Drive Formation of Pancreatic Precancerous Lesions. *Cell Rep* **14**, 2325–2336 (2016).
146. Murtaugh, L. C. & Keefe, M. D. Regeneration and Repair of the Exocrine Pancreas. *Annu Rev Physiol* **77**, 229–249 (2015).
147. Longnecker, D. S., Gorelick, F. & Thompson, E. D. Anatomy, Histology, and Fine Structure of the Pancreas. in *The Pancreas* 10–23 (Wiley, 2018). doi:10.1002/9781119188421.ch2.
148. Mizrahi, J. D., Surana, R., Valle, J. W. & Shroff, R. T. Pancreatic cancer. *The Lancet* **395**, 2008–2020 (2020).
149. Rahib, L. *et al.* Projecting Cancer Incidence and Deaths to 2030: The Unexpected Burden of Thyroid, Liver, and Pancreas Cancers in the United States. *Cancer Res* **74**, 2913–2921 (2014).
150. Mukhopadhyay, S., Vander Heiden, M. G. & McCormick, F. The metabolic landscape of RAS-driven cancers from biology to therapy. *Nat Cancer* **2**, 271–283 (2021).

151. Halbrook, C. J., Lyssiotis, C. A., Pasca di Magliano, M. & Maitra, A. Pancreatic cancer: Advances and challenges. *Cell* **186**, 1729–1754 (2023).
152. Li, J.-T., Wang, Y.-P., Yin, M. & Lei, Q.-Y. Metabolism remodeling in pancreatic ductal adenocarcinoma. *Cell Stress* **3**, 361–368 (2019).
153. Hanahan, D. Hallmarks of Cancer: New Dimensions. *Cancer Discov* **12**, 31–46 (2022).
154. Huang, H. *et al.* Oncogenic K-Ras requires activation for enhanced activity. *Oncogene* **33**, 532–535 (2014).
155. Ciernikova, S. *et al.* Epigenetic Landscape in Pancreatic Ductal Adenocarcinoma: On the Way to Overcoming Drug Resistance? *Int J Mol Sci* **21**, 4091 (2020).
156. McDonald, O. G. *et al.* Epigenomic reprogramming during pancreatic cancer progression links anabolic glucose metabolism to distant metastasis. *Nat Genet* **49**, 367–376 (2017).
157. Cleveland, M. H., Sawyer, J. M., Afelik, S., Jensen, J. & Leach, S. D. Exocrine ontogenies: On the development of pancreatic acinar, ductal and centroacinar cells. *Semin Cell Dev Biol* **23**, 711–719 (2012).
158. Hezel, A. F., Kimmelman, A. C., Stanger, B. Z., Bardeesy, N. & DePinho, R. A. Genetics and biology of pancreatic ductal adenocarcinoma. *Genes Dev* **20**, 1218–1249 (2006).
159. Paoli, C. & Carrer, A. Organotypic culture of acinar cells for the study of pancreatic cancer initiation. *Cancers (Basel)* **12**, 1–22 (2020).
160. Wong, M. C. S. *et al.* Global temporal patterns of pancreatic cancer and association with socioeconomic development. *Sci Rep* **7**, 3165 (2017).
161. Rawla, P., Sunkara, T. & Gaduputi, V. Epidemiology of Pancreatic Cancer: Global Trends, Etiology and Risk Factors. *World J Oncol* **10**, 10–27 (2019).
162. Hu, J.-X. *et al.* Pancreatic cancer: A review of epidemiology, trend, and risk factors. *World J Gastroenterol* **27**, 4298–4321 (2021).
163. Siegel, R. L., Miller, K. D., Fuchs, H. E. & Jemal, A. Cancer statistics, 2022. *CA Cancer J Clin* **72**, 7–33 (2022).
164. Wood, L. D., Canto, M. I., Jaffee, E. M. & Simeone, D. M. Pancreatic Cancer: Pathogenesis, Screening, Diagnosis, and Treatment. *Gastroenterology* **163**, 386-402.e1 (2022).
165. Bosetti, C. *et al.* Cigarette smoking and pancreatic cancer: an analysis from the International Pancreatic Cancer Case-Control Consortium (Panc4). *Annals of Oncology* **23**, 1880–1888 (2012).
166. Wood, L. D. & Hruban, R. H. Pathology and Molecular Genetics of Pancreatic Neoplasms. *The Cancer Journal* **18**, 492–501 (2012).
167. Arslan, A. A. Anthropometric Measures, Body Mass Index, and Pancreatic Cancer. *Arch Intern Med* **170**, 791 (2010).
168. Hu, J.-X. *et al.* Pancreatic cancer: A review of epidemiology, trend, and risk factors. *World J Gastroenterol* **27**, 4298–4321 (2021).
169. Yadav, D. & Lowenfels, A. B. The Epidemiology of Pancreatitis and Pancreatic Cancer. *Gastroenterology* **144**, 1252–1261 (2013).
170. Singhi, A. D., Koay, E. J., Chari, S. T. & Maitra, A. Early Detection of Pancreatic Cancer: Opportunities and Challenges. *Gastroenterology* **156**, 2024–2040 (2019).
171. Ying, H. *et al.* Genetics and biology of pancreatic ductal adenocarcinoma. *Genes Dev* **30**, 355–385 (2016).
172. Storz, P. Acinar cell plasticity and development of pancreatic ductal adenocarcinoma. *Nat Rev Gastroenterol Hepatol* **14**, 296–304 (2017).

173. Kopp, J. L. & Sander, M. New insights into the cell lineage of pancreatic ductal adenocarcinoma: Evidence for tumor stem cells in premalignant lesions? *Gastroenterology* **146**, 24–26 (2014).
174. Storz, P. & Crawford, H. C. Carcinogenesis of Pancreatic Ductal Adenocarcinoma. *Gastroenterology* **158**, 2072–2081 (2020).
175. Pamonsinlapatham, P. *et al.* P120-Ras GTPase activating protein (RasGAP): A multi-interacting protein in downstream signaling. *Biochimie* **91**, 320–328 (2009).
176. Huang, L., Guo, Z., Wang, F. & Fu, L. KRAS mutation: from undruggable to druggable in cancer. *Signal Transduct Target Ther* **6**, 386 (2021).
177. Raphael, B. J. *et al.* Integrated Genomic Characterization of Pancreatic Ductal Adenocarcinoma. *Cancer Cell* **32**, 185-203.e13 (2017).
178. Haigis, K. M. *et al.* Differential effects of oncogenic K-Ras and N-Ras on proliferation, differentiation and tumor progression in the colon. *Nat Genet* **40**, 600–608 (2008).
179. Hayashi, H. *et al.* Biological Significance of YAP/TAZ in Pancreatic Ductal Adenocarcinoma. *Front Oncol* **11**, (2021).
180. Grant, T. J., Hua, K. & Singh, A. Molecular Pathogenesis of Pancreatic Cancer. in 241–275 (2016). doi:10.1016/bs.pmbts.2016.09.008.
181. Sipos, B., Frank, S., Gress, T., Hahn, S. & Klöppel, G. Pancreatic Intraepithelial Neoplasia Revisited and Updated. *Pancreatology* **9**, 45–54 (2009).
182. Wilentz, R. E. and H. R. H. Pathology of cancer of the pancreas. *Surg Oncol Clin N Am* **7,1**, 43–65 (1998).
183. Massagué, J. TGFβ in Cancer. *Cell* **134**, 215–230 (2008).
184. Iacobuzio-Donahue, C. A., Velculescu, V. E., Wolfgang, C. L. & Hruban, R. H. Genetic basis of pancreas cancer development and progression: insights from whole-exome and whole-genome sequencing. *Clin Cancer Res* **18**, 4257–65 (2012).
185. Vogelstein, B., Lane, D. & Levine, A. J. Surfing the p53 network. *Nature* **408**, 307–310 (2000).
186. Collisson, E. A. *et al.* Subtypes of pancreatic ductal adenocarcinoma and their differing responses to therapy. *Nat Med* **17**, 500–503 (2011).
187. Moffitt, R. A. *et al.* Virtual microdissection identifies distinct tumor- and stroma-specific subtypes of pancreatic ductal adenocarcinoma. *Nat Genet* **47**, 1168–1178 (2015).
188. Bailey, P. *et al.* Genomic analyses identify molecular subtypes of pancreatic cancer. *Nature* **531**, 47–52 (2016).
189. Hessmann, E. *et al.* Microenvironmental Determinants of Pancreatic Cancer. *Physiol Rev* **100**, 1707–1751 (2020).
190. Hosein, A. N., Brekken, R. A. & Maitra, A. Pancreatic cancer stroma: an update on therapeutic targeting strategies. *Nat Rev Gastroenterol Hepatol* **17**, 487–505 (2020).
191. Jacobetz, M. A. *et al.* Hyaluronan impairs vascular function and drug delivery in a mouse model of pancreatic cancer. *Gut* **62**, 112–120 (2013).
192. Provenzano, P. P. *et al.* Enzymatic Targeting of the Stroma Ablates Physical Barriers to Treatment of Pancreatic Ductal Adenocarcinoma. *Cancer Cell* **21**, 418–429 (2012).
193. Collins, M. A. *et al.* Oncogenic Kras is required for both the initiation and maintenance of pancreatic cancer in mice. *Journal of Clinical Investigation* **122**, 639–653 (2012).
194. Ying, H. *et al.* Oncogenic kras maintains pancreatic tumors through regulation of anabolic glucose metabolism. *Cell* **149**, 656–670 (2012).
195. Helms, E., Onate, M. K. & Sherman, M. H. Fibroblast Heterogeneity in the Pancreatic Tumor Microenvironment. *Cancer Discov* **10**, 648–656 (2020).

196. Neuzillet, C. *et al.* Inter- and intra-tumoural heterogeneity in cancer-associated fibroblasts of human pancreatic ductal adenocarcinoma. *J Pathol* **248**, 51–65 (2019).
197. Schneider, G. *et al.* Lymphangioma of the pancreas and the duodenal wall: MR imaging findings. *Eur Radiol* **11**, 2232–2235 (2001).
198. Vonlaufen, A., Wilson, J. S. & Apte, M. V. Molecular mechanisms of pancreatitis: Current opinion. *J Gastroenterol Hepatol* **23**, 1339–1348 (2008).
199. Corcoran, R. B. *et al. STAT3* Plays a Critical Role in *KRAS* -Induced Pancreatic Tumorigenesis. *Cancer Res* **71**, 5020–5029 (2011).
200. Lesina, M. *et al.* Stat3/Socs3 Activation by IL-6 Transsignaling Promotes Progression of Pancreatic Intraepithelial Neoplasia and Development of Pancreatic Cancer. *Cancer Cell* **19**, 456–469 (2011).
201. LING, S., FENG, T., JIA, K., TIAN, Y. & LI, Y. Inflammation to cancer: The molecular biology in the pancreas (Review). *Oncol Lett* **7**, 1747–1754 (2014).
202. Liou, G.-Y. *et al.* Mutant KRAS–Induced Expression of ICAM-1 in Pancreatic Acinar Cells Causes Attraction of Macrophages to Expedite the Formation of Precancerous Lesions. *Cancer Discov* **5**, 52–63 (2015).
203. Liou, G.-Y. *et al.* The Presence of Interleukin-13 at Pancreatic ADM/PanIN Lesions Alters Macrophage Populations and Mediates Pancreatic Tumorigenesis. *Cell Rep* **19**, 1322–1333 (2017).
204. Liou, G.-Y. & Storz, P. Inflammatory macrophages in pancreatic acinar cell metaplasia and initiation of pancreatic cancer. *Oncoscience* **2**, 247–251 (2015).
205. Karamitopoulou, E. Tumour microenvironment of pancreatic cancer: immune landscape is dictated by molecular and histopathological features. *Br J Cancer* **121**, 5–14 (2019).
206. Perera, R. M. & Bardeesy, N. Pancreatic Cancer Metabolism: Breaking It Down to Build It Back Up. *Cancer Discov* **5**, 1247–1261 (2015).
207. Wang, S. *et al.* The molecular biology of pancreatic adenocarcinoma: translational challenges and clinical perspectives. *Signal Transduct Target Ther* **6**, 249 (2021).
208. Guillaumond, F. & Vasseur, S. The metabolic facet of pancreatic cancer: How hypoxia shapes fatal cancer cells. *Cell Cycle* **12**, 1155–1156 (2013).
209. Santana-Codina, N. *et al.* Oncogenic KRAS supports pancreatic cancer through regulation of nucleotide synthesis. *Nat Commun* **9**, 4945 (2018).
210. Dey, P. *et al.* Oncogenic KRAS-Driven Metabolic Reprogramming in Pancreatic Cancer Cells Utilizes Cytokines from the Tumor Microenvironment. *Cancer Discov* **10**, 608–625 (2020).
211. Lee, J. V. *et al.* Akt-dependent metabolic reprogramming regulates tumor cell Histone acetylation. *Cell Metab* **20**, 306–319 (2014).
212. Hao, X., Ren, Y., Feng, M., Wang, Q. & Wang, Y. Metabolic reprogramming due to hypoxia in pancreatic cancer: Implications for tumor formation, immunity, and more. *Biomedicine & Pharmacotherapy* **141**, 111798 (2021).
213. Sonveaux, P. *et al.* Targeting lactate-fueled respiration selectively kills hypoxic tumor cells in mice. *Journal of Clinical Investigation* (2008) doi:10.1172/JCI36843.
214. Baek, G. *et al.* MCT4 Defines a Glycolytic Subtype of Pancreatic Cancer with Poor Prognosis and Unique Metabolic Dependencies. *Cell Rep* **9**, 2233–2249 (2014).
215. Hosein, A. N. & Beg, M. S. Pancreatic Cancer Metabolism: Molecular Mechanisms and Clinical Applications. *Curr Oncol Rep* **20**, 56 (2018).
216. Lyssiotis, C. A., Son, J., Cantley, L. C. & Kimmelman, A. C. Pancreatic cancers rely on a novel glutamine metabolism pathway to maintain redox balance. *Cell Cycle* **12**, 1987–1988 (2013).
217. DeNicola, G. M. *et al.* Oncogene-induced Nrf2 transcription promotes ROS detoxification and tumorigenesis. *Nature* **475**, 106–109 (2011).

218. Mitsuishi, Y. *et al.* Nrf2 Redirects Glucose and Glutamine into Anabolic Pathways in Metabolic Reprogramming. *Cancer Cell* **22**, 66–79 (2012).
219. Maddocks, O. D. K. *et al.* Modulating the therapeutic response of tumours to dietary serine and glycine starvation. *Nature* **544**, 372–376 (2017).
220. Kottakis, F. *et al.* LKB1 loss links serine metabolism to DNA methylation and tumorigenesis. *Nature* **539**, 390–395 (2016).
221. Kimmelman, A. C. & White, E. Autophagy and Tumor Metabolism. *Cell Metab* **25**, 1037–1043 (2017).
222. Perera, R. M. *et al.* Transcriptional control of autophagy–lysosome function drives pancreatic cancer metabolism. *Nature* **524**, 361–365 (2015).
223. Yang, A. *et al.* Autophagy Sustains Pancreatic Cancer Growth through Both Cell-Autonomous and Nonautonomous Mechanisms. *Cancer Discov* **8**, 276–287 (2018).
224. Yang, S. *et al.* Pancreatic cancers require autophagy for tumor growth. *Genes Dev* **25**, 717–729 (2011).
225. Commisso, C. *et al.* Macropinocytosis of protein is an amino acid supply route in Ras-transformed cells. *Nature* **497**, 633–637 (2013).
226. Sousa, C. M. & Kimmelman, A. C. The complex landscape of pancreatic cancer metabolism. *Carcinogenesis* **35**, 1441–50 (2014).
227. Guillaumond, F. *et al.* Cholesterol uptake disruption, in association with chemotherapy, is a promising combined metabolic therapy for pancreatic adenocarcinoma. *Proceedings of the National Academy of Sciences* **112**, 2473–2478 (2015).
228. Sancho, P. *et al.* MYC/PGC-1α Balance Determines the Metabolic Phenotype and Plasticity of Pancreatic Cancer Stem Cells. *Cell Metab* **22**, 590–605 (2015).
229. Karasinska, J. M. *et al.* Altered Gene Expression along the Glycolysis–Cholesterol Synthesis Axis Is Associated with Outcome in Pancreatic Cancer. *Clinical Cancer Research* **26**, 135–146 (2020).
230. Izzo, L. T., Affronti, H. C. & Wellen, K. E. The Bidirectional Relationship Between Cancer Epigenetics and Metabolism. *Annu Rev Cancer Biol* **5**, 235–257 (2021).
231. Juliano, C. N. *et al.* H4K12 and H3K18 Acetylation Associates With Poor Prognosis in Pancreatic Cancer. *Applied Immunohistochemistry & Molecular Morphology* **24**, 337–344 (2016).
232. Benitz, S. *et al.* Polycomb repressor complex 1 promotes gene silencing through H2AK119 mono-ubiquitination in acinar-to-ductal metaplasia and pancreatic cancer cells. *Oncotarget* **7**, 11424–11433 (2016).
233. Vincent, A., Herman, J., Schulick, R., Hruban, R. H. & Goggins, M. Pancreatic cancer. *The Lancet* **378**, 607–620 (2011).
234. Azizi, M. *et al.* MicroRNA-148b and microRNA-152 reactivate tumor suppressor genes through suppression of DNA methyltransferase-1 gene in pancreatic cancer cell lines. *Cancer Biol Ther* **15**, 419–427 (2014).
235. Panatta, E. *et al.* Metabolic regulation by p53 prevents R-loop-associated genomic instability. *Cell Rep* **41**, 111568 (2022).
236. Morris, J. P. *et al.* α-Ketoglutarate links p53 to cell fate during tumour suppression. *Nature* **573**, 595–599 (2019).
237. Mann, K. M. *et al. Sleeping Beauty* mutagenesis reveals cooperating mutations and pathways in pancreatic adenocarcinoma. *Proceedings of the National Academy of Sciences* **109**, 5934–5941 (2012).
238. Wang, S. C. *et al.* SWI/SNF component ARID1A restrains pancreatic neoplasia formation. *Gut* **68**, 1259 (2019).

239. Chen, W. W., Freinkman, E., Wang, T., Birsoy, K. & Sabatini, D. M. Absolute Quantification of Matrix Metabolites Reveals the Dynamics of Mitochondrial Metabolism. *Cell* **166**, 1324-1337.e11 (2016).
240. Nagdas, S. *et al.* Drp1 Promotes KRas-Driven Metabolic Changes to Drive Pancreatic Tumor Growth. *Cell Rep* **28**, 1845-1859.e5 (2019).
241. Huang, G. *et al.* WBSCR16 Is a Guanine Nucleotide Exchange Factor Important for Mitochondrial Fusion. *Cell Rep* **20**, 923–934 (2017).
242. Lacombe, M.-L., Tokarska-Schlattner, M., Boissan, M. & Schlattner, U. The mitochondrial nucleoside diphosphate kinase (NDPK-D/NME4), a moonlighting protein for cell homeostasis. *Laboratory Investigation* **98**, 582–588 (2018).
243. Schlattner, U. *et al.* Dual Function of Mitochondrial Nm23-H4 Protein in Phosphotransfer and Intermembrane Lipid Transfer. *Journal of Biological Chemistry* **288**, 111–121 (2013).
244. Hu, C. *et al.* OPA1 and MICOS Regulate mitochondrial crista dynamics and formation. *Cell Death Dis* **11**, 940 (2020).
245. Glytsou, C. *et al.* Optic Atrophy 1 Is Epistatic to the Core MICOS Component MIC60 in Mitochondrial Cristae Shape Control. *Cell Rep* **17**, 3024–3034 (2016).
246. Schlattner, U. *et al.* Mitochondrial NM23-H4/NDPK-D: a bifunctional nanoswitch for bioenergetics and lipid signaling. *Naunyn Schmiedebergs Arch Pharmacol* **388**, 271–278 (2015).
247. Stephens, A. D. *et al.* Chromatin histone modifications and rigidity affect nuclear morphology independent of lamins. *Mol Biol Cell* **29**, 220–233 (2018).
248. Cantwell, H. & Dey, G. Nuclear size and shape control. *Semin Cell Dev Biol* **130**, 90–97 (2022).
249. Amiad-Pavlov, D. *et al.* Live imaging of chromatin distribution reveals novel principles of nuclear architecture and chromatin compartmentalization. *Sci Adv* **7**, (2021).
250. McDonald, O. G. *et al.* Epigenomic reprogramming during pancreatic cancer progression links anabolic glucose metabolism to distant metastasis. *Nat Genet* **49**, 367–376 (2017).
251. Wellen, K. E. *et al.* ATP-citrate lyase links cellular metabolism to histone acetylation. *Science (1979)* **324**, 1076–1080 (2009).
252. Arnold, P. K. *et al.* A non-canonical tricarboxylic acid cycle underlies cellular identity. *Nature* **603**, 477–481 (2022).
253. Hingorani, S. R. *et al.* Preinvasive and invasive ductal pancreatic cancer and its early detection in the mouse. *Cancer Cell* **4**, 437–450 (2003).
254. Ariston Gabriel, A. N. *et al.* Differences between KC and KPC pancreatic ductal adenocarcinoma mice models, in terms of their modeling biology and their clinical relevance. *Pancreatology* **20**, 79–88 (2020).
255. Hingorani, S. R. *et al.* Trp53R172H and KrasG12D cooperate to promote chromosomal instability and widely metastatic pancreatic ductal adenocarcinoma in mice. *Cancer Cell* **7**, (2005).
256. Herkenne, S. *et al.* Developmental and Tumor Angiogenesis Requires the Mitochondria-Shaping Protein Opa1. *Cell Metab* **31**, 987-1003.e8 (2020).
257. Hanahan, D. & Weinberg, R. A. Hallmarks of Cancer: The Next Generation. *Cell* **144**, 646–674 (2011).
258. Edens, L. J., White, K. H., Jevtic, P., Li, X. & Levy, D. L. Nuclear size regulation: from single cells to development and disease. *Trends Cell Biol* **23**, 151–159 (2013).
259. Nitsch, S., Zorro Shahidian, L. & Schneider, R. Histone acylations and chromatin dynamics: concepts, challenges, and links to metabolism. *EMBO Rep* **22**, (2021).

260. Chatterjee, N. & Walker, G. C. Mechanisms of DNA damage, repair, and mutagenesis. *Environ Mol Mutagen* **58**, 235–263 (2017).
261. Matthews, H. K., Bertoli, C. & de Bruin, R. A. M. Cell cycle control in cancer. *Nat Rev Mol Cell Biol* **23**, 74–88 (2022).
262. Cogliati, S., Enriquez, J. A. & Scorrano, L. Mitochondrial Cristae: Where Beauty Meets Functionality. *Trends Biochem Sci* **41**, 261–273 (2016).
263. Ilic, M. & Ilic, I. Epidemiology of pancreatic cancer. *World J Gastroenterol* **22**, 9694–9705 (2016).
264. Weinberg, F. *et al.* Mitochondrial metabolism and ROS generation are essential for Kras-mediated tumorigenicity. *Proc Natl Acad Sci U S A* **107**, 8788–8793 (2010).
265. Eser, S., Schnieke, A., Schneider, G. & Saur, D. Oncogenic KRAS signalling in pancreatic cancer. *Br J Cancer* **111**, 817–822 (2014).
266. Liu, J. *et al.* Critical role of oncogenic KRAS in pancreatic cancer (Review). *Mol Med Rep* **13**, 4943–4949 (2016).
267. Ying, H. *et al.* Oncogenic Kras Maintains Pancreatic Tumors through Regulation of Anabolic Glucose Metabolism. *Cell* **149**, 656–670 (2012).
268. Carpenter, E. S. *et al.* Analysis of Donor Pancreata Defines the Transcriptomic Signature and Microenvironment of Early Neoplastic Lesions. *Cancer Discov* **13**, 1324–1345 (2023).
269. Rodrigues, T. & Ferraz, L. S. Therapeutic potential of targeting mitochondrial dynamics in cancer. *Biochem Pharmacol* **182**, 114282 (2020).
270. Kurelac, I. *et al.* Inducing cancer indolence by targeting mitochondrial Complex I is potentiated by blocking macrophage-mediated adaptive responses. *Nat Commun* **10**, 903 (2019).
271. Yang, Q. *et al.* Targeting the complex I and III of mitochondrial electron transport chain as a potentially viable option in liver cancer management. *Cell Death Discov* **7**, 293 (2021).
272. Martínez-Reyes, I. *et al.* Mitochondrial ubiquinol oxidation is necessary for tumour growth. *Nature* **585**, 288–292 (2020).
273. Civiletto, G. *et al.* Opa1 Overexpression Ameliorates the Phenotype of Two Mitochondrial Disease Mouse Models. *Cell Metab* **21**, 845–854 (2015).
274. Millet, A. M. C. *et al.* OPA1 deficiency impairs oxidative metabolism in cycling cells, underlining a translational approach for degenerative diseases. *Dis Model Mech* **16**, (2023).
275. Grotehans, N. *et al.* Ribonucleotide synthesis by <scp>NME6</scp> fuels mitochondrial gene expression. *EMBO J* **42**, (2023).
276. Kramer, N. J. *et al.* Regulators of mitonuclear balance link mitochondrial metabolism to mtDNA expression. *Nat Cell Biol* **25**, 1575–1589 (2023).
277. Wanrooij, P. H. & Chabes, A. NME6: ribonucleotide salvage sustains mitochondrial transcription. *EMBO J* **42**, (2023).
278. Gemble, S. *et al.* A balanced pyrimidine pool is required for optimal Chk1 activation to prevent ultrafine anaphase bridge formation. *J Cell Sci* (2016) doi:10.1242/jcs.187781.
279. Abt, E. R. *et al.* Reprogramming of nucleotide metabolism by interferon confers dependence on the replication stress response pathway in pancreatic cancer cells. *Cell Rep* **38**, 110236 (2022).
280. Mizenina, O. A. & Moasser, M. M. S-phase Inhibition of Cell Cycle Progression by a Novel Class of Pyridopyrimidine Tyrosine Kinase Inhibitors. *Cell Cycle* **3**, 794–801 (2004).
281. Ali, E. S. & Ben-Sahra, I. Regulation of nucleotide metabolism in cancers and immune disorders. *Trends Cell Biol* **33**, 950–966 (2023).

282. Diehl, F. F. *et al.* Nucleotide imbalance decouples cell growth from cell proliferation. *Nat Cell Biol* **24**, 1252–1264 (2022).
283. Frey, A. J. *et al.* LC-quadrupole/Orbitrap high-resolution mass spectrometry enables stable isotope-resolved simultaneous quantification and 13C-isotopic labeling of acyl-coenzyme A thioesters. *Anal Bioanal Chem* **408**, 3651–3658 (2016).
284. Frezza, C., Cipolat, S. & Scorrano, L. Organelle isolation: functional mitochondria from mouse liver, muscle and cultured filroblasts. *Nat Protoc* **2**, 287–295 (2007).